UNIVERSITY OF OKLAHOMA

GRADUATE COLLEGE

IMPACT OF EDGE DIFFRACTION IN DUAL-POLARIZED

PHASED ARRAY ANTENNAS

A DISSERTATION

SUBMITTED TO THE GRADUATE FACULTY

in partial fulfillment of the requirements for the

Degree of

DOCTOR OF PHILOSOPHY

By

JAVIER ALEJANDRO ORTIZ GARCÍA
Norman, Oklahoma
2020

IMPACT OF EDGE DIFFRACTION IN DUAL-POLARIZED
PHASED ARRAY ANTENNAS

A DISSERTATION APPROVED FOR THE
SCHOOL OF ELECTRICAL AND COMPUTER ENGINEERING

BY THE COMMITTEE CONSISTING OF

Dr. Jorge L. Salazar Cerreño, Chair

Dr. Nafati Aboserwal

Dr. Hjalti H. Sigmarsson

Dr. Robert Palmer

Dr. Tian-You Yu

Dr. Alberto Marino

To my parents, Gilberto and Amagie,

for their endless love and support.

Acknowledgments

Firstly, I would like to thank my advisor, Dr. Jorge Salazar, for giving me the opportunity to work under his team's incredible projects and for his invaluable support and guidance throughout the years. I'd also like to thank Dr. Nafati Aboserwal for his incredible insight, patience, and willingness to teach and pass on his expertise on the subject of diffraction.

This work is made possible because of the Advanced Radar Research Center (ARRC) and all the amazing members and facilities that help us as students bring value to the community and grow as individuals. Among them, I'd like to thank all of my committee and colleagues at the ARRC, with special mention to José Díaz, Dr. Rodrigo Lebrón, Arturo Umeyama, Dr. Robin Irazoqui, Blake James, and all of those who turned into very close friends that were of great influence in my growth as a student, professional, and a person overall. Moments of clarity came with all of their insights, discussions, and laughs, which helped tremendously with my research and made all the experience more than worthwhile.

In the University of Puerto Rico at Mayagüez is where my interest for applications in electromagnetics was born. Therefore, I would like to express deep gratitude to all my advisors and professors that willingly and kindly sat with me, taught me, and welcomed me in their projects. They were a source of inspiration and my experience there helped me grow as well as opened many

doors, including the opportunity for me to get to this point, and for that also, I am grateful.

Finally, a special thank you to my family for all their support, especially my father, Gilberto, for all of his wisdom and for laying down a path for me to follow by believing in myself. To my mother, Amagie, whose love and kind words of encouragement always composed me through the tough times. Without them, none of this or any other accomplishments would be possible. Also, to my younger brothers, Eduardo and Armando, both of whom I look up to in many ways. I would also give a special thank you to my beloved grandmother, Amanda, for her infinite love and for being my first teacher. I admire her strength more than anyone. Finally, to my late grandfather, Ramón, for supporting me throughout my life until the beginning of this journey and for teaching me how to learn.

Table of Contents

List of Tables

List of Figures

xiv

Abstract

An analytical model is proposed to characterize and quantify the effects that diffracted fields have on the performance of phased array antennas. The work involves the combination of diffraction theory techniques and how each can be used to analyze this phenomena with the use of antenna elements as sources. As these antenna elements are placed along a ground plane of relatively large size in terms of λ diffracted fields can perturb the expected cross-polarization radiation performance of the element. As the element is moved along the ground plane and at different relative distances from the edges, depending on the electromagnetic radiation nature of the antenna structure, these edges produce diffracted fields that can affect the performance of the co- as well as the cross-polarized fields of the antenna. This is of great importance when working with highly pure polarized elements for applications that require low cross-polarization. The expansion of an equivalent current model is proposed where the antenna element can be expressed at a distance from the edges and the diffracted fields generated from such edges are calculated from these equivalent currents. Every element position over the ground plane will generate a theoretical equivalent current that would radiate the diffracted fields, which then contribute to the overall array pattern. This work shows a successful implementation of the proposed technique and how this can be combines with finite element method (FEM) analysis in order to predict the radiated fields

from different element positions providing an advantage over resource hungry simulations. This proves to be an effective tool by reducing the calculation time substantially for scalable applications where the phased array can be over thousands of elements and extremely difficult to gather resources to produce a predicted pattern.

Chapter 1

Introduction

1.1 Motivation

A phased array antenna consists of a number of radiating elements spaced out in some lattice configuration and fed by variable attenuators and phase shifters or time-delay controls. This allows for a coherent summation of the elements' radiation patterns to form a beam that can be electrically shaped and steered to certain angles while having a fixed aperture [1]. Since the 1950s, phased array radars (PARs) have been used for military surveillance with the ability to detect multiple targets from many directions [2]. As the development of radar technology progresses, the potentials for PAR applications become far more attainable. The development of technology in computer processing and electronically controlled attenuators and phased shifters as well as analog to digital converters grants rapid beam steering and different beam shapes. This capability of rapid scanning is now of special interest for weather and air surveillance applications to perform multiple functions in one radar unit with fast temporal resolution [3].

PAR technology, as that shown in Figure 1.1, continues to be a growing interest in the weather radar community due to the overcoming of limitations
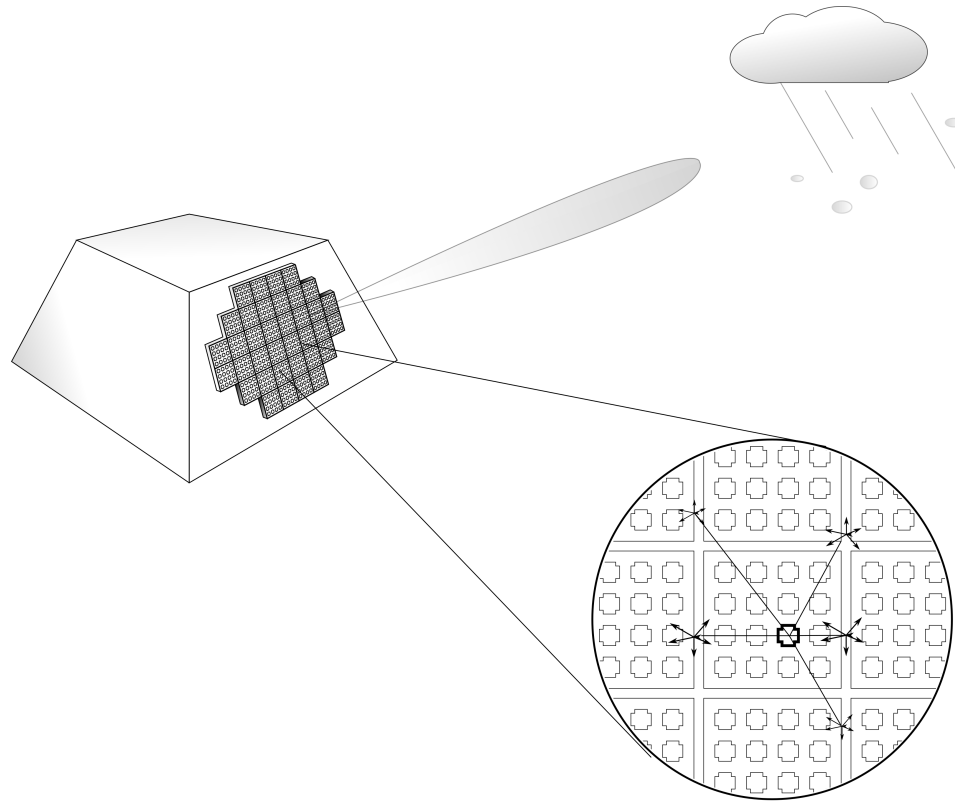
Figure 1.1: Sketch of a PAR with electronic beam steering. The PAR is composed of an arrangement of subarrays, which introduces internal gaps between them.

that mechanically steered radars have. Mechanically scanned radars have high operational costs and disadvantageous reliability due to the limited operational units, which is usually a single unit or transmitter. Furthermore, they are constrained by sweeping the beam through a specific elevation angle for each revolution with slow update times of about four minutes or more due to the size and weight [3]. Alternatively, PARs provide much better reliability due to the number of operational transmitters and high temporal resolution (< 1 min) and dynamic flexibility for diverse scanning modes. Subsequently, in the past 10 years, PAR technology has been used for dual-polarized atmospheric applications, where the system typically will transmit two orthogonal com-

ponents; one component in horizontal (H) polarization and the other one in vertical (V) polarization. Nonetheless, dual-polarized PARs for polarimetric weather applications require high polarization purity (-20 to -40 dB) and an excellent mismatch between the co-polar patterns (< 0.1 dB) of both polarizations for accurate measurements when operating various polarization modes [3], [4].

Typically for dual-polarized PARs, one waveform generator is operated and the signal is divided and distributed to each V- and H-pol port across the array. To transmit and receive the waveform signals, analog transmit and receive (T/R) module architectures, consisting of high-power amplifiers, low-noise amplifier receivers, phase shifters, and attenuators are integrated and placed immediately behind the antenna element terminals. With continued evolution in PAR architecture and technology, waveform generation functions can now be placed either behind subarrays or every individual element [5]. This "holy grail" of PAR technology, other-wise known as fully-digital phased array radars have more significant beamforming flexibility, bringing forth the multi-function phased array radar (MPAR) as a vision to implement both ground-based weather and air traffic surveillance [6]. Digital beamforming with the use of a fully-digital phased arrays allows for simultaneous tracking of multiple types of targets and faster update times. This brings an interest in operating PARs to the individual element level with the ability to selectively illuminate the aperture at arbitrary locations of the array for multiple scanning strategies and beamforming techniques [5]. Therefore, adding to the demand for high-performance radiating elements to have desired performance requirements down to the element level.

Having such strict radiation requirements for cross-polarization purity and

scanning capabilities, leads to challenges in antenna element design. When designing for high isolation of up to 30 dB or more between polarization ports, antenna losses in the form of spurious radiation can significantly impact the isolation between H and V field components. This is measured as cross-polarization fields. It is well known that antenna elements produce spurious radiation due to imperfections in the radiator and feeding structures. In addition, surface waves contribute to cross-polarization degradation, especially when placed over a flat conductor that usually contains a dielectric surface, adding conductor and dielectric losses in the form of spurious radiation [7]. This unintended radiation, as well as intended radiation produced by the antenna source, strikes discontinuities in the ground plane and produce diffracted fields that also affect the cross-polarization and sidelobe levels of the array. Nevertheless, PARs are composed of linear or planar array configurations with antenna elements usually spaced in rectangular lattices and a flat ground plane to shield the backend of the radar system from the antenna radiation. Therefore, this conductive sheet located between the antenna elements and the backend architecture exposes this spurious radiation to discontinuities where diffracted fields are generated.

Overall, diffraction fields are dependent on many factors that are present in a phased array antenna. Space and surface waves produced by different antenna elements strike the edges and produce diffracted fields based on the wedge geometry and the amplitude, phase, and polarization of the incident wave generated by the radiating element source. Therefore, the location of the element with respect to the edges is a critical factor as well as the radiation characteristics determined by the type of antenna element. Furthermore, since diffracted fields are a local phenomena that interacts with the antenna.

These interactions cause changes in its S-parameters, frequency response, and impedance. All these effects translate to changes in mutual coupling between the elements, especially those closer to the edge.

Little to no work is done to predict the behavior of diffraction phenomena in an array environment and how the performance is affected. The impact of edge diffracted fields on the antenna element performance and the overall scanning performance of dual-pol PARs is mainly addressed. The diffracted fields are analytically approximated and would prove to be a helpful tool for PAR design and integration in multiple applications, including weather surveillance. Nonetheless, this is more true for larger-scale radar systems that contain multiple panels that introduce a large number of discontinuities throughout the antenna aperture.

1.2 Problem Statement

As microwave component technology becomes more affordable for phased array systems, the weather radar community has brought their attention to the use of agile electronic beam steering for meteorological measurements [8]. However, with the added dynamic capabilities of electronic scanning and shaping of the beam, phased array antennas face many design challenges. Typical desired performance requirements, e.g., in weather applications, are: wide-angle scanning, narrow beamwidth, high-gain, low sidelobe levels (SLL), very low co-polarization mismatch and low cross-polarization levels throughout the whole scanning range [3], [9]–[11].

For weather radar, accurate measurements of hydrometeor and severe storm formations are of utmost importance. PARs offer high temporal resolution (< 1 min) and dynamic scanning modes that reveal more details of the scanned

volume in comparison to a conventional dish antenna radar. Furthermore, to obtain detailed description of the shape of hydrometeors and other objects that would compose a storm, polarimetric weather radars transmit and receive horizontally (H) and vertically (V) polarized electromagnetic waves. With dual-pol capabilities, different polarization modes can be used to analyze the covariance between backscattering H and V components from particles. Therefore, polarimetric weather radars can either operate in alternate modes, such as alternate transmit and alternate receive (ATAR), or hybrid modes, like simultaneous transmit and simultaneous receive (STSR). STSR is by far more versatile and easier to algorithmically implement due to no lag between signals providing more accurate measurements [12]. However, it is more sensitive to perturbations in the polarization states produced by errors in the radar system. Consequently, these errors will affect the measurement's accuracy [4].

An important polarimetric measurement parameter that helps determine a hydrometeor's shape is differential reflectivity (Z_{dr}). It is produced by the ratio between the backscattered power estimates in both H and V polarizations. To successfully obtain this parameter, in STSR for instance, measurements need to have a bias in differential reflectivity (ΔZ_{dr}) of no greater than 0.1 dB, meaning cross-polarization levels of less than -40 dB [4]. However, as previously mentioned, perturbations in the radar system can translate to errors in the measurements. Therefore, the design of antennas with high polarization isolation is necessary and requires reducing any small contributions to cross-polarized fields into the system's performance.

Small spurious radiation in the array can significantly impact the cross-polarization when an isolation higher than 30 dB is required. Spurious radiation may be found in the feeding mechanism of the antenna element, as well

6

as conductor and dielectric losses in the form of surface waves. In addition, radiation produced by the antenna element strikes the edges of the ground planes where diffraction phenomena is produced. These diffracted fields will impact the cross-polarization levels of the antenna. Therefore, achieving low cross-polarization (< -40 dB) for phased array technology is extremely difficult, especially when scanning at nonprincipal planes, e.g., the diagonal plane (D-plane).

Diffracted fields from a single element may be found around its perimeter, including neighboring panels in a larger-scaled phased array antenna, where panels can be added to expand the size of the antenna aperture. To predict the behavior of the PAR accurately, the system can be simulated. However, the amount of resources needed to calculate the fields of a large number of elements and discontinuities in the ground plane is exorbitant. Therefore, an analytical model that predicts diffracted fields in the array is proposed to evaluate the overall performance of the array that would include cross-polarization levels for dual-pol applications. However, little insight is found in literature of the effects that diffraction at the edges have on the cross-polarization pattern of the antenna and overall array performance. This research hypothesizes that one of the main contributors to cross-polarization degradation in phased array antennas is produced by diffraction phenomena. The extent to which spurious radiation affects the performance of a dual-polarized array is explored.

1.3   Proposed Research

In this research, the components that contribute to the contamination of cross-polarized fields in an array antenna are evaluated. An overview of desirable antenna element prospects is taken into consideration. A study into the an-

tenna element structures can give a better understanding of their radiating properties and how they fit into weather radar applications. With an understanding of possible influences in the polarization errors of an antenna element, a deep study is done as to how the element behaves when introduced into a finite edged ground plane. The uniform theory of diffraction (UTD) and equivalent current method are used to evaluate the effects that the edges have on the radiation characteristics of different radiating elements. This will provide an analytical model for evaluating the cross-polarization of an array that includes diffraction.

Array scanned pattern performance will greatly be influenced by the edge effects. Therefore, quantification of the influence in scanned patterns should be possible with the analytical model and will answer questions about the behavior of edges in an array. This model will take into account the geometrical aspects of the ground plane where the antennas are placed with respect to every point of diffraction. Hence, an expansion can be made to larger-scaled arrays with multiple diffraction points inside of the aperture, i.e., internal gaps between panels of the array.

When considering the scattering from an illuminated conductive plane, two dominant mechanisms are to be considered, reflected and diffracted fields. These fields are determined using methods such as geometric optics (GO) and the geometrical theory of diffraction (GTD), respectively. An extension to refine the GTD, was the UTD and the equivalent current method. The equivalent current method models every diffraction point as intervals along a half-plane edge as an equivalent magnetic or electric current and proves to be useful to predict the pattern for cross-polarized field components at principal and nonprincipal planes.

To validate the results of the new analytical model, which incorporates the techniques mentioned, a set of measurements will be made for various antenna elements. The model predicts individual patterns based on their placement along the ground plane and differentiates between contributions from effects such as mutual coupling and others that might have an impact on cross-polarization. Having a clearer insight as to how diffracted fields play a role with the radiation characteristics of an antenna source, opens a discussion about how to deal with edge effects.

A direct relationship between the geometrical aspects of antenna placements for phased arrays plays a role in how diffraction will interact with the antenna's performance. This will be evaluated by placing several elements along with different positions of a modifiable ground sheet. A linear array can be placed asymmetrically from the sheet to see its performance variation. Also, the location of the element with respect to other neighboring elements and their distance with relation to the edges can change the mutual coupling parameters and this can be experimented with how edge effects can affect these parameters.

Since UTD can assume that the incident fields are at far-field, it is simple to produce resulting far-field patterns in all planes by combining finite element method (FEM) results from antenna elements and with the diffracted fields around all points of incidence. The advantage of having a dynamic analytical model is that it can be expanded to calculate array patterns with details such as multiple panels with a certain distance between them. Therefore, the array can be evaluated with different configurations of panels for a large-scale PARs.

1.4 Contribution

The main contribution of this research is an analytical model that predicts the perturbation that edge diffraction has in the overall radiation pattern of a phased array antenna, including the cross-polarization contamination. Furthermore, a much clearer insight as to how electromagnetic waves behave under the effects of diffraction is drawn, and a much better understanding of what changes in impedance and mutual coupling take effect on each antenna element spaced around the array relative to the edges. The model is scaleable for larger structures with multiple panels, making it an effective tool to combine with other numerical methods such as FEM, PO, etc.

The studies done take into account different element types with different ground plane sizes in the element level. Analytical experiments include different locations and array sizes to further complete a study that can be expanded to larger scale structures. Included in these experiments are the analytical quantification of edge effect contributions to element pattern's cross-polarization and how it affects the array performance. This model can then be extended to be applicable to expandable arrays with multiple tiles and gap separations between them and how these separations impact the performance of the array.

A better prediction of the array pattern behavior is achieved with experiments on element frequency response, element patterns based on location over a ground plane, and the analytical model for predicting the effects of diffracted fields on the radiation pattern of each individual element of the array. With this model, it is shown that a more accurate representation of a phased array performance is possible by including edge effects into the calculations. Making this analytical model valuable for in-detailed predictions of

high-performance PARs.

1.5   Literature Review

In the topic of antennas and electromagnetic theory, diffraction is the process of spreading of a wave when incident upon an edge, corner, or vertices of boundary surfaces. It has been discussed so far that diffraction of the edges of the ground plane and the effects it has on the far-field radiation pattern of an antenna are due to the presence of the discontinuities of a finite ground plane [13]–[23]. These effects become more predominant at edges where the dimensions exceeds a wavelength. Diffracted fields, therefore, depend on the edge's geometry (straight or curved) and the amplitude, phase, and polarization of the incident wave. The interest of this work comprises on the modeling of diffraction from a finite ground plane. The geometrical theory of diffraction (GTD) was introduced to extend on geometric optics (GO) and was introduced by Keller in the 1950s [16], [24]. GO has been often used to determine the distribution of light intensity as a ray tracing technique that accounts for direct, reflected, and refracted rays. However, it does not account for the local phenomena of diffraction, which is analogous to the laws of reflection and refraction.

In the same way that the GO pattern is the sum of all the rays (direct, reflected, and refracted) at the point of observation, in GTD, a field is associated with each diffracted ray and the total field is then the sum of all rays at that point [25]. The GTD treats electromagnetic waves as rays and does not require integration of currents as in physical optics (PO) by use of dyadic diffraction coefficients, similar as to how reflected rays are calculated by reflection coefficients. The treatment of electromagnetic waves in the form of rays helps

simplify for high-frequency problems, since the spreading of waves is the same as if they where propagating rays from the point of incidence. However, GTD, in its original form, exhibited singularities near its ray-shadow and caustic regions. Therefore, to compensate for these discontinuities, a uniform asymptotic high-frequency method is necessary to smoothen the transition between these regions [26].

A widely popular approach to correct for the singularities near the boundaries is the uniform theory of diffraction (UTD) [15]. The use of the UTD in modeling the effects of diffraction in antenna patterns is fairly popular since proven to be accurate [27]. The application of UTD has been used at the aperture of antennas as well as antennas placed on finite ground plane structures [28]. When finite ground plane edges are close enough to the radiating structure of an antenna UTD can accurately represent the effects that local diffraction has on the far-field patterns in both principal (E and H) planes [29]. After being modeled in an infinite ground plane structure, the study shows how the amplitude of the pattern changes as the antenna is introduced to a finite ground plane due to edge diffraction. The use of UTD was also introduced for the calculation of radiation patterns to better predict the diffracted fields including backlobe and cross-pol radiation of the microstrip patch antenna (MPA) based on the fields generated by a cavity model and modal expansion [14]. This suggests that a combination of UTD and equivalent current methods are appropriate to predict the far-field radiation pattern of different antenna elements, including the MPA. The study also suggests that with the use of corner diffraction coefficients, the diagonal plane can be predicted [30].

An equivalent current method (ECM) was developed to make corrections for inaccuracies of diffracted field singularities and inaccuracies near caustic

regions, specifically for curved edges [18], [31]. The method involves evaluating multiple points of diffraction along the edge of a conductive strip or ground plane and modeling the total diffracted fields by using equivalent magnetic or electric current along the rim of the edges. The farfield patterns of the induced equivalent currents in the ground edge have been derived using vector potentials [32]. The induced equivalent currents on the ground plane edges are estimated first and the total radiated fields are computed based on the induced currents in the ground edges and the equivalent sources of the antenna aperture. The gain was shown to vary widely, increasing the radiation intensity as the ground plane size increases by preventing radiation in the shadow region. The effects of the ground plane size on the radiation pattern, gain and axial ratio have been studied using a moment methods analysis [33]. For each cavity mode there is an optimum ground plane radius and thickness that maximizes gain. The ground plane size for each mode is shown to have an effect on its radiation pattern for optimum gain and axial ratio. This implies that it affects higher-order modes in rectangular MPAs, consequently affecting the cross-polarization levels of dual-polarized antennas. The accuracy of the models, however, are questionable for ground plane sizes of less than one free space wavelength.

Not only the size but also the thickness of the ground plane may affect performance of the mounted antenna due to edge diffraction [17]. Radiation conductance is also computed to be much less than it being with an infinite ground plane [34]. The conductance determines the input impedance of the patch, causing a change in the position of feeding of a 50 ohm match, therefore, it does make sense that for dual-polarized MPAs, the effects of the ground plane reflections will affect port isolation, making the inclusion of edge effects

into the calculation of antenna performance critical.

Limited studies have been done of the effects edges have on dual-polarized and low cross-pol antennas [13], [35], [36]. The effects of diffraction in a linear array of dual-polarized wideband elements that contain thick substrates are shown [36]. The change in ground place size can be appreciated by the changes in ripples in the co- and cross-pol patterns of the antenna. Copper pillars are added below the antenna source to suppress such ripples caused by ground edge effects and shows an improvement in cross-pol especially in the H-plane. However, for large arrays of more complicated structures for high-performance, where devices are located in the back panel, these approaches seem impractical.

An analysis that includes the effects of finite ground planes in microstrip patch antennas is shown in [21]. However, there is no good accurate agreement, especially in the backlobe radiation. This is due to the lack of diffraction analysis. The utilization of UTD to account for the finite ground plane edge diffraction does provide a more accurate agreement [37]. The effects of ground plane sizes on the radiation pattern of a patch are also shown in [38] and a solution to reduce its effects is demonstrated increasing the gain at broadside. Cross-polarization level increases are shown with increasing ground plane size [36]. This also takes into account thick substrate antennas for broadband applications where surface waves tend to be stronger. To reduce the cross-pol of the array, the ground plane size has to be reduced. However, this is not possible for low-sidelobe and wideband array applications. A solution to improve the degradation of axial ratio of circularly polarized antennas by making EBG modifications to the ground plane are presented in [39]. This solution, however, is complicated to model accurately and design.

In regards to phased array antennas, as the array is larger, all elements

14

will see a uniform contribution in the element patterns [22]. However, when it is not large, elements do see differences in patterns due to the effects of the edges of the array that have to be accounted for especially when dealing with low-cross polarization levels. Ground planes where the microstrip array or other structures are mounted, can diffract surface and space waves [23]. The diffraction effects shown in [35] pointed out the effects of a finite ground plane on low cross-pol and wideband antennas. There are also cases where the ground plane is distorted and changes in shape to reduce the effects of the edges [39]. They show that for thicker arrays, the gain is reduced, meaning the efficiency is lost due to surface waves and this could greatly impact the cross-pol levels. This is to be considered when arrays are mounted on big tiled structures, where there should be a metallic structure in the back. Effects from gap separations between tiles are a known possible issue of diffraction for embedded elements, affecting the scanning of the array [13].

For the modeling and measurement of microstrip patch arrays, a more accurate representation of the diffracted fields and edge effects have to be implemented if we want to do rigorous calibration of high-performance, low-cross pol, wide bandwidth, and wide angle scanning arrays. This impact in the performance of phased arrays due to diffraction is due not only to external ground plane edges, but also internal gaps between subarrays [13]. Based on the literature found of external edges, if the edges are far enough from elements and the gaps are to have a significant separation between sub arrays, there can be additional significant degradation in element patterns same as with external edges. This is to be an important observation in dual-polarized elements in a large array, since due to fabrication limitations they have to be fabricated and tiled in subarray components. Quantification of grating lobe effects due

to these gaps has been shown in [40].

Added discontinuities and therefore sources of diffraction that can compromise the performance of the elements throughout the array has been shown to degrade cross-polarization levels even further than outer edge effects would to a large array [13]. Another sensitive mechanism in phased array antennas that can be affected by diffraction phenomena is the mutual coupling between array elements [41]–[45]. It is shown that edge diffraction should be added to computations to represent the mutual coupling in an array more accurately where the edge is exposed.

The level of diffraction effects experienced by the radiation patterns and impedance of the antennas in an array is mainly due to the size of the ground plane and the location of the element source [13], [23], [35]. Co-polar patterns experience components added in phase to the pattern causing ripples in both broadside and the back radiation. It has also been shown that these effects are even more noticeable in polarization isolation in the axial ratio of circularly polarized antennas [39] and of low cross-pol dual-polarized elements reducing from 10 to 20 dB in the polarization isolation [13], [35]. Changing the size of the ground plane, where the antenna element is placed in the center, the cross-polarization contamination increases and changes shape as it gets larger. The isolation of the between ports, however, seem to improve as the ground plane size is increased because of the reduction in reflections from the edges. Nonetheless, the cross-polarization isolation is decreased as the ground plane is increased.

There is more work needed in analyzing what these edge effects do in an active array environment. How the asymmetrical contributions of diffraction actually contribute to the cross-pol of individual embedded elements and how

internal gaps play an additional role in the degradation of mutual coupling and radiation patterns. Also, to quantify edge diffraction using current field modeling techniques, shows the significance of different internal gap separations and its influence in the performance on active phased arrays.

1.6 Dissertation Overview

The dissertation is organized to present the diffraction impact on dual-polarized phased array antennas. In Chapter 2, PAR requirements for polarimetric weather radars are reviewed. A clear explanation as to what are the performance challenges for PAR and the design considerations for low cross-polarization antennas are presented. The theory that predicts the impact of edge diffractions in the overall radiation pattern of an antenna is discussed in Chapter 3. The diffraction theory with its uses and limitations is also presented. This includes the "two-point diffraction", equivalent current methods, and the proposed utilization of these tools for the proposed analytical method to predict cross-polarization fields. In Chapter 4, the impact of edge diffraction is expressed with the use of these tools and numerical simulations to show how diffracted fields potentially affect the array's performance. The tools mentioned in these chapters are then applied to specific antenna elements in Chapter 5 where the proposed analytical tool is used to validate the antenna element patterns for different scenarios. Several experiments based on numerical simulations are presented in order to validate these tools to be implemented in phased array environments. Detailed effects of diffraction on an individual element level are shown along with how these effects change with respect to ground plane size and the location of the element. Nonetheless, the addition of multiple elements for different array sizes are introduced to look

deeper into how edge effects contribute to impedance, mutual coupling, gain and cross-polarization measurements on different element types. Finally, an epilogue in Chapter 6 will summarize the findings and explores on possible methods to mitigate diffraction as well as suggestions on what the next steps would be to further improve this study.

Chapter 2

Fundamentals

2.1 Introduction

This chapter will present the requirements for polarimetric weather radars and challenges. Starting with the current operational challenges that conventional weather radars, which usually are comprised of reflector antennas, face for dual-polarized polarimetric weather measurements. A brief explanation of dual-polarization operation and techniques are discussed to provide an understanding of what are the requirements for different type of operational configurations. Polarization definitions are then defined for the application of dual-pol PAR and what are the trade-offs in designing antennas for PAR. Since the main study in this work will be the impact diffraction has in overall phased array antenna performance with emphasis in polarization performance, this chapter's focus is in design challenges to achieve low cross-polarization.

2.2 Polarization Requirements for Weather Radars

Weather radars are used to detect and measure rain intensity as well as the hydrometeor contents in the volume. Accuracy is of the highest interest for meteorological measurements. In order to obtain adequate measurements, a

weather radar antenna must be capable of producing high enough gain for receiving sufficient power from reflected signals, low sidelobes to mitigate any type of clutter or contaminated signals from other sources, as well as narrow beamwidth for good spacial resolution. Besides these general requirements for radar, it is of general interest that the system be able to identify different weather patterns and hydrometeor detection.

Efficient hydrometeor classification is dependent upon received backscattered components of a transmitted wave. Single polarized weather radars would use sensitivity metrics, like reflectivity (Z in mm^6m^{-3}) from the backscattered wave in order to determine characteristics of the scanned phenomena. Reflectivity is the amount of power that is backscattered from precipitation after being hit by a transmitted wave. A high-reflectivity measurement can indicate that the volume contains a large amount of rain drops, which can translate to a large amount of rain rate, or it can indicate the volume contains large drop sizes that can generate large backscattering to the receiver as well. The same can be said of other hydrometeors, such as hail or snow, which generate a much higher backscatter reflection than water would.

Besides the ability to measure rain fall, in order to detect and identify content characteristics in a volume, such as the amount and shape of water droplets, polarimetric measurements are extremely useful. Polarimetric weather radars are generally composed of an antenna with dual-polarized capabilities and a system for processing the signals to be transmitted and received in two well isolated channels for horizontal (H) and vertical (V) polarizations. The use of two electric field components opens a wide variety of operational modes and polarimetric variables that provide a significant amount of metrics to detect and analyze weather radar phenomena. Therefore, the received elec-

tric field components for both polarizations will be dependent on the transmitted wave upon an object and the backscattering produced by it. The scattering can be represnted by the following matrix:

$$\mathbf{S} = \left[\begin{array}{cc} s_{hh}(\hat{\theta}, \hat{\phi}) & s_{hv}(\hat{\theta}, \hat{\phi}) \\ s_{vh}(\hat{\theta}, \hat{\phi}) & s_{vv}(\hat{\theta}, \hat{\phi}) \end{array} \right] \qquad (2.1)$$

where the s_{hh} and s_{vv} are the co-polarized backscattering coefficients and s_{hv} and s_{vh} would represent the cross-coupling components introduced mainly by depolarization from the scattering object. These, as well as cross-polarized fields that are inherent in the design of the antenna would add to any type of biasing errors in polarimetric variables.

One such polarimetric variable, very much relevant to the motivation of this research, is the differential reflectivity (Z_{dr}) seen in (2.2). This parameter provides important physical information of the scattering object that helps identify the detection of water content in a radar resolution volume.

$$Z_{dr} = \frac{\langle |s_{hh}| \rangle^2}{\langle |s_{vv}| \rangle^2} \qquad (2.2)$$

In order to obtain this information, a signal is transmitted and received in both polarizations. The ratio between the backscattered signal's power from a H-polarized wave (Z_{hh}) and the backscattered power from a transmitted V-polarized wave (Z_{vv}) provides information about the shape of the droplets in the contained volume. As the droplets fall they can have an oblong shape based on their size and weight. This, for example, will provide a larger return

21

for backscattered wave signals in the H polarization rather than in the V polarization. These indicators are also useful in the overall detection of what is water.

With advancements in technological efforts to provide accurate measurements, polarimetric weather radars, depending on the versatility of the system design, may use a combination dual-polarized polarization transmission and reception modes. Mainly, these modes are composed of a combination of alternate or hybrid transmission and reception modes. Alternate transmit and alternate receive (ATAR) mode performs both transmission and reception of the signals in both H- and V-polarizations alternately, while hybrid mode may transmit or receive both simultaneously, such as simultaneous transmit and simultaneous receive (STSR). However, antenna structures in practice do not purely radiate in one polarization and some form of contamination occurs as the wave is depolarized by imperfections and the nature of the particular antennas radiation mechanism. Hence, contamination between channels is a common occurrence that can be mitigated to some extent by the design of more purely polarized radiating elements or biasing correction of the signals [8].

Requirements for such polarization modes depend on the use of parameters such as Z_{dr} and depend on the meteorological measurements needed to detect and classify hydrometeor's shape, size, density, and composition. Z_{dr} measurements vary from smallest particles like drizze and larger rain drops between 0.1 dB to about 3-4 dB. As Z_{dr} increases, biasing errors are more tolerable. However, tolerances for lower Z_{dr} measurements require a bias error of no more than 0.1 dB. To attain this tolerance level, peak cross-polarization levels of -20 dB for ATAR and -40 dB for STSR with respect to the co-polarizationhave

been determined [46]. In order to achieve these low levels of cross-polarization, effective calibration techniques and error correcting algorithms need to be implemented.

2.3 Polarization Definition for Dual-pol Phased Arrays

As PAR technology has evolved, the use of electronically steered beam has become more attractive to polarimetric weather radar applications. With the advantages in two-dimensional electronic scanning of the beam comes challenges when accurate polarimetric radar measurements are required. Unlike a dish antenna radar, which has a fixed beam and rotates mechanically, ground-based PAR are physically fixed and as it electronically steers the beam in two dimensions, its properties change. Theoretically, an idealized formulation for a polarimetric PAR is in the form of two crossed dipoles [8]. To understand the impact that polarization has on polarimetric PAR, formulations are made to relate the electric fields of the individual array element with the scattered components of hydrometeors. The electric field for the radiating element is then based by a dipole moment $\vec{M}$ and is given by:

$$\vec{E}_q(\vec{r}) = -\frac{k^2 e^{-jkr}}{4\pi\epsilon r}\left\{\hat{a}_r \times \left[\hat{a}_r \times \vec{M}_q\right]\right\} \tag{2.3}$$

where q denotes the dipole 1 or 2, which lie along $\hat{a}_y$ and $\hat{a}_z$ respectively, as seen in Figure 2.1. The dipole moment $\vec{M}_q = \hat{a}_q A_q e^{j\Phi_q}$, the has an amplitude A_q and phase Φ_q.

The transmitted electric fields by the antenna are polarized in the y or z directions. Both of these antennas will have spherical components $\hat{a}_\theta$ and $\hat{a}_\phi$ as follows:
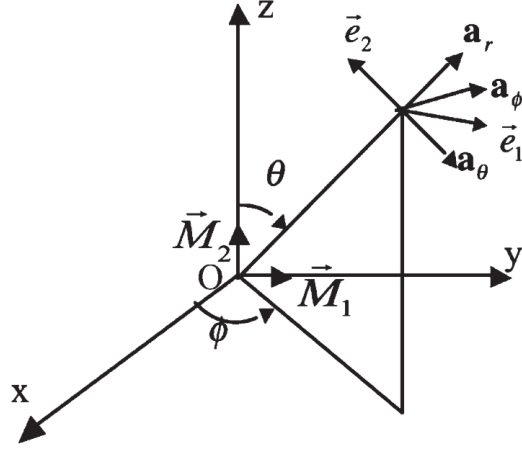
Figure 2.1: Spherical coordinate system of the electric fields for the orthogonal dipole moment $\vec{M}_1$ and $\vec{M}_2$ [8].

$$\vec{E}_q(\vec{r}) = \hat{a}_\theta E_{\theta q} + \hat{a}_\phi E_{\phi q} \tag{2.4}$$

Hence, the transmitted fields by each source will be then dipole moment for the horizontal dipole ($M_1 \hat{a}_y$) and the vertical dipole ($M_2 \hat{a}_y$) in their respective cross products from (2.3) will then be a product of the electric field and their vector identities [8].

$$\vec{E}_1 = E_{t1} \left[\hat{a}_y - (\hat{a}_x \sin\theta \cos\phi + \hat{a}_y \sin\theta \sin\phi + \hat{a}_z \cos\theta) \sin\theta \sin\phi \right]$$
$$= E_{t1}\vec{e}_1 \quad (2.5a)$$

$$\vec{E}_2 = E_{t2} \left[\hat{a}_z \sin^2\theta - (\hat{a}_x \cos\phi + \hat{a}_y \sin\phi) \sin\theta \cos\theta \right] = E_{t2}\vec{e}_2 \tag{2.5b}$$

where

$$E_{tq} = \frac{k^2 e^{-jkr}}{4\pi\epsilon r} M_q \tag{2.6}$$

24

The characteristics of the H and V waves from a PAR as a function of the beam's direction (θ,ϕ) is then corresponding to the projections of the dipoles and generates the intensities along $\hat{a}_h$ and $\hat{a}_v$ directions. These projections toward a local H and V polarizations are formulated in the **P** projection matrix. Hence, the electric fields generated by the dipoles are projected into the local H and V directions as follows:

$$\hat{a}_h \cdot \vec{e}_1 = \hat{a}_\phi \cdot \vec{e}_1 = \cos \phi \tag{2.7a}$$

$$\hat{a}_v \cdot \vec{e}_1 = -\hat{a}_\theta \cdot \vec{e}_1 = -\cos \theta \sin \phi \tag{2.7b}$$

$$\hat{a}_h \cdot \vec{e}_2 = \hat{a}_\phi \cdot \vec{e}_2 = 0 \tag{2.7c}$$

$$\hat{a}_v \cdot \vec{e}_2 = -\hat{a}_\theta \cdot \vec{e}_2 = \sin \theta \tag{2.7d}$$

$$\mathbf{P} = \begin{bmatrix} \hat{a}_h \cdot \vec{e}_1 & \hat{a}_h \cdot \vec{e}_2 \\ \hat{a}_v \cdot \vec{e}_1 & \hat{a}_v \cdot \vec{e}_2 \end{bmatrix} = \begin{bmatrix} \cos \phi & 0 \\ -\cos \theta \sin \phi & \sin \theta \end{bmatrix} \tag{2.8}$$

$$\begin{bmatrix} E_{ih} \\ E_{iv} \end{bmatrix} = \mathbf{P} \begin{bmatrix} E_{t1} \\ E_{t2} \end{bmatrix} \tag{2.9}$$

This matrix shows that a PAR produces a cross-polar component as a product of the projection to the local H ($\hat{a}_h$) and V ($\hat{a}_v$) coordinates in terms of (θ,ϕ). This projection is then used to convert the wave that is to be incident upon the precipitation medium and expressed in (2.9). With the existence of

a medium that the electric field will be backscattered from, a backscattering matrix will produce the electric fields $\vec{E}_r$ that would be received by the PAR. The complete representation of the backscattered fields that would be received at the radar would be:

$$\begin{bmatrix} E_{r1} \\ E_{r2} \end{bmatrix} = \frac{e^{-jkr}}{r} \mathbf{P}^T \mathbf{S}' \mathbf{P} \begin{bmatrix} E_{t1} \\ E_{t2} \end{bmatrix} \tag{2.10}$$

where $\mathbf{P}^T$ is the transpose of the polarization projection matrix $\mathbf{P}$ and $\mathbf{S}'$ is the backscattering matrix from the hydrometeor and incident fields $\vec{E}_i$ including all of the propagation effects. Hence, this equation (2.10) is the expression for the received electric fields at each polarized dipole radiator in a PAR including all polarimetric effects [8].

It is common practice to use linearly polarized elements for weather applications, specifically for dual-polarized PARs. As, previously mentioned the projection matrix provides the polarization of the field in space with regards to spherical coordinates, showing the dependency of polarization with scan angle. However, since a PAR is meant to scan at principal and nonprincipal planes, the adequate co- and cross-polarization expression based on Ludwig definitions needs to be used in order to accurately determine the cross-polarized fields when steering the beam [47]. It is shown, that the adequate definition used for the projected fields depends on what the antenna source is and what cartesian plane it lies on.

26

2.4 Polarization Challenges in Phased Array Antennas

With the added capabilities of beam steering, many challenges have to be addressed over a standalone conventional reflector antenna. A PAR will be composed of multiple radiating elements compared to a conventional radar, where a number of transmit and receive (T/R) modules are distributed along the radiating aperture. Due to the increase in radiating elements and T/R channels, a big roll in the design and fabrication of these systems involves reducing the costs of implementation as much as possible while still attaining a level of quality performance. Technical attributes such as scanning performance can be translated into several contingencies such as the radiating elements design structure and how this interacts with the overall composed structure of the phased array antenna. This includes the presence of neighboring elements, the materials and platforms on which they are built on, and the unwanted spurious radiation generated by such. Hence, the arrangement of these elements and structures play a significant roll on the performance of the overall PAR.

2.4.1 Radiating Elements

One of the main challenges in the design of a PAR is the selection of the appropriate radiating element. Things to pay attention to in the utilization of a radiating element structure is the radiation characteristics, such as directivity, beamwidth, bandwidth, and polarization purity. One of the widely used elements is the microstrip patch antenna. One of the main advantages of MPAs is the ease of fabrication and the ability to obtain high-performance capabilities in a low-profile structure.

The MPA antenna is chosen for its dual-polarized capabilities. Given its

(a) Top view
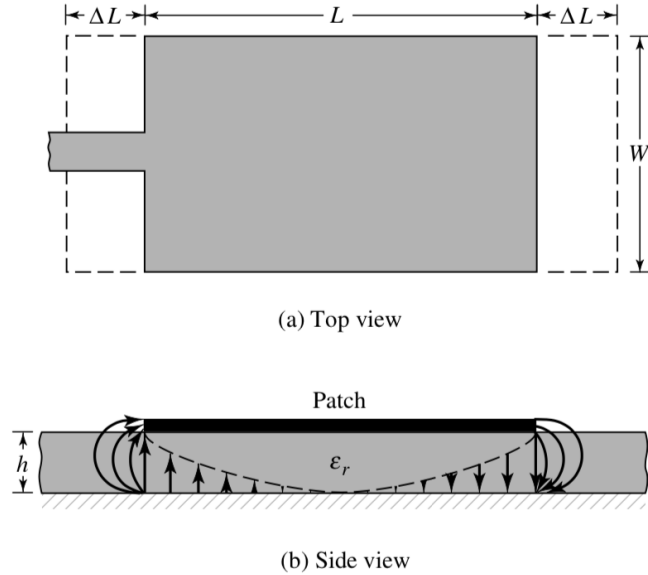
(b) Side view

Figure 2.2: Top view and side view illustrations of the MPA and its radiation mechanism [51].

wide flexibility in design, many feeding techniques are used in order to excite the element in different positions to generate orthogonal polarizations. This can be done with the use of conventional feeding, as seen in Figure 2.2, as well as other coupling techniques such as probe feeding, proximity or aperture coupling [48], [49]. Coupled feeding techniques, shown in Figure 2.3, produce less spurious radiation due to magnetic coupling excitation and can be more suitable for extremely low cross-polarization situations, however design is more complicated [50]. In Figure 2.2(b), the MPA radiation mechanism is illustrated. It shows that the electric fields are perpendicular to the ground plane under the cavity, hence, the electric fields that are theoretically produced are TM modes. The bending of the waves, otherwise called fringing, are caused at the aperture and produce the radiation fields that are added in phase between the two radiating slots.

The resulting radiation pattern of the microstrip patch antenna is then

28
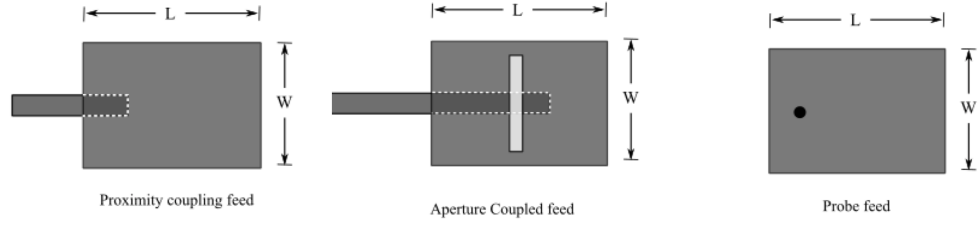
Figure 2.3: Some examples of common feeding techniques for MPAs [51].
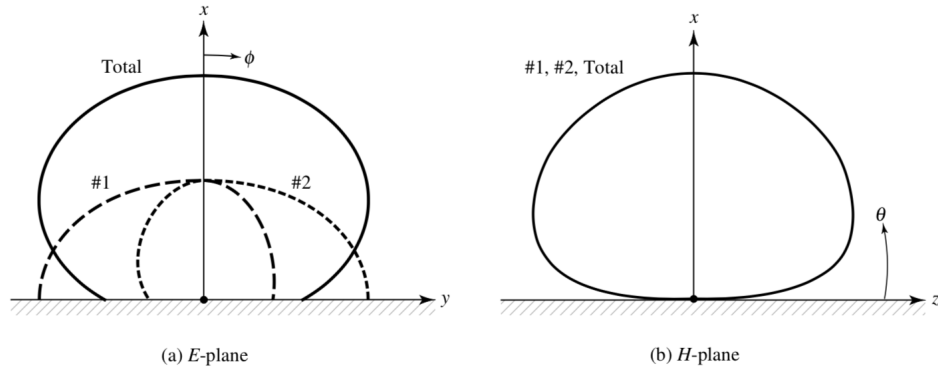
(a) *E*-plane

(b) *H*-plane

Figure 2.4: Radiation pattern for the MPA [51].

shown in Figure 2.4. The E-plane is the radiation pattern cut along the alignment of the electric field's polarization. H-plane is the orthogonal cut to the alignment of the electric fields or along the magnetic field's component. Due to the aperture radiation currents, the case of the MPA two main electric field components are present, E_θ and E_ϕ, and can be calculated in the E- and H-planes respectively. If the polarization is aligned the y-axis ($\phi = 90°$) then the E-plane cut will give the spherical E_θ component and orthogonal to that ($\phi = 0°$) the H-plane cut will contain the E_ϕ component. It is fair to note that the E_ϕ component, since it is orthogonal to the E_θ component and tangent to the ground plane goes to 0, due to image theory. Hence, the electric field in this cut is negligible at the surface. This will be useful in the following chapters when discussing diffraction in this cut.

29

The design of this radiating elements is dependent upon what material properties, like permittivity (ϵ), it is being built on and its thickness h. Depending on the requirements of the antenna performance in terms of bandwidth and efficiency the material properties are chosen (see Figure 2.5). It can be observed that as the material thickness increases, bandwidth increases but efficiency decreases. Furthermore, as the dielectric permittivity increases, bandwidth and the efficiency decreases. The material properties will then determine the dimensions of the patch shown in Figure 2.2, which will be calculated as follows:

$$\epsilon_{eff} = \frac{\epsilon_r + 1}{2} + \frac{\epsilon_r - 1}{2} \left[1 + 12\frac{h}{W} \right]^{-\frac{1}{2}} \tag{2.11}$$

assuming $W/h > 1$

$$W = \frac{1}{2f_r\sqrt{\mu_0\epsilon_0}} \sqrt{\frac{2}{\epsilon_r + 1}} \tag{2.12}$$

$$\Delta L = 0.412 \ h \ \frac{\left(\epsilon_{reff} + 0.3\right)\left(\frac{W}{h} + 0.264\right)}{\left(\epsilon_{reff} - 0.258\right)\left(\frac{W}{h} + 0.8\right)} \tag{2.13a}$$

$$L = L_{eff} - \frac{\Delta L}{2} \tag{2.13b}$$

Having the dimension of the MPA, the bandwidth (BW) can be predicted and approximated using several methods [53]. As an example one of the methods can be calculated by:

$$BW = \frac{16}{3\sqrt{2}} \frac{p}{e_r} \frac{1}{\epsilon_r} \frac{h}{\lambda_0} \frac{W}{L} q \tag{2.14a}$$
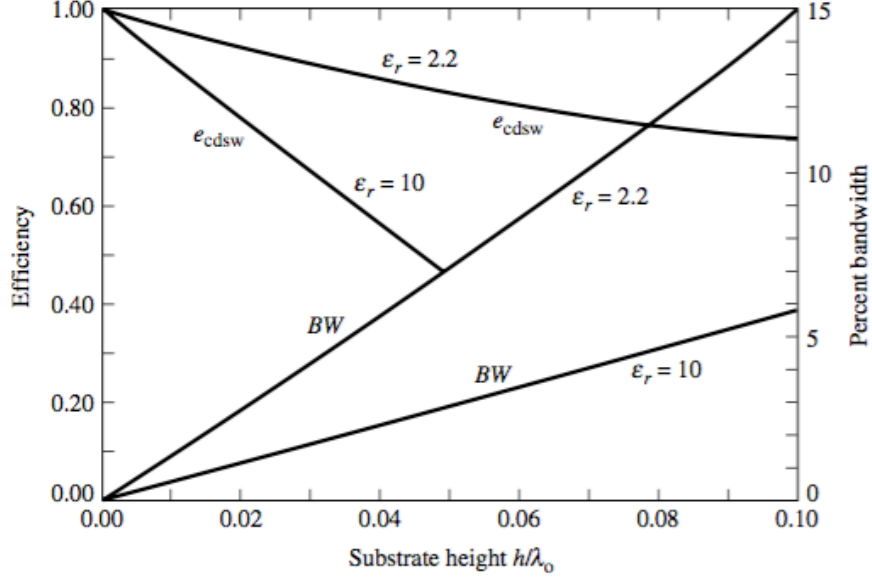
Figure 2.5: MPA efficiency and bandwidth as a function of substrate thickness [52].

$$p = 1 - \frac{0.16605}{20}(k_0 W)^2 + \frac{0.02283}{560}(k_0 W)^4 - 0.009142(k_0 L)^2 \qquad (2.14\text{b})$$

$$q = 1 - \frac{1}{\epsilon_r} + \frac{2}{5\epsilon_r^2} \qquad (2.14\text{c})$$

One of the main advantages for using MPA in this work is the ability to mitigate cross-polarized fields that are being produced by the spurious radiation from the antenna structure including its feeding structure. The antenna's physical and material parameters take an effect on the level of cross-polarization [54]. Besides the antenna structure, projection of fields can also be a generator of cross-pol [47]. In the case there is cross-polarized fields, they will cause a pressence of E_ϕ components in the E-plane where E_θ is predominant and E_θ components in the H-plane where E_ϕ is predominant. In nonprincipal planes, cross-polarization definitions must be taken into account. This is highly impor-
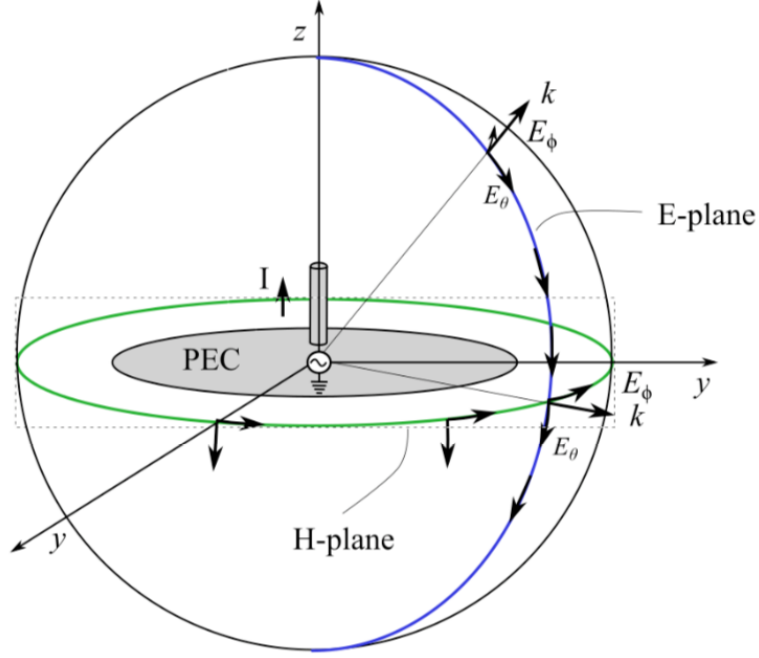
Figure 2.6: Bandwidth calculation method comparison (courtesy of J. Salazar).

tant for PAR applications where the antenna has a fixed coordinate placement and the beam has its own local coordinate for scanning, as discussed before.

Another important radiating element that is used for this study is the quarter-wave ($\lambda/4$) monopole. This element is extremely useful as a study case for diffracted fields. One of the main reasons is that it being wire antenna (a line of current), a monopole, in theory, generates purely E_θ components (see Figure 2.6) along all of the element's radiation projection in space. This, as will be discussed in Chapter 3, will produce equal radiation in the azimuth cut and where hard diffraction is generated on the ground plane. This proves to be a practical design for cross-polarization studies as well, due to the element being of pure polarization and theoretically has an E_ϕ component of 0. In practice then, the cross-polarized fields are solely generated by the element's imperfections, such as the excitation and the presence of edge effects.
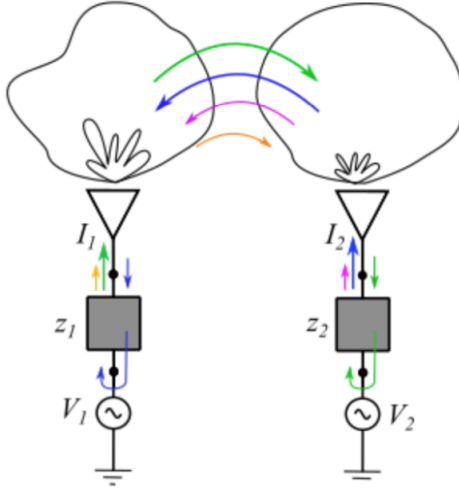
Figure 2.7: Representation of mutual coupling between antenna elements (courtesy of J. Salazar).

2.4.2 Mutual Coupling

Mutual coupling is the electromagnetic interaction between elements when they are in vicinity, as seen in Figure 2.7. The distance between elements will determine the mutual impedance response between the elements at their point of excitation, as shown in Figure 2.8 and can also affect their individual radiation pattern characteristics, as seen in Figure 2.9. This, in turn, will affect the phased array antenna performance, especially in its scanning characteristics [55]. The mutual coupling in an array can be expressed as an impedance matrix with a number of arranged current distributions with complex amplitude I_n for each element related to an applied voltage V_m.

$$V_m = \sum Z_{mn} I_n \qquad (2.15)$$

Therefore, as the distance between elements changes, the mutual coupling changes, as seen in a two-element half-wavelength dipole case in Figure 2.8.

33
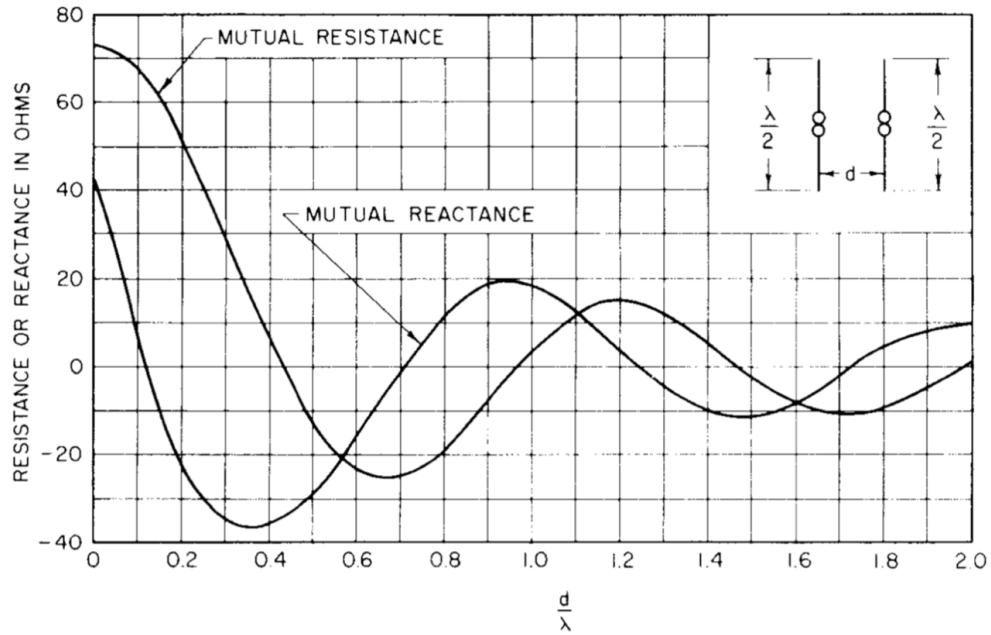
Figure 2.8: Mutual impedance Z_{12} between two dipoles as a function of separation distance [1].
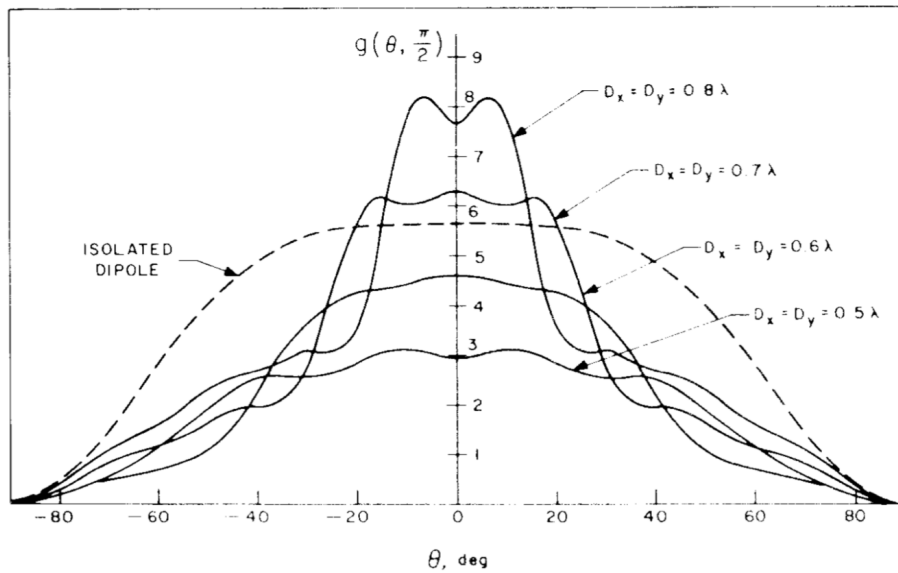
Figure 2.9: H-plane element gain functions for a center element of a 7-by-9-element dipole array ($\lambda/2$ dipoles, $\lambda/4$ above ground.) Element spacings denoted D_x and D_y. Note: dashed curve is for isolated dipole over ground [1].

As the distance in terms of λ is increased, the variation in mutual impedance lowers. The variation would also depend on the orientation of the dipoles due to the difference in electric field orientations. Therefore, for an arrangement of dipoles where their placement is by the ends of the wire, the mutual coupling would be much different.

A PAR's efficiency can be degraded due to mutual coupling. For a dual-polarized array, the efficiency of one of the ports, e.g., the H port, can be given by:

$$\eta_H = 1 - |S_{11}^{HH}|^2 - \sum_{i=2}^{N+1} |S_{i1}^{HH}|^2 - \sum_{i=1}^{N+1} |S_{i1}^{VH}|^2 \tag{2.16}$$

Another important aspect in the PAR performance is the scanning performance which is affected by mutual coupling. The element's impedance changes once it is exposed to other elements near by and therefore, the mnth element will now have an active impedance in the array environment [56], [57].

The active impedance is then a function of the mutual coupling parameters relative to the neighboring element's position in space. This parameter can then be translated into what the scanning capabilities of the active array element is and will provide the overall scanning range that the array potentially has. The active reflection coefficient is then expressed as:

$$\Gamma_{mn}^a(\theta, \phi) = \sum_{p=-P}^{P} \sum_{q=-Q}^{Q} \bar{S}_{mn,pq} e^{[-jk(p-m)d_x u_0 + (q-n)d_y v_0)]} \tag{2.17}$$

where

$$u_0 = \sin\theta_0 \cos\phi_0 \tag{2.18a}$$
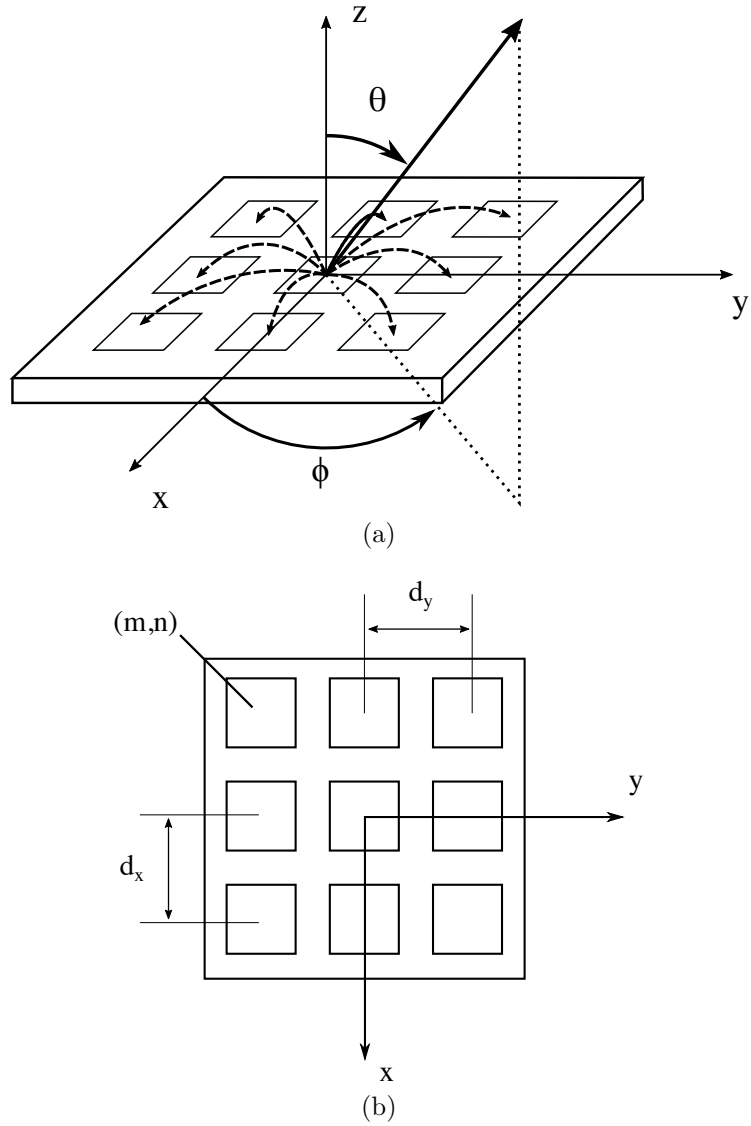
Figure 2.10: (a) Illustration of mutual coupling between elements with respect to the center elements. (b) Top view of the coordinates and arrangement of elements.

and

$$v_0 = \sin\theta_0 \sin\phi_0. \tag{2.18b}$$

It is now evident that the active impedance of the element in the array is then dependent on the scan angle (θ_0,ϕ_0). Assuming the array is large

enough making all of the Γ^a_{mn} of the same magnitude, the phased array's gain performance as it scans the beam can then be predicted by each embedded element pattern gain (G^e):

$$G^e(\theta_0, \phi_0) = G^i(\theta_0, \phi_0) \left[1 - |\Gamma^a(\theta_0, \phi_0)|^2\right] \tag{2.19}$$

where G^i is the gain of the isolated element and Γ^a is the active reflection coefficient expressed in (2.19).

2.4.3 Surface Waves

Surface waves are fields excited in some dielectric bounded medium, usually in the form of a grounded or ungrounded dielectric slab. In the case of PAR, surface waves can be usually present in printed antennas such as printed dipoles or MPAs, where the radiating elements are placed over a grounded dielectric substrate. This substrate can then contain the surface wave that can potentially degrade the array pattern by means of mutual coupling or scanning performance.

In MPAs, both TE and TM modes of surface waves are possible to be excited in the grounded substrate. The excitation of these modes introduces scan blindness in a phased array. Scan blindness is possible whenever the wavenumber, (k_c) coincides with the surface wave propagation constant (β_{sw}) [58]. Since TM$_0$ has a zero cut-off frequency, it will always occur in all substrate-based antennas. In this case study, the mentioned mode is the only introductor of scan blindness.

An antenna sub-assembly of 0.1 λ_o thickness with a low dielectric constant (ϵ_r: 2.2) is used to mitigate the impact of surface waves on overall scanning performance [59]. A set of simultaneous and transcendental equations where
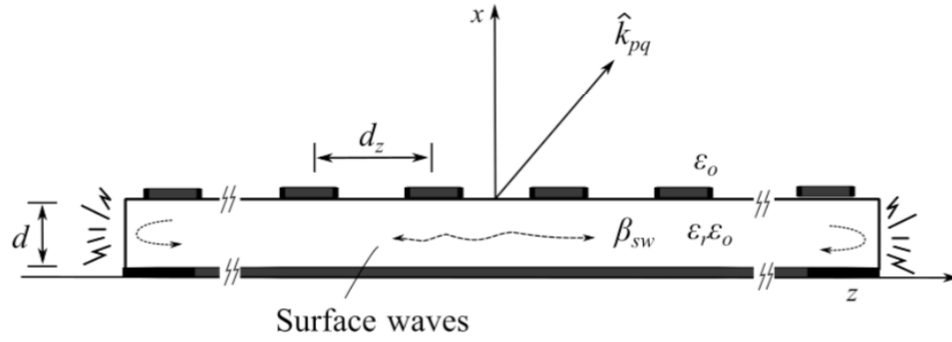
Figure 2.11: Diagram of surface waves in a dielectric surface (courtesy of J. Salazar).
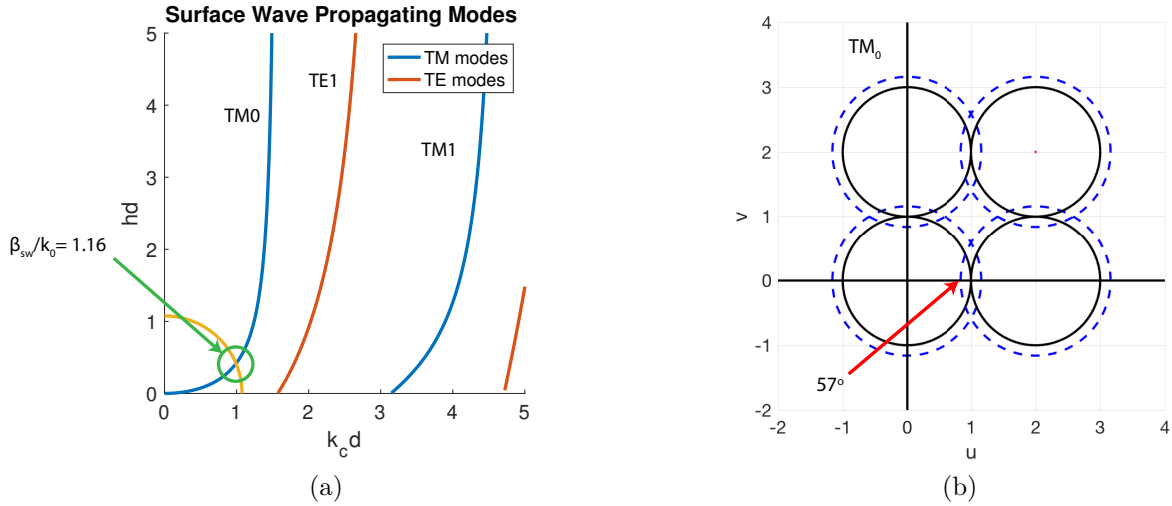
Figure 2.12: (a) Graphical illustration of the propagation constant. (b) Grating lobe diagram with surface waves showing.

used to estimate the propagation constant of surface waves (2.22) in the antenna sub-assembly is given by:

$$(k_c d)^2 + (hd)^2 = (k_o d)^2 (\epsilon_r - 1) \tag{2.20}$$

$$k_c d + \tan k_c d = hd\epsilon_r \tag{2.21}$$

38
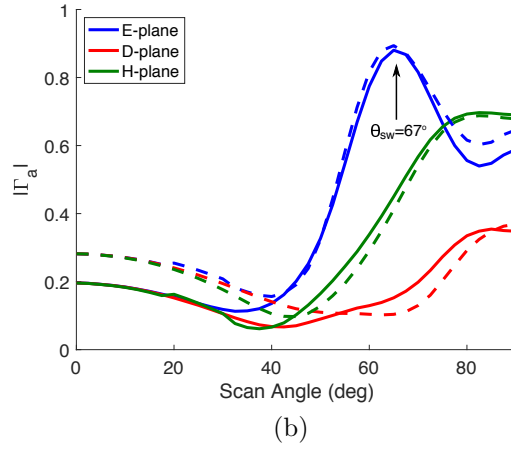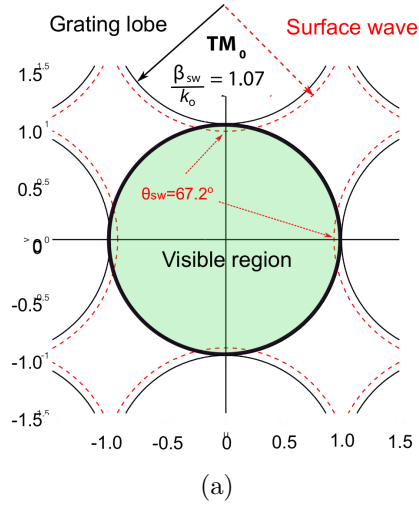
Figure 2.13: (a) Grating lobe diagram showing calculated scanning performance for the proposed antenna array, (b) simulated active reflection coefficient as a function of scan angle at 9.5 GHz for H- (—) and V-ports (- - -).

where $h^2 = \beta^2 - k_o^2$, and d represents the substrate thickness of the antenna subassembly.

$$\beta_{sw}/k_o = \sqrt{(\epsilon_r k_o^2 - k_c^2)}/k_o \tag{2.22}$$

An example of the graphical representation of the solutions of the propagation constants and the location of the scan blindness can be seen in Figure 2.12.

The intersection of the solutions for a TM_0 means that only one surface wave propagation mode is excited. The propagation constant value of this mode is then calculated to determine if a scanning blindness will be introduced.

Figure 2.13(a) shows the graphical solution for the surface wave propagation constant (β_{sw}/k_o) for the dominant mode (TM_0) in both polarizations. Higher-order modes for surface waves and parallel plate modes are not excited using this antenna. For the antenna sub-assembly, the normalized propagation constant for the dominant mode (β_{sw}/k_o) is 1.07, producing a scan blindness at 67.2° for the H-pol and V-pol in the respective E-planes (see Fig. 2.13(b)). Numerical simulation using an infinite array approach in HFSS validates the theoretical estimation of the scan blindness in the antenna sub-assembly. The scan blindness was found to be around 67° in the E-plane for both H- and V-polarizations. The active reflection coefficient (Γ_a) versus the scan angles for the E-, D-, and H-planes are represented in Figure 3.17b. Using the acquired active reflection coefficient, a calculation of a gain variation $(G_o(1 - |\Gamma_a|^2))$ of 1 dB was obtained for the scanning range of ±45°.

2.4.4   Edge Effects/Diffraction

Edge effects are a widely known phenomena in the antenna and phased array antenna community. It has been observed how the diffracted fields affect the antenna element patterns [13]. However, it is fairly complicated to analyze and quantify and therefore, little to no work has been done to quantify the effects analytically, especially for cross-pol. However, it is a substantial effect to take into account under many scenarios, like that shown in Figure 2.14, where multiple sources of discontinuity can be present in a phased array configuration. In this specific scenario where there is interest in low cross-polarization anten-
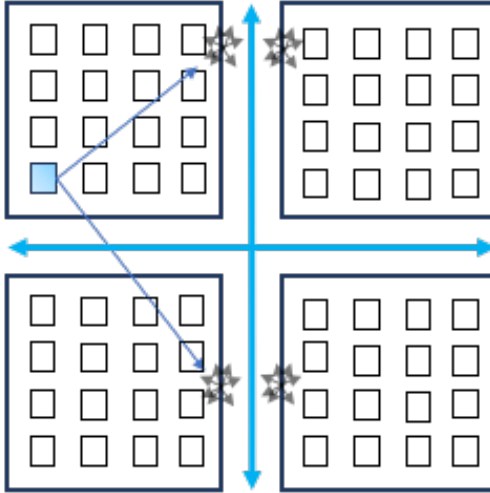
Figure 2.14: A representation of currents generated by internal gaps between subarray panels.

nas, diffraction can play a very critical goal in assuring good cross-polarization performance. Furthermore, edge diffractions affect the elements impedance response as it gets to closer locations to the edges. Mutual coupling calibration techniques are affected once the edges are taken into account. Figure 2.15 shows how some particular edges show some unwanted edge effects, which due to diffraction increases the variability in the magnitude estimations mostly [23], [60], [61].

Furthermore, besides calibration issues related to the mutual coupling of the elements along edges, diffracted fields play an important role in the performance of the active element pattern. As seen in Figure 2.16, very high cross-polarization levels occur with slight movement of the element along the edges and is highly dependent on the location of the element with respect to these edges [62].
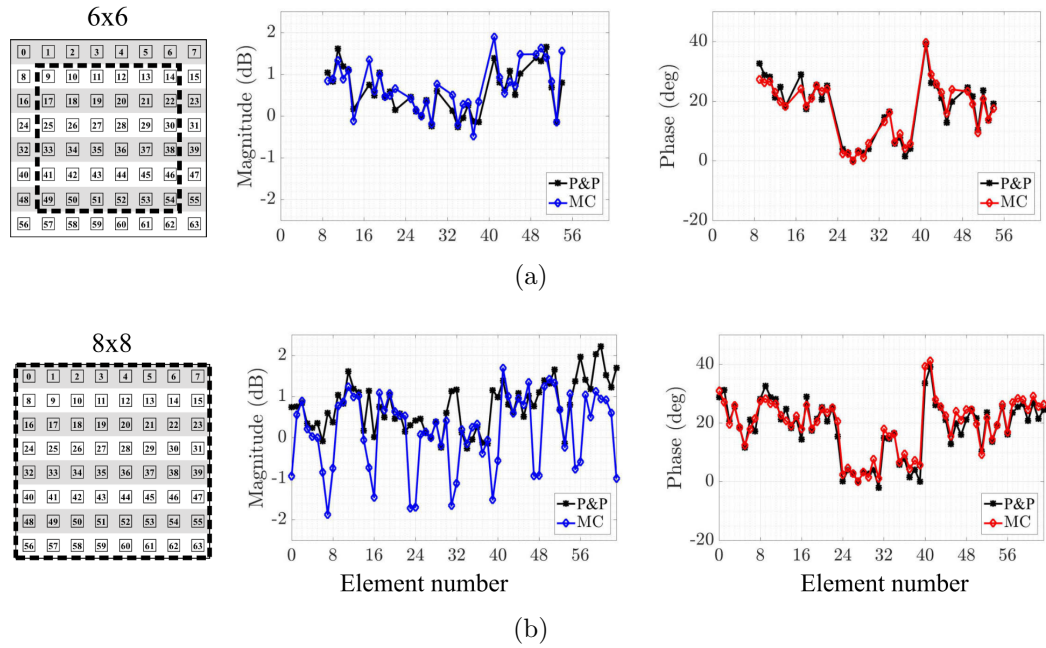
Figure 2.15: The park and probe (P&P) results are compared to the ones obtained using the mutual coupling-based (MC) technique for different subarray configurations. (a) Shows the estimations for the central elements while (b) shows the inclusion of the elements at the edges [60].
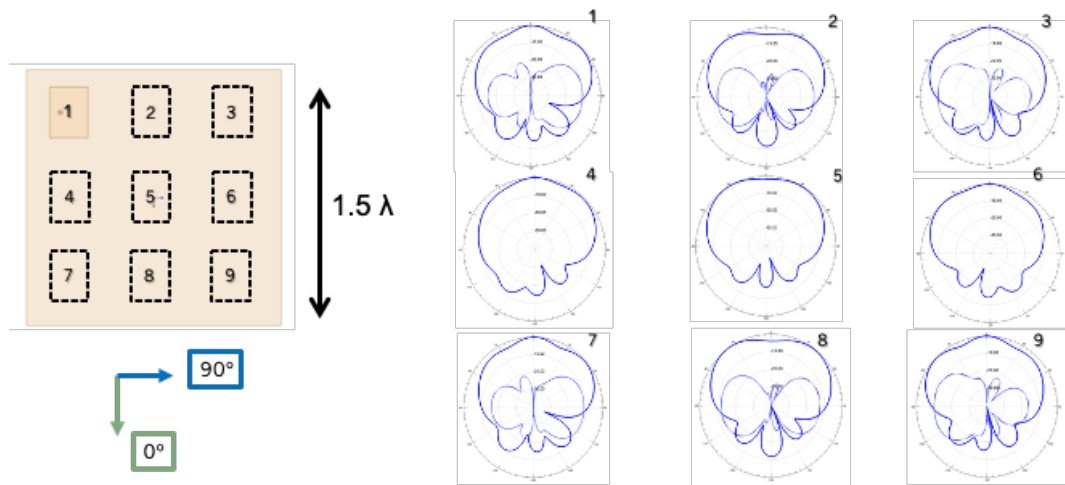
Figure 2.16: 3x3 MPA array showing the element patterns at each position of the array.

Figure 2.17: Diagram of a phased array antenna with its independent sources of excitation V_n with element separation d. (courtesy of J. Salazar).

2.5 Array Antenna Fundamentals

Weather PARs require agile beam steering as well as the need to control important array parameters in order to reduce sidelobe levels while mantaining narrow beamwidth and high gain, avoid scanning nulls for wide angle scanning and wider bandwidths for flexibility in signal processing techniques. This requires control at the element level of the array where amplitude and phase are varied independently as well as a consideration of the array performance at the element level including all of the considerable components that have to

be taken into account to calculate the desired array pattern and excitations at the element level. In this section the fundamental concepts in the calculation of a phased array antenna are discussed.

Having discussed mutual coupling and edge effects and the contribution they have towards the element pattern we can get into what the array calculations entail. A phased array antenna is the arrangement of radiating elements with the ability to change the phase at the element excitation so they add coherently and can point the beam in a certain direction (θ_0, ϕ_0). An array pattern is the superposition of embedded element radiation patterns with their respective amplitudes and phases. This gives the ability for the antenna to be directional and steer the beam, as well as configure a variety of amplitude distributions in order to reduce sidelobe levels.

It has been shown that the array pattern is a function of the active element patterns and the individual excitation coefficients at the terminal of the array. Furthermore, the active element pattern is a function of the scattering parameters of all the ports in the array and the isolated pattern [22], [56], [63]. Figure 2.17 shows a representation of a phased array antenna with independent excitation sources containing phase shifters and attenuators. Each element is excited with a terminal voltage V_0. Hence, the electric field radiated by a single isolated element can be expressed as:

$$E_0(r, \theta) = V_0 f(\theta) \frac{e^{-jkr}}{r} \tag{2.23}$$

where f is the polarized field of the element in space and k is the propagation constant equal to $2\pi/\lambda$. For a linear array of N elements, the total radiated field of the array is then

$$E^A(r,\theta) = f(\theta)\frac{e^{-jkr}}{r}\sum_{n=1}^{N}V_n e^{jk(n-1)d\sin\theta} \tag{2.24}$$

where V_n is the total voltage at the nth antenna element expressed as

$$V_n = V_n^+ + V_n^- \tag{2.25}$$

In order to scan the array to the angle θ_0, the incident voltage V_n^+ at the nth terminal is

$$V_n^+ = V_0 e^{-jk(n-1)d\sin\theta_0} \tag{2.26}$$

As previously discussed in Section 2.4.2, an array of antennas has an input impedance at the termination of each antenna. Hence, the set of N antennas has incident and reflected voltages that are characterized by an $N \times N$ scattering matrix. The S-parameters for each element with respect to the mth element can be written then as

$$S_{mn} = \left.\frac{V_m^-}{V_n^+}\right|_{V_k^+=0 \text{ for } k\neq n} \tag{2.27a}$$

$$V_m^- = V_n^+ \sum_{n=1}^{N} S_{mn} \tag{2.27b}$$

Then at the mth element, where all the elements would be excited, the active reflection coefficient Γ_m^a can be expressed as
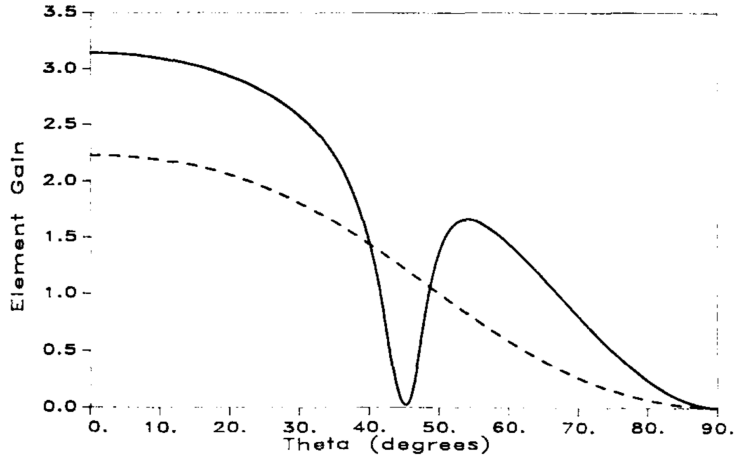
Figure 2.18: Active (——) and isolated (- - -) element pattern of [22].

$$\Gamma_m^a(\theta_0) = \frac{V_m^-}{V_m^+} = \sum_{n=1}^N S_{mn} e^{-jk(n-m)d\sin\theta_0} \tag{2.28}$$

The most accurate representation of the array pattern is the inclusion of all of the effects that are present in the array (see Figure 2.18). These are mutual coupling, edge effects, and any other reflections or scattering sources in the array's design. An isolated radiation pattern f^i is generally used as a predictor of the overall phased array performance, however it does not include all the aforementioned characteristics that are crucial for the most accurate representation of the array's efficiency, scanning capabilities, and cross-polarization levels, which are crucial in this work. Usually, the array elements are passive and therefore when all other elements are terminated except the mth element the active element radiation field, otherwise called here the embedded element field can be expressed as

46

$$E_m^e(\theta) = f^i(\theta) \frac{e^{-jkr}}{r} V_0 \left[1 + \sum_{n=1}^{N} S_{mn} \frac{e^{jk(n-1)d\sin\theta}}{e^{jk(m-1)d\sin\theta}} \right] e^{jk(m-1)d\sin\theta} \qquad (2.29)$$

where the embedded element pattern is

$$f_m^e(\theta) = f^i(\theta) \left[1 + \sum_{n=1}^{N} S_{mn} \frac{e^{jk(n-1)d\sin\theta}}{e^{jk(m-1)d\sin\theta}} \right] \qquad (2.30)$$

And so, the most complete representation of an array pattern is

$$E_{Total}(r, \theta, \phi) = \frac{e^{-jkr}}{r} \sum_{m=1}^{M} a_m f_m^e(\theta) e^{jk(m-1)d\sin\theta} \qquad (2.31)$$

where a_m is the excitation amplitude at the mth element.

2.6   Summary

To this point all of the relevant topic's fundamentals have been discussed. The polarization definitions for PAR have been presented giving context to the necessity of accurate measurements to provide the required polarimetric parameters for the better forecasting of weather phenomena. Hence, it is important to address challenges in the design of phased array antennas that are discussed. Those included the limitations and structural challenges of radiating elements. The selection of an appropriate radiating element has to take into account many aspects such as, efficiency, bandwidth, polarization purity, and other radiation performances such as gain. The latter mentioned is

of importance to the scanning capabilities of the array. Scanning performance is then is expressed as a direct effect of the mutual coupling parameters and the overall radiation performance of the antenna elements in the array. This is proven with the run through the phased array antenna fundamentals which is essentially a superposition of all the elements radiation performance and the interactions between them.

Chapter 3

Edge Diffraction Theory

3.1   Introduction

Diffraction, in electromagnetic theory, is a local phenomena that occurs when a field is introduced to a discontinuity over a conductive surface. It involves the spreading of electromagnetic energy of a given source when incident upon the discontinuity in the forma of a vertex, corner, or wedge, see Figure 3.1. The diffracted field's characteristics are dependent on the geometry at the point of diffraction and the amplitude, phase, and polarization of the incident field at the point of diffraction.

This spreading of energy can be a detrimental factor for high-performance radiating elements and active phased array antenna performance. Different methods can aid in the prediction of diffracted fields. However, with the challenges that come when analyzing electromagnetic problems is the evaluation of scattered fields and its unknowns. Diffracted fields are in all regions of space (see Figure 3.2), and is the only component present in the shadow region (III), since it lies below the reflected and incident boundaries.

Of the most widely used methods that provide accurate numerical solutions for scattered fields for antenna patterns today are full-wave analysis methods,
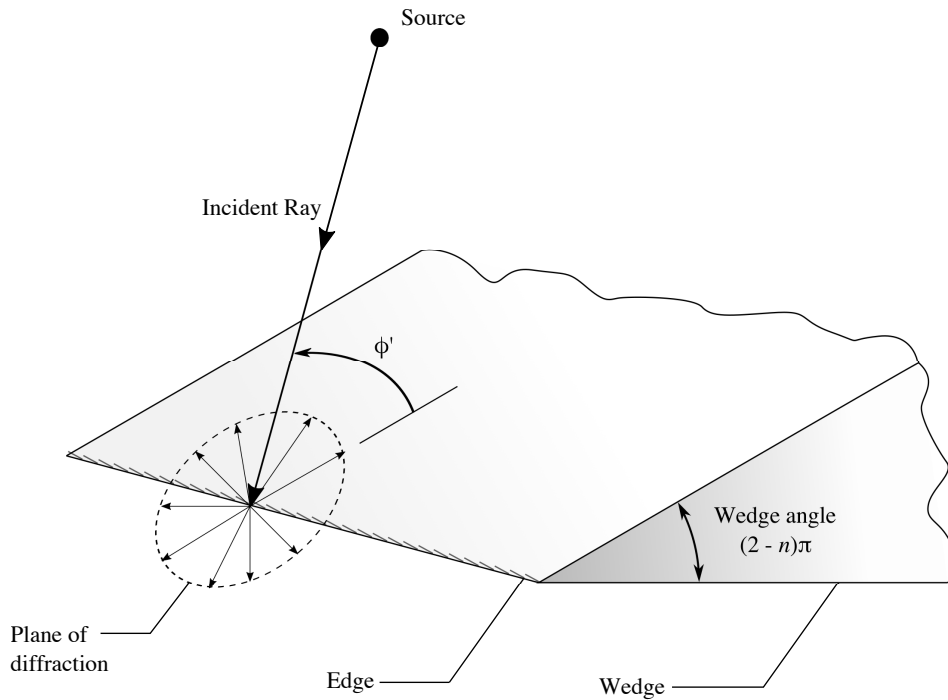
Figure 3.1: Diffraction by a wedge with a straight edge.

which include the method of moments (MoM) and the finite element method (FEM). These methods are proven to provide accurate representation of the scattering and diffraction of electromagnetic radiation. However, these full-wave methods require a lot of computational time and memory resources, especially when electrically large objects are considered. This is particularly the case with phased array antennas, where antennas are placed over larger ground planes and have scalable the applications that involve the placement of several panels in order to increase the size of the array.

For electrically large geometries, high-frequency asymptotic solutions to Maxwell's equations have been commonly preferred methods [64]. Two widely-adopted techniques are GO and PO and their extensions to account for diffracted fields. PO is an integral method involving the numerical calculations of induced currents over an illuminated perfect electric conductor (PEC) plane.
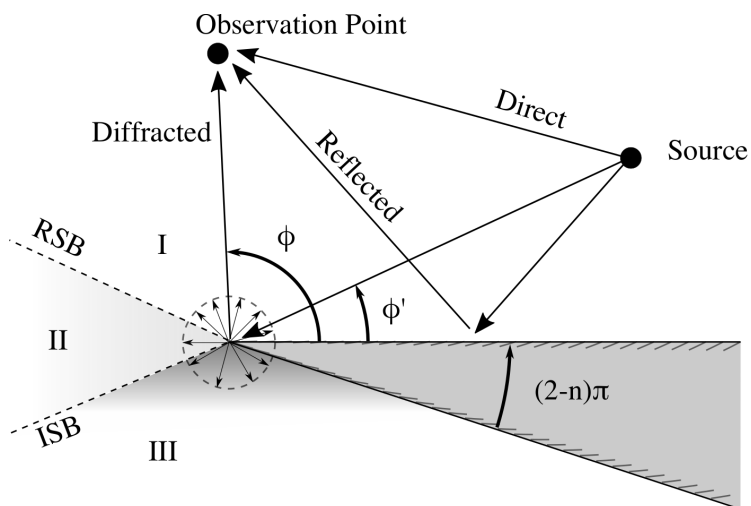
Figure 3.2: Ray tracing of a source to the point of diffraction and the point of observation with respective regions and fields that are present. The regions are separated by the reflected shadow boundary (RSB) where the reflected rays stop to exist and the incident shadow boundary (ISB), where only diffracted fields are present below it [25].

Therefore, PO provides an approximation to the surface fields of the plane and gives an accurate representation of the radiation pattern close to the caustic regions of the reflective surface. However, when edge contributions are of close vicinity and wider angles are of interest the physical theory of diffraction (PTD) provides corrections for PO outside of these caustics regions [65]. The resulting field would be the superposition of the PO field generated by the currents induced on the radiating object and the corrections produced by the diffracted component for edged bodies regarded as the "edge wave field" [27].

About the same time PTD was developed, a similar approach, the geo-metrical theory of diffraction (GTD) is presented as an extension to GO for a generally closed-form solution without the need of integrations [16]. GTD, as an extension of GO, adds the diffracted ray components missing from the direct, reflected, and refracted rays of a GO solution. GTD is later extended

51

to the uniform theory of diffraction (UTD), which, as the name implies, provides uniform solutions with smoothened transitions around singularities in the calculation of the diffracted fields and is to be used throughout this work. GTD/UTD, can also be used to account for multiple diffraction easily in the form of higher-order multiple wave interactions. This is useful when analyzing multiple edges close to a radiating object [27].

Some important assumptions made for the purposes of these studies is the use of flat, perfectly conductive surfaces and straight edges where the fields are incident upon. No surface impedance is taken into account, if so, surface wave analysis would then be needed to be applied into the diffraction models study, especially for phased array architectures where surface waves evidently impact scanning performance and can potentially amplify the effects caused by diffracted fields.

This chapter will discuss GO solutions and total field calculations for several radiating sources in order to understand direct and reflected rays as well as polarization characteristics. These cases will include plane waves, monopole, and microstrip patch antenna (MPA). Plane waves give a general introduction to polarized cases of incident and reflected fields, while the monopole and MPA are more practical cases for different scenarios. To the mentioned GO examples the UTD will be applied in order to understand how the diffracted fields behave under certain scenarios and how they are applied to the specific cases. Furthermore, higher-order techniques will be presented, specifically the equivalent current method (ECM) and how they will help complete the proposed analytical model of this work.

3.2 Geometric Optics

In diffraction theory, GO is used to represent what the total radiation pattern of an antenna would be once placed over an infinite conductive surface. In all the cases to be shown, the ground plan is assumed to be a perfect conductor and will have a zero impedance surface. Therefore, only the direct and reflected components are to be considered in the calculations. These components are characterized by being of hard or soft polarization (see Figure 3.3). Soft polarization is referent to an electric field component that is tangential to the edge and hard polarization to an electric field component normal to the edge. To obtain the GO pattern of both cases, the direct fields from the radiating element and the reflected fields from the ground plane are added.

$$\mathbf{E}^{GO} = \mathbf{E}^{Direct} + \mathbf{E}^{Reflected} \tag{3.1}$$

where the direct components ($\mathbf{E}^{Direct}$) are coming directly from the antenna source and the reflected components ($\mathbf{E}^{Reflected}$) are reflections at the conductive surface, as seen in Figure 3.2. Even though radiated fields do exist in the space all around a wedge, these calculated components do not. To have a clear view of where these fields are present, the space around the wedge will be divided into three sections, as seen in Table **??**.

Table 3.1: Regions around a PEC wedge and their existing components.

Region	Components	Angular Space
I	Direct + Reflected + Diffracted	$0 \leq \phi \leq \pi - \phi'$
II	Direct + Diffracted	$\pi - \phi' \leq \phi \leq \pi + \phi'$
III	Diffracted	$\pi + \phi' \leq \phi \leq n\pi$
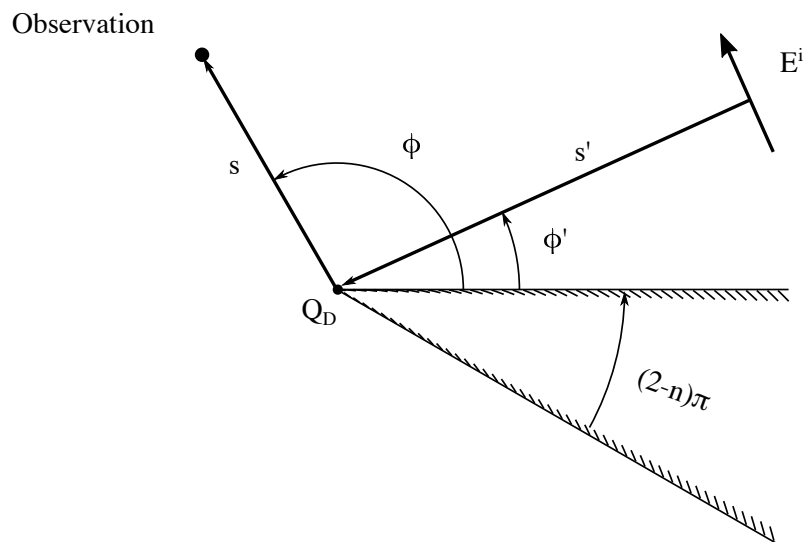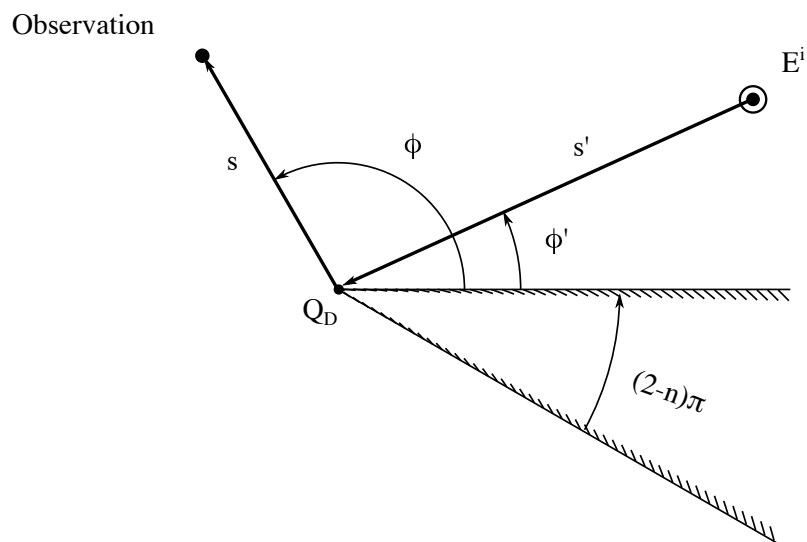
Figure 3.3: A plane wave of (a) hard and (b) soft polarization incident upon a PEC wedge.

3.2.1 Plane Wave

As a basic example, a plane wave incident upon a wedge is studied. This plane wave can be perpendicular or parallel to the plane of incidence. These polarization cases are respectfully denoted as soft and hard polarizations (see
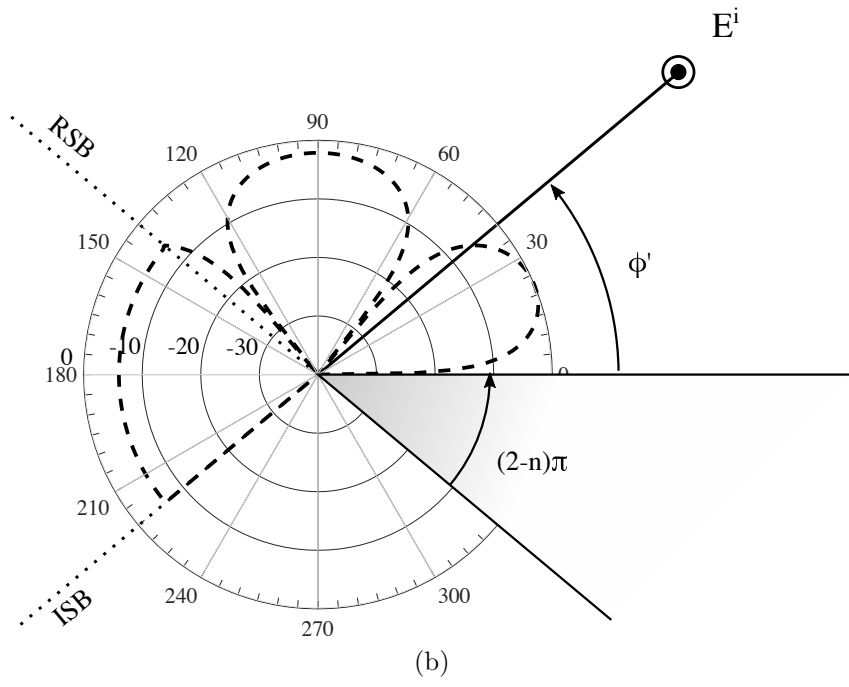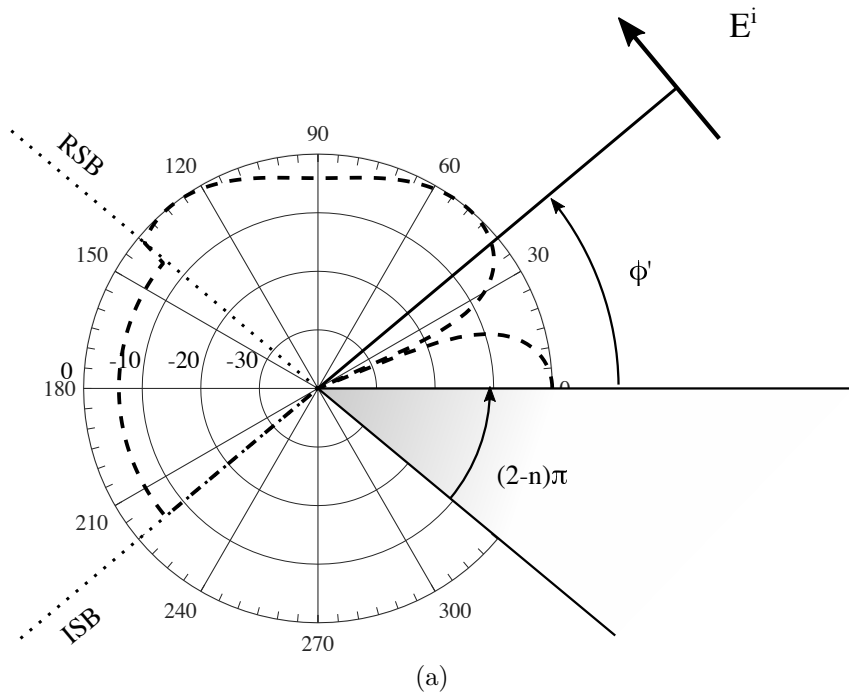
Figure 3.4: Normalized GO pattern solution in dB for a plane wave with (a) hard and (b) soft polarizations with incident angle $\phi' = 40°$ upon a PEC wedge at distance $\rho = \lambda$.

Figure 3.3). Due to boundary conditions, different equations are used to represent the respective GO pattern and to calculate the diffracted fields, which will be discussed in the following section. Each plane wave of unit amplitude will be incident upon a two-dimensional wedge and its GO pattern is calculated by means of contour integration and a method of steepest descent [25] and results in (3.2).

$$
E_{h,s}^{GO} = \begin{cases} e^{jk\rho\cos(\phi-\phi')} \pm e^{jk\rho\cos(\phi+\phi')} & 0 \leq \phi \leq \pi - \phi' \\ e^{jk\rho\cos(\phi-\phi')} & \pi - \phi' \leq \phi \leq \pi + \phi' \\ 0 & \pi + \phi' \leq \phi \leq n\pi \end{cases} \tag{3.2}
$$

The top line of the equation represents region I, the incident and reflected components are added for the hard polarization case and subtracted for the soft polarization case. As for region II, only the incident component is considered and in region III there is zero contributions from GO. The normalized radiation patterns for both polarization cases are shown in Figure 3.4 for an incidence at a 40° angle (ϕ') to the wedge. It is worth knowing that if the incident angle approaches 0° then the image (reflected) component cancels with the incident and produces zero pattern for a soft polarization. The next section will introduce the practicality of the monopole in this study. The monopole produces purely hard polarized radiation with equal magnitude along the azimuthal cut. This helps understand better what effects does hard diffraction have on the performance of an antenna that is placed directly on top of a ground plane.
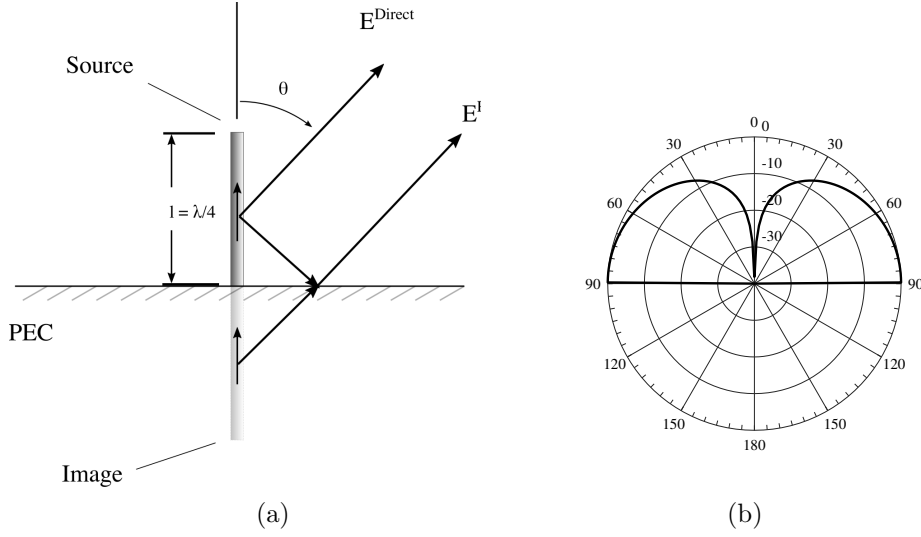
Figure 3.5: (a) Representation of GO rays for the case of a $\lambda/4$ monopole with respective direct and reflected fields. (b) Normalized GO pattern of the monopole over an infinite ground plane.

3.2.2 Monopole

A useful example to represent an object that uniformly illuminated the edges of a ground plane is the quarter-wavelength $(\lambda/4)$ monopole. The monopole has been a widely used antenna for mobile communications. Essentially it is a wire antenna placed vertically over a ground plane. Due to image theory, the vertically placed line of current will be added with its image along the ground plane, it is an equivalent of a half-wavelength $(\lambda/2)$ dipole for the region above the ground plane $(-90° < \theta < 90°)$. Therefore, the expression would be the same as for a half-wavelength dipole (3.3) [51] except that the values are to be zero for anything below the ground plane, as expressed in (3.4).

$$
E_\theta \simeq j\eta\frac{kI_0 e^{-jkr}}{4\pi r}\sin\theta \left\{ \int_{-l/2}^{0} \sin\left[k\left(\frac{l}{2}+z'\right)\right]e^{jkz'\cos\theta}dz' \right.
$$
$$
\left. + \int_{0}^{l/2} \sin\left[k\left(\frac{l}{2}-z'\right)\right]e^{jkz'\cos\theta}dz' \right\} \qquad (3.3)
$$

57

$$E_\theta^{GO}(r,\theta) = \begin{cases} E_0 \left[\dfrac{\cos\left(\frac{\pi}{2}\cos\theta\right)}{\sin\theta} \right] \dfrac{e^{-jkr}}{r} & -\pi/2 \leq \theta \leq \pi/2 \\[12pt] 0 & -\pi/2 > \theta > \pi/2 \end{cases} \tag{3.4}$$

In the GO pattern of the antenna, only the direct, and reflected components are shown in Figure 3.3. The antennas are assumed to be on top of an uncoated ground plane, therefore, refracted components are generally not included in these cases.

3.2.3 Microstrip Patch Antenna

The microstrip patch antenna (MPA) is widely used for high-performance applications and is common in communications and radar technology. It is composed of a dielectric material in between a strip of conductor and a ground plane. Unlike the end-fire radiation produced by a monopole, the MPA produces a maximum normal to the surface of the patch for broadside radiation. The fields formed under the patch can be modeled as a cavity bounded by perfect magnetic walls, where higher-order resonances can be calculated. These, otherwise called higher-order modes, contribute to the overall electric field radiation pattern produced by the MPA and can be one of the main causes of cross-polarization. Using (3.5) and (3.6) one can calculate the electric fields bounded under the patch. These fields are characterized by different propagating modes.

In the general case, the MPA is usually composed by a dominant TM_{01} mode and a TM_{20} mode in the orthogonal dimension of the patch, or along the dimension W, which is usually considered to be the cause of cross-polar radiation as seen in Figure 3.7. Besides the TM_{01} and TM_{20} modes, any other higher-order modes have little to no contribution. For this study, only these
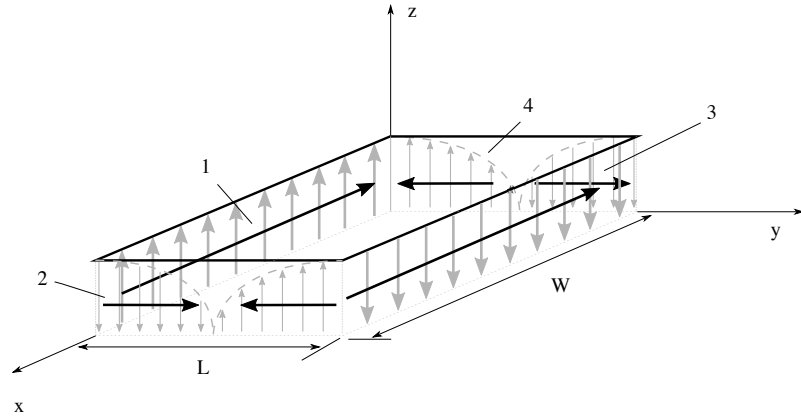
Figure 3.6: Representation of the currents generated by each aperture of the MPA cavity. These currents are determined by the field distribution under the patch and is the radiation mechanism by with the radiation patterns are calculated.
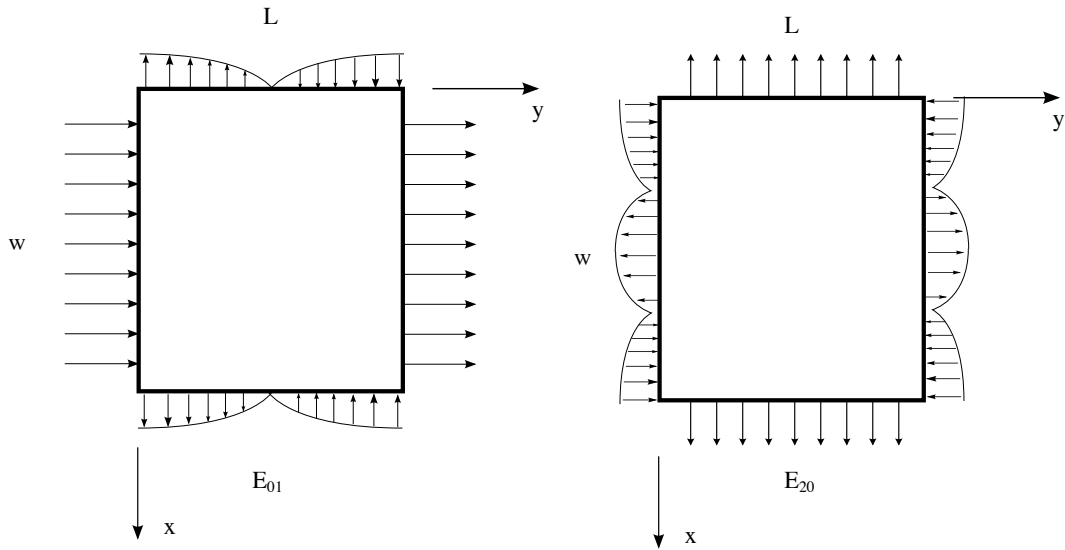
Figure 3.7: Orientation of electric fields bounded by the cavity produced by the two main propagating modes E_{01} and E_{20}.

two will be considered for the analysis to represent co- and cross-polar fields and how they interact with edges and the diffraction fields produced by them. Each mode will be analyzed independently. The equation for calculating the propagating field modes E_{mn}^z and respective coefficients C_{mn} under the patch are given by [66] as

$$E_{mn}^z = \sum_{m=0}^{i} \sum_{n=0}^{j} C_{mn} \cos\left(\frac{m\pi}{W}x'\right) \cos\left(\frac{n\pi}{L}y'\right) \tag{3.5}$$

$$C_{mn} = \left(\frac{\epsilon_{0m}\epsilon_{0n}}{WL}\right) \frac{\cos\left(\frac{m\pi}{W}x_f\right)\cos\left(\frac{n\pi}{L}y_f\right)}{k^2 - k_{mn}^2} j_0\left(\frac{m\pi d}{2W}\right) \tag{3.6}$$

where $k^2 = \epsilon_r(1 - j\delta)k_0^2$, ϵ_r being the dielectric constant under the patch, δ is the dielectric loss tangent, k_0 is the propagation constant, and x_f and y_f resembles the position of the feed. $e_{0m} = 1$ for $m = 0$ and 2 for $m \neq 0$ $k_{mn}^2 = (m\pi/W)^2 + (n\pi/L)^2$ and $j_0 = \sin x/x$ where d is the "effective width" of a uniform strip of a source of current in the z-direction, where for the case of a coax, the authors in [66] use five times the diameter of the coaxial feed cable center conductor.

The design parameters for the dimensions of the cavity are determined using the equations found in [51] and other text books for the design of MPAs. Having the field distribution underneath the patch, the fields at each edge of the cavity is used to calculate the radiated fields by the apertures shown in Figure 3.6. In the principal planes, slots 1 and 3 determine the fields for the TM_{01} mode, while 2 and 4 are used to calculate the fields for the TM_{20} mode. First, the fields at each edge is considered uniform due to the boundary conditions applied to the cavity model, where each boundary is assumed to be a perfect magnetic conducting boundary where all fields are perpendicular to the electric conducting boundaries in the top and bottom. Hence, a magnetic current density is calculated at the apertures by

$$M_s^i = -2\hat{n} \times \hat{a}_z E_z \tag{3.7}$$

where $\hat{n}$ is the unit normal to the field perimeter for each slot;

$$M_s^1 = -2(-\hat{a}_y) \times \hat{a}_z E_z\big|_{y'=0} = 2\hat{a}_x C_{mn} \cos\left(\frac{m\pi}{W}x'\right)$$

$$M_s^3 = -2(\hat{a}_y) \times \hat{a}_z E_z\big|_{y'=L} = -2\hat{a}_x C_{mn} \cos\left(\frac{m\pi}{W}x'\right)\cos(n\pi)$$

$$M_s^4 = -2(-\hat{a}_x) \times \hat{a}_z E_z\big|_{x'=0} = -2\hat{a}_x C_{mn} \cos\left(\frac{n\pi}{L}y'\right)$$

$$M_s^2 = -2(\hat{a}_x) \times \hat{a}_z E_z\big|_{x'=W} = 2\hat{a}_x C_{mn} \cos\left(\frac{m\pi}{L}y'\right)\cos(m\pi)$$

Now that the current densities are determined, the radiated fields are represented by the sum of the fields radiated by all four slots, where two opposing slots account for most of the radiated fields. In this study slots 1 and 3 account for the dominant mode (TM_{01}) that comprises the linearly polarized fields in the y-direction and the higher-order mode (TM_{20}) using slots 2 and 4 to account for the cross-polarization found on most conventional rectangular microstrip patch antennas (RMPAs).

A similar procedure used for calculating the fields radiated by an aperture [51] is applied to each slot of the RMPA. Using spatial factors and disregarding components in z because all current densities are at either x or y

$$L_\theta = \iint_S [M_x \cos\theta\cos\phi + M_y \cos\theta\cos\phi]e^{jkr'\cos\psi}ds' \qquad (3.8)$$

$$L_\phi = \iint_S [-M_x sin\phi + M_y \cos\phi]e^{jkr'\cos\psi}ds'$$

The total electric fields for the respective slot (i) can be written as

$$E_\theta^i = -\frac{jke^{-jkr_i}}{4\pi r_i} L_\phi^i \tag{3.9}$$

$$E_\phi^i = \frac{jke^{-jkr_i}}{4\pi r_i} L_\theta^i$$

Simplifying integration for both M_x and M_y currents

$$L_x = \int_0^h \int_{-\frac{L}{2}}^{\frac{L}{2}} \cos\left(\frac{m\pi}{W}x'\right) e^{jk(x'\sin\theta\cos\phi+z'\cos\theta)} dx'dz' \tag{3.10}$$

$$L_y = \int_0^h \int_{-\frac{W}{2}}^{\frac{W}{2}} \cos\left(\frac{n\pi}{L}y'\right) e^{jk(y'\sin\theta\sin\phi+z'\cos\theta)} dy'dz'$$

The resulting E_θ field expression for each slot is

$$E_\theta^1 = 2C_{mn}\frac{jke^{-jkr_1}}{4\pi r_1} (\sin\phi) L_x \tag{3.11}$$

$$E_\theta^3 = -2C_{mn}\frac{jke^{-jkr_3}}{4\pi r_3} (\sin\phi\cos(n\pi)) L_x$$

$$E_\theta^2 = -2C_{mn}\frac{jke^{-jkr_2}}{2\pi r_2} (\cos\phi\cos(m\pi)) L_y$$

$$E_\theta^4 = 2C_{mn}\frac{jke^{-jkr_4}}{2\pi r_4} (\cos\phi) L_y$$

The resulting E_ϕ field expression for each slot is

Figure 3.8: Calculated patterns for the rectangular microstrip patch antenna in (a) E- and (b) H-plane for co- (—) and cross-pol (- - -).

$$E_\phi^1 = 2C_{mn}\frac{jke^{-jkr_1}}{4\pi r_1}\left(\cos\theta\cos\phi\right)L_x \tag{3.12}$$

$$E_\phi^3 = -2C_{mn}\frac{jke^{-jkr_3}}{4\pi r_3}\left(\cos\theta\cos\phi\cos(n\pi)\right)L_x$$

$$E_\phi^2 = 2C_{mn}\frac{jke^{-jkr_2}}{2\pi r_2}\left(\cos\theta\sin\phi\cos(m\pi)\right)L_y$$

$$E_\phi^4 = -2C_{mn}\frac{jke^{-jkr_4}}{2\pi r_4}\left(\cos\theta\sin\phi\right)L_y$$

where $r_1 = r$, $r_3 = r - L\sin\phi\sin\theta$, $r_2 = r - W\sin\theta\cos\phi$, and $r_4 = r$. The corresponding patterns for the dominant mode (co-pol) and the higher-order mode (cross-pol) will be represented mainly by the addition of apertures 1, 3, 2, and 4, respectively. The patterns produced by the equations are shown in Figure 3.8.

3.3 Geometrical Theory of Diffraction

As an extension to GO, the geometrical theory of diffraction (GTD) introduces diffracted rays, which are added to the total representation of the field. Diffracted rays are produced when the rays known from GO are incident upon an edge, corner, or vertex of a surface boundary. Analogous to how reflection coefficients are applied to incident fields, diffraction coefficients, introduced by the GTD method, provide a relation between the incident field and the diffracted fields. The diffracted field seen at an observation point (s) in space has the form

$$\mathbf{E}^D\left(s\right) = \mathbf{E}^i(Q_D) \cdot \bar{\mathbf{D}} A\left(s', s\right) e^{-jks} \tag{3.13}$$

where $\bar{\mathbf{D}}$ is a dyadic, which is analogous to the reflection coefficient used for an incident electric field (E^i) with parallel or perpendicular incidence upon a the diffraction point (Q_D). A is the spatial attenuation factor and is dependent on the geometrical nature of incidence at the point Q_D.

Both polarizations are denoted as soft and hard polarizations. Soft polarization is identified as a wave that is polarized parallel to a conductive surface and hard polarization as a wave that is perpendicular to the conductive surface. When each polarized field is incident upon a wedge, a respective diffraction coefficient is applied. With the addition of the diffracted field, it is now possible to provide an approximate representation of the total field (3.14) around all regions including the shadow region where, according to GOs, has no field.

$$E^{Total} = E^{Direct} + E^{Reflected} + E^{Diffracted} \tag{3.14}$$

In accordance to the GTD, correction factors and asymptotic solution for angles other than normal incidence ($\beta_0' \neq 90°$) are derived [67]. Furthermore, introducing the dyadic coefficient $\bar{\mathbf{D}}$ as a diagonal matrix the polarization of the scattered field is related to the polarization of the incident wave. This dyadic coefficient is found by introducing asymptotic high-frequency methods and is shown to be practical for applying GTD to antenna and other three-dimensional scattering problems with edges [67].

According to GTD, the diffracted electric field E^d can be obtained by:

$$\mathbf{E}^d(s) = \mathbf{E}^i(Q_D) \cdot \bar{\mathbf{D}}\left(L; \phi, \phi'; n; \beta_0'\right) A(s', s) \frac{e^{-jks}}{s} \qquad (3.15)$$

where

L is the is the distance parameter

A is a spatial attenuation factor

Q_D is the point of diffraction

ϕ is the angle perpendicular to the edge of incidence

ϕ' is the angle perpendicular to the diffraction

n determines the wedge angle

β_0' is the oblique incident angle to the edge of incidence

s' is the point toward the edge of diffraction

s points from the point of diffraction to the point of observation

Incident and diffracted electric fields can be solved as individual components of parallel and perpendicular polarizations. Therefore this equation can be written as:

$$
\begin{bmatrix} E_\phi^D(s) \\ E_\theta^D(s) \end{bmatrix} = - \begin{bmatrix} D_s & 0 \\ 0 & D_h \end{bmatrix} \begin{bmatrix} E_\phi^i(Q_D) \\ E_\theta^i(Q_D) \end{bmatrix} A(s', s) e^{-jks} \tag{3.16}
$$

where the diagonal components D_h and D_s are the diffraction coefficients for the hard and soft boundary conditions, respectively. The respective hard diffraction coefficient and soft diffraction coefficient are then applied to both hard and soft polarized electric field components respectively, seen in Figure 3.3.

The coefficients depend on trigonometric functions involving a Fresnel integral, which is used as a correction factor for the transition regions along the incident shadow boundary and reflection shadow boundary. These transition regions produce singularities which generate errors and become more pronounced as the edge of diffraction is closer to the source. In order to correct for these inaccuracies and extend the formulation of the asymptotic expansions for a more general type of illumination of the wedge the uniform theory of diffraction (UTD) is introduced [15].

3.3.1 Uniform Theory of Diffraction

Previous high-frequency methods to calculate the fields in the shadow region, where the GO is zero to account for non-vanishing fields, produce discontinuities at the shadow and reflection boundaries. However, fields in these region do exist and have a continuous nature. As such, sources closer to the edges must be excluded because the GTD approach is no longer valid. Therefore, the diffracted field solution must provide a correction for the transition between

66

regions illuminated by the source and shadowed by the edge [15].

UTD is introduced to smoothen the results obtained by the high-frequency method where it shows discontinuities in vanishing points between the shadow and reflection boundaries. In reality, there are fields to exist in these boundaries, therefore, the UTD is a uniform asymptotic method which introduces transition function expansions in its diffraction coefficients (D^i, D^r).

Diffraction coefficients for incident and reflected diffraction for oblique incidence including corresponding expanded Fresnel functions for bounding discontinuous boundaries are:

$$
D^i\left(L, \phi - \phi', n, \beta_0'\right) = -\frac{e^{-jk\pi/4}}{2n\sqrt{2\pi k}\sin\beta_0'}
$$
$$
\cdot\left(\left\{\cot\left[\frac{\pi + (\phi - \phi')}{2n}\right] F\left[kLg^+\left(\phi - \phi'\right)\right]\right.\right.
$$
$$
\left.\left. + \cot\left[\frac{\pi + (\phi - \phi')}{2n}\right] F\left[kLg^-\left(\phi - \phi'\right)\right]\right\}\right) \quad (3.17\text{a})
$$

$$
D^r\left(L, \phi + \phi', n, \beta_0'\right) = -\frac{e^{-jk\pi/4}}{2n\sqrt{2\pi k}\sin\beta_0'}
$$
$$
\cdot\left(\left\{\cot\left[\frac{\pi + (\phi + \phi')}{2n}\right] F\left[kLg^+\left(\phi + \phi'\right)\right]\right.\right.
$$
$$
\left.\left. + \cot\left[\frac{\pi - (\phi + \phi')}{2n}\right] F\left[kLg^-\left(\phi + \phi'\right)\right]\right\}\right) \quad (3.17\text{b})
$$

where F is the Fresnel transition function

$$
F(X) = 2j\sqrt{X}e^{jX}\int_{\sqrt{X}}^{\infty} e^{-j\tau^2}d\tau \quad (3.17\text{c})
$$

where (3.17c) is used, along with functions g^- and g^+, to relate the angular separation between the observation point and the incident and reflection shadow boundaries [15], [25]. These functions introduce integral values of importance in order to provide non-abrupt changes as a function of ϕ near the boundaries.

There are two main polarizations that are assumed to be incident upon an edge, as seen in Figure 3.3, and for each case a diffraction coefficient is applied in (3.16). Depending on the polarization and boundary conditions of the incident wave with respect to the wedge, equations (3.17a) and (3.17b) then determine the soft and hard diffraction coefficients, seen in (3.16), as:

$$D_h\left(L; \phi, \phi', n; \beta_0'\right) = D^i\left(L, \phi - \phi', n, \beta_0'\right) + D^r\left(L, \phi + \phi', n, \beta_0'\right) \qquad (3.18a)$$

$$D_s\left(L; \phi, \phi', n; \beta_0'\right) = D^i\left(L, \phi - \phi', n, \beta_0'\right) - D^r\left(L, \phi + \phi', n, \beta_0'\right) \qquad (3.18b)$$

To verify that these coefficients are related to boundary conditions and image assumptions, whenever the wave is incident at grazing incidence $\phi' = 0°$ both incident and reflected diffraction coefficients are the same. Therefore, (3.18b) and (3.18a) become 0 and $2D^{i,r}$ respectively. This means that incident field that is parallel (or of soft polarization) to the perfectly conductive surface cancels itself out with its image and the opposite is true for the perpendicular (or hard) polarization.
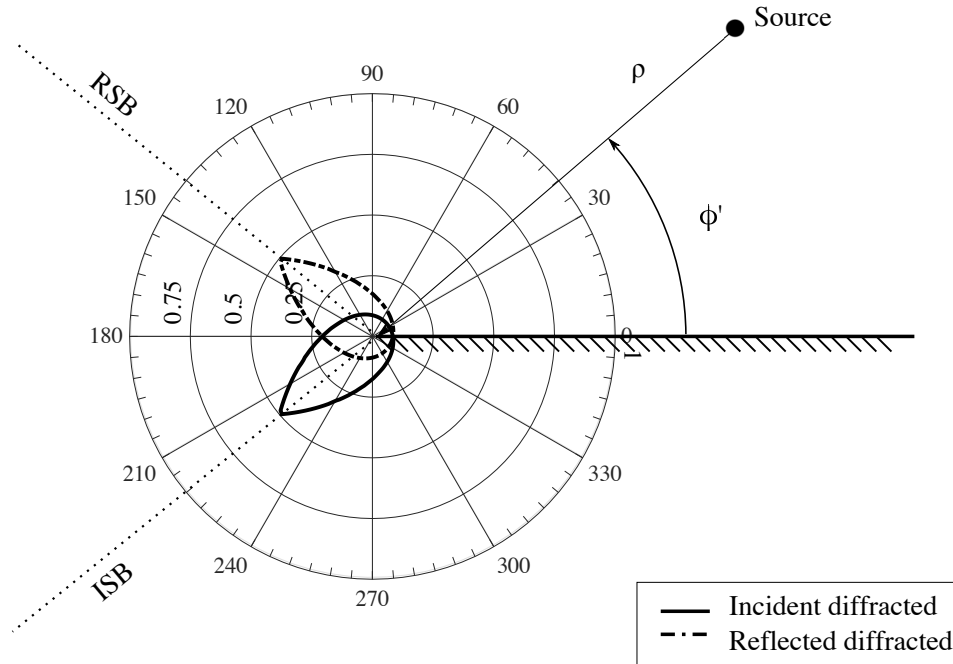
Figure 3.9: Incident and reflected diffracted fields from a plane wave source with incidence angle $\phi' = 40°$ upon a flat half-plane ($n = 2$).

3.3.2 Diffracted Fields

The total field of an antenna element placed in a finite ground sheet will be the superposition of the GO pattern and the diffracted fields. Diffracted fields exist in all space surrounding a wedge where the wave of an arbitrary source is incident upon. The relation between the incident wave and the diffracted wave is determined by diffraction coefficients. These coefficients will mainly be dependent upon the geometry of the wedge, the distance at which the wave travels to reach the edge and the angle of incidence. As previously mentioned, the incident and reflected diffraction coefficients, expressed in (3.17a) and (3.17b) respectively, have singularities that are corrected using transition functions (3.17c) and their extensions when the observation is close to the

incident shadow boundary (ISB) and reflection shadow boundary (RSB).

$$V_{i,r}\left(\rho;\phi,\phi',n;\beta_0'\right) = D_{i,r}\left(\rho;\phi\mp\phi';n;\beta_0'\right)\frac{e^{-jk\rho}}{\sqrt{\rho}} \tag{3.19}$$

$$V_{s,h}\left(\rho;\phi,\phi',n;\beta_0'\right) = \left[D_i\left(\rho;\phi-\phi';n;\beta_0'\right)\mp D_r\left(\rho;\phi+\phi';n;\beta_0'\right)\right]\frac{e^{-jk\rho}}{\sqrt{\rho}} \tag{3.20}$$

The fields generated by the diffraction coefficients are shown in Figure 3.9. This diagram shows how the diffracted fields are seen with respect to the surface of the wedge at the distance to observation point (ρ) and an incident angle from the face of the wedge to the source (ϕ'). The incident diffracted field (V_i) and reflected diffracted field (V_r) are calculated with the UTD method and shows the smoothened discontinuity at both ISB at $\pi - \phi'$ and RSB at $\pi + \phi'$, respectively. These fields will provide the corrections to the transitions between boundaries necessary to represent the total electric fields of a source. For instance, the hard diffraction coefficient (D_h), in (3.18a), will provide the missing components to a parallel polarized wave upon the incident plane. Therefore, adding to the GO solution, shown in Figure 3.4a the missing diffracted field components, resulting in the pattern seen in Figure 3.10a. In a similar manner the field for the perpendicular polarization case is shown in Figure 3.10b. From these results it is easy to appreciate how the boundary conditions work at $\phi = 0°$ and $\phi = n\pi$ where the soft polarization approaches an amplitude of 0 at the boundary or PEC surface while the hard polarization does not.

The cases shown here are for a straight wedge of infinite length. In order
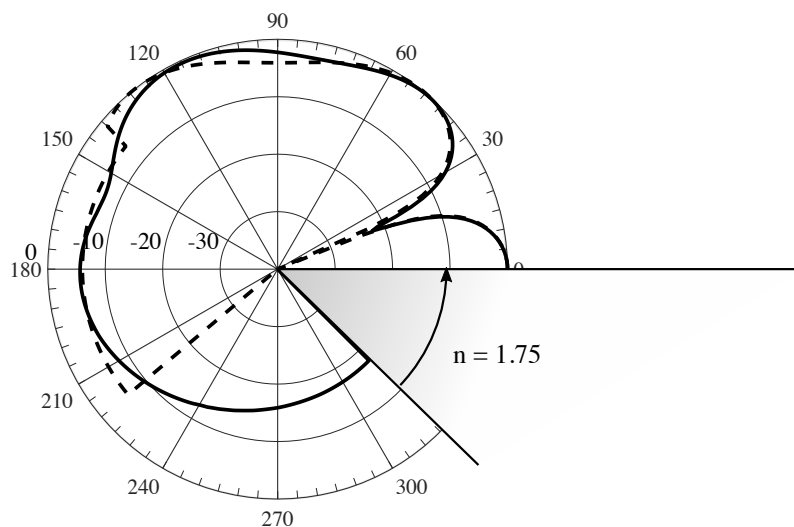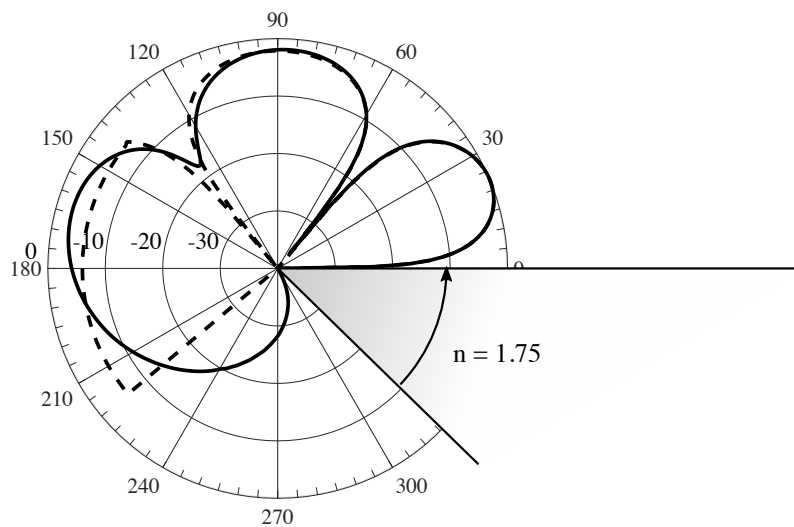
Figure 3.10: Normalized total field (——) and GO solution (- - -) of an incident plane wave in (a) hard (b) soft polarizations with incident angle of $\phi' = 40°$ upon a 45° wedge at distance $\rho = \lambda$.

to evaluate the effects that these fields have on the pattern from a source radiation, the parameters that determine the behavior of change in the diffraction coefficients are explored. Since the diffraction coefficient is inherently a complex value, the effects it has on the overall pattern will be in amplitude and phase. The variation can be due to the different parameters the diffraction
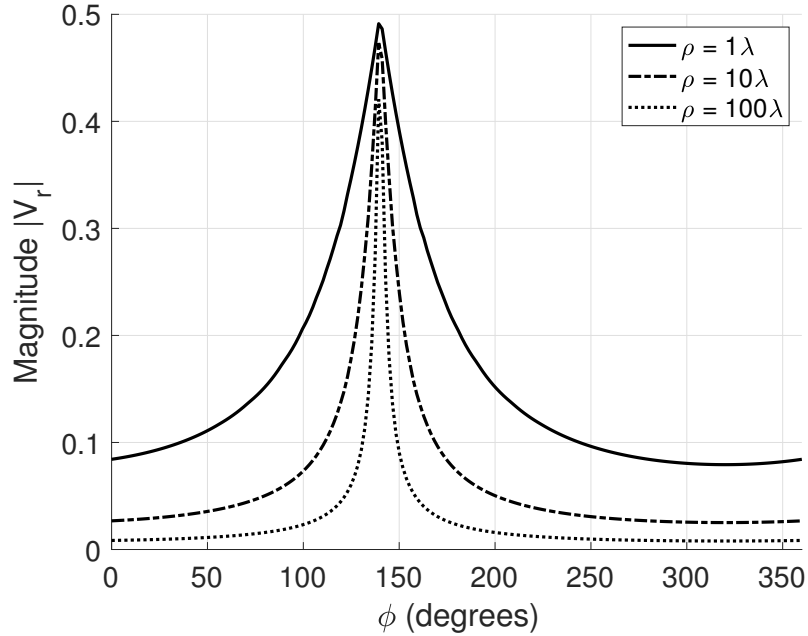
Figure 3.11: Reflected diffracted fields for different source positions ρ and a fixed incident angle of $\phi' = 40°$ and a wedge angle of $n = 2$.

coefficient is dependent on, the diffracted field can vary with changing the distance from the source to the edge, the angles at which the wave is incident upon the edge, and the angle of the wedge.

The amplitude of the reflected diffracted fields at different distances (ρ) can be viewed in Figure 3.11. It shows a maximum at the angle of incidence with respect to the RSB at $\pi - \phi'$, while the maximum of the incident diffracted field will be at the ISB at $\pi + \phi'$. The total of the reflected and incident diffracted is shown in Figure 3.12. As the diffracted field is formed farther from the source, the spreading is reduced. However, it will introduce phase alterations which produces more ripples in the total radiation pattern. Figure 3.13 shows how the pattern for both hard and soft diffraction coefficients changes with length towards the edge. A noticeable difference can be seen in the shadow region $(\pi + \phi')$, especially for the hard polarization case (see Figure 3.13a), where the reduction in amplitude can be seen as the distance to the source is increased.
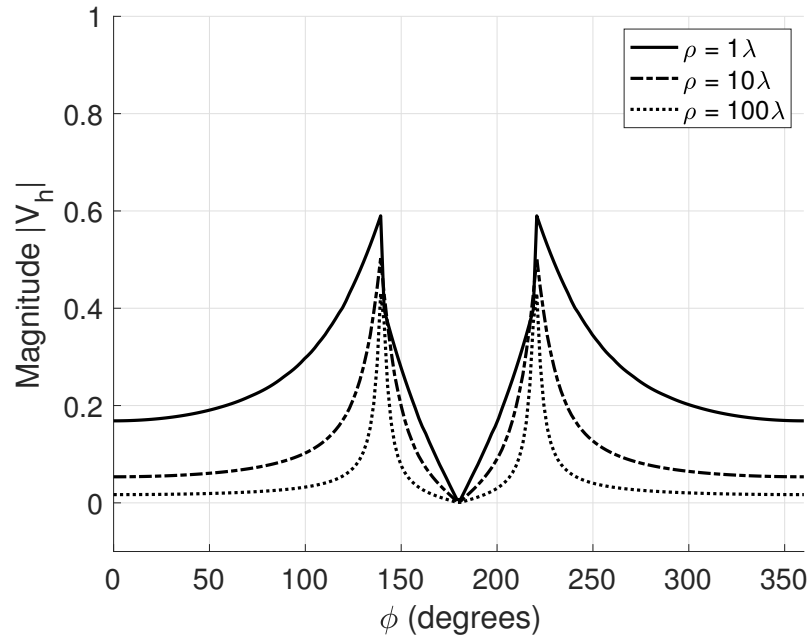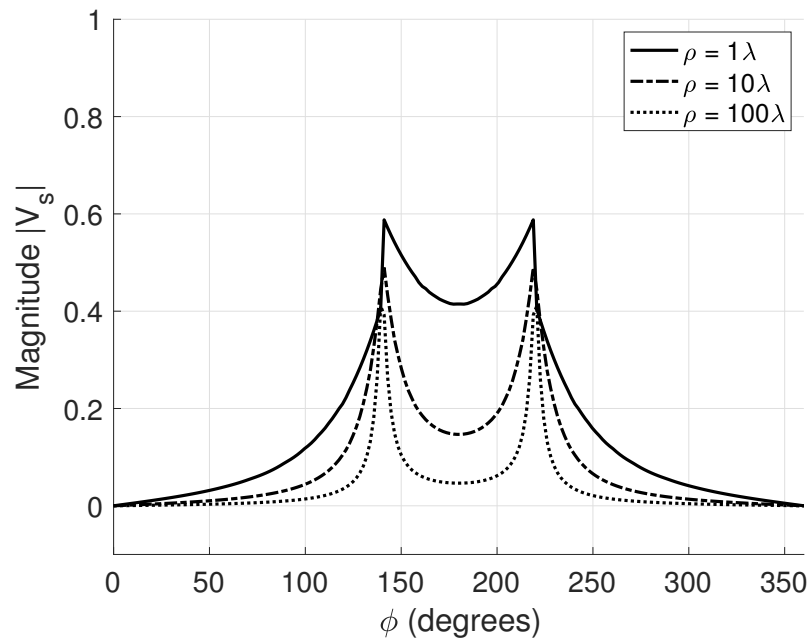
Figure 3.12: Incident diffracted fields for (a) soft and (b) hard diffraction for different source distances ρ and a fixed incident angle of $\phi' = 40°$ and a wedge angle of $n = 2$.
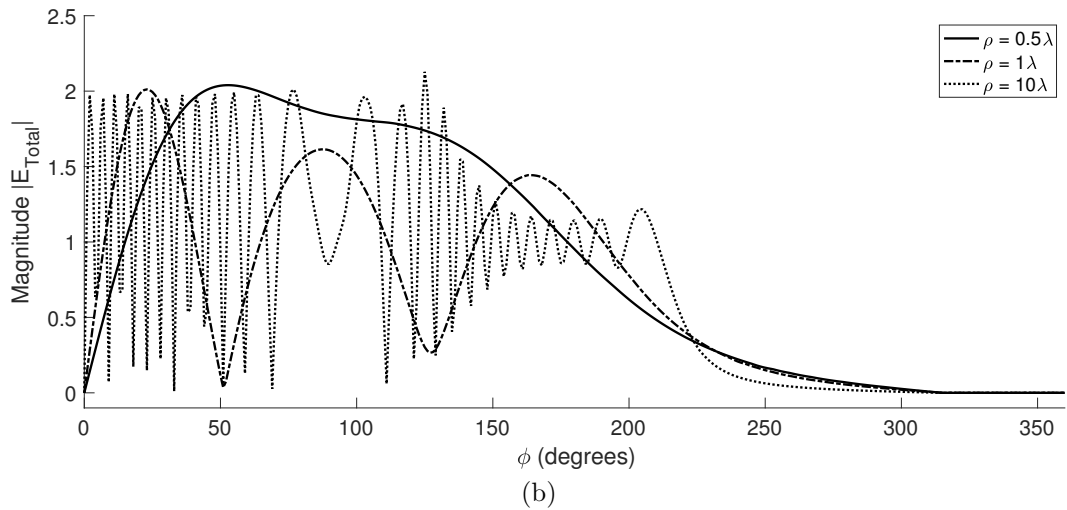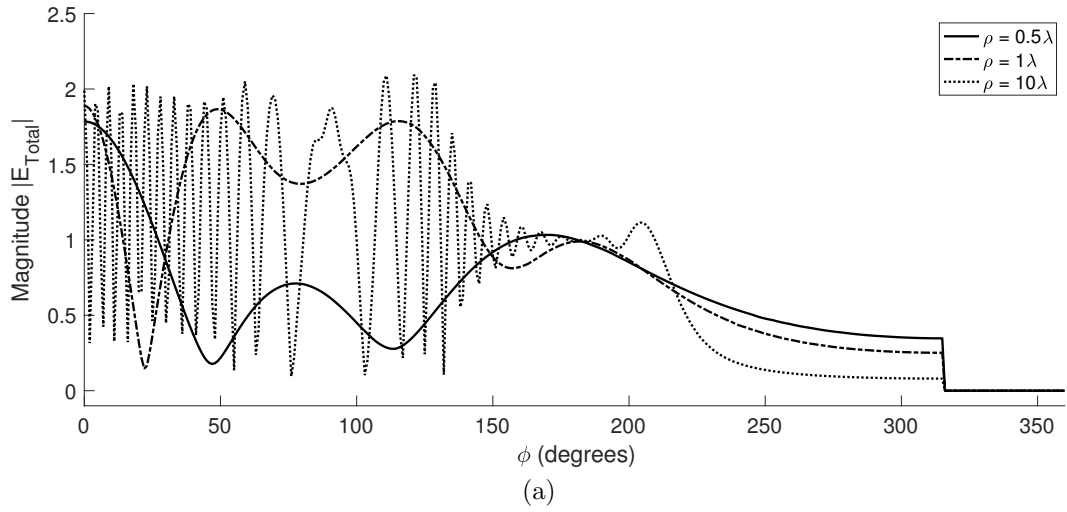
Figure 3.13: Total field of an incident plane wave for different distances in (a) hard (b) soft polarizations with incident angle of $\phi' = 40°$ upon a flat half-plane where $n = 2$.

In both polarization cases, the effect the diffracted fields have on the pattern is adding ripples to the pattern. Meaning, edge can affect the magnitude of the individual source depending on its position along a ground plane.

Furthermore, analyzing how the incident angle approaches grazing incidence ($\phi' = 0°$) can give a view as to how the diffracted fields interaction with the source varies. Figure 3.14 shows the total hard and soft diffracted fields that would be added to the source GO solution to get the total representation
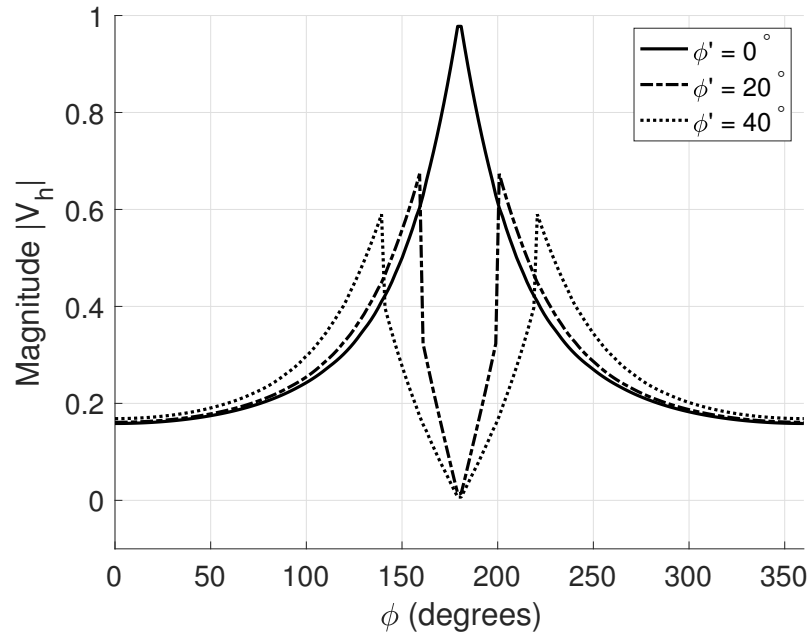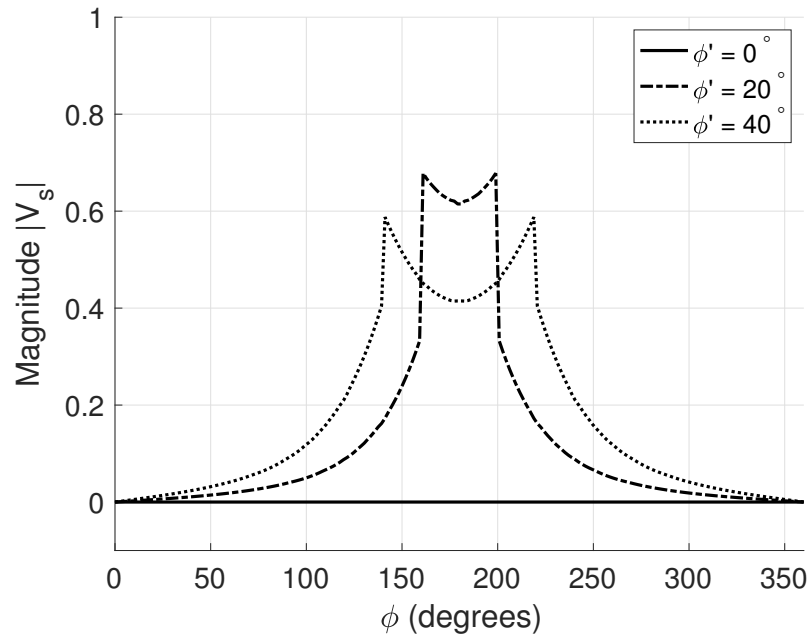
Figure 3.14: (a) Soft and (b) hard diffracted fields of an incident plane wave upon a flat half-plane at distance $\rho = \lambda$ and a wedge angle of $n = 2$.

of the electric field. Here, as the incident angle ϕ' approaches grazing, proves what was mentioned before, that for a hard polarization case the diffraction
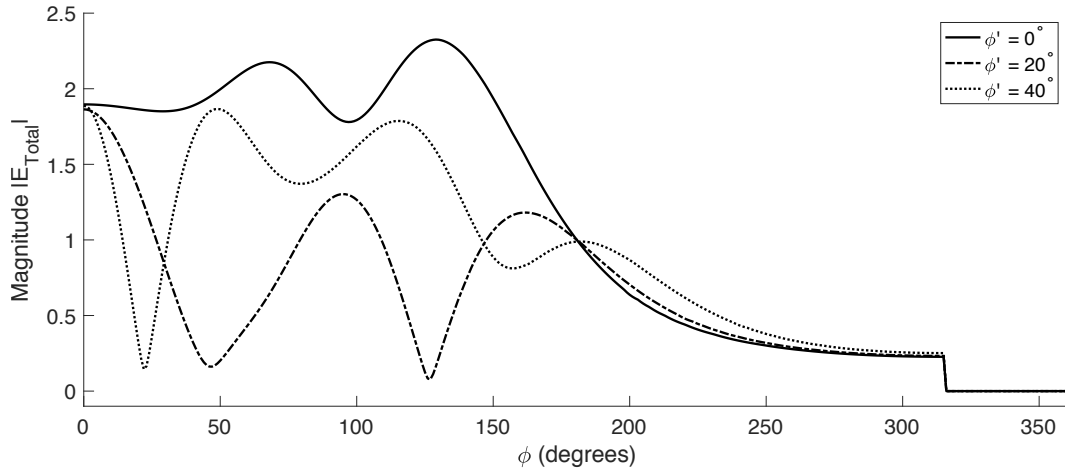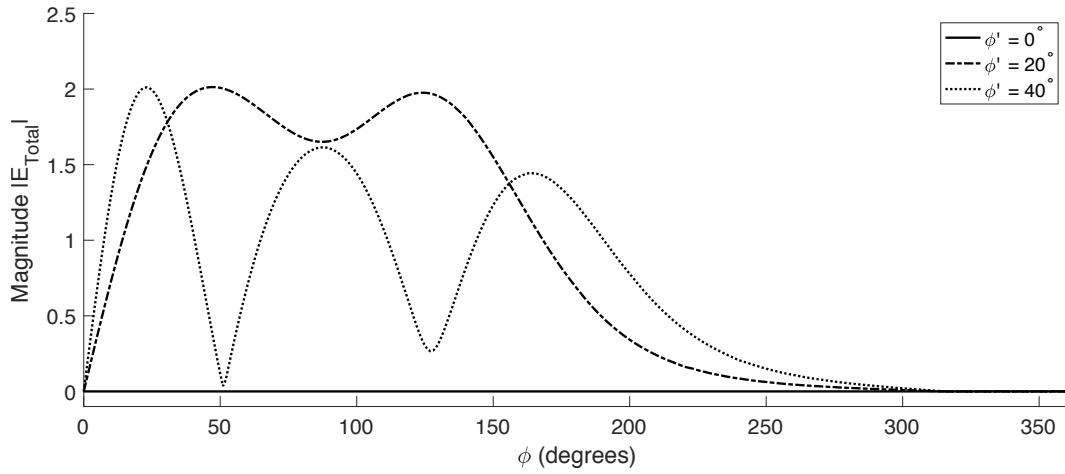
Figure 3.15: Total field of an incident plane wave in (a) hard (b) soft polarizations with a fixed distance of $\rho = \lambda$ upon a flat half-plane where $n = 2$.

coefficients would be equal, hence when added would result in $2V_{i,r}$ in case of hard diffraction and 0 in the case of soft diffraction. This would comply with boundary conditions where a tangential component to the edge would be zero when no distance is between it and the PEC boundary and twice the value when it is perpendicular to it. With changing incidence, both polarization cases experience different conditions where the pattern changes as the transition region between both RSB and ISB narrows, resulting in 0 for the soft

cases seen in Figure 3.14b and 3.15b.

3.4   Analytical Model

Having discussed the theory behind diffracted fields and how they are calculated, this section will discuss the analytical tools to build the proposed model. One of the main objectives with the use of an analytical model is to capture the effects diffracted fields have on an antenna element's radiation performance placed in a finite array environment. In order to implement this, a method that is dependent on the location of the element with respect to the edges will provide enough information of the diffracted fields produced in space.

The proposed analytical model will be composed of a combination of techniques. The two-point diffraction will lay down the basic parameters that will be useful to calculate the diffracted fields with respect to the location of the source along the sheet or conductive surface. As an extension of this, the equivalent current method, can represent each edge of the finite array as a current source induced by each element's diffracted fields and provide a view of the element's radiation field in all space around it. Hence, this method has the ability to analyze the fields in all of its components as well as principal and non-principal cuts.

3.4.1   Two-point Diffraction Method

The two-point diffraction is a method that is useful to calculate how diffraction from two points over a finite ground plane interacts with the radiation pattern from a source between them. This is what would usually happen when dealing with a finite phased array, where the elements will have two edges on either side of the ground plane for each azimuthal (ϕ) cut. The main element of this
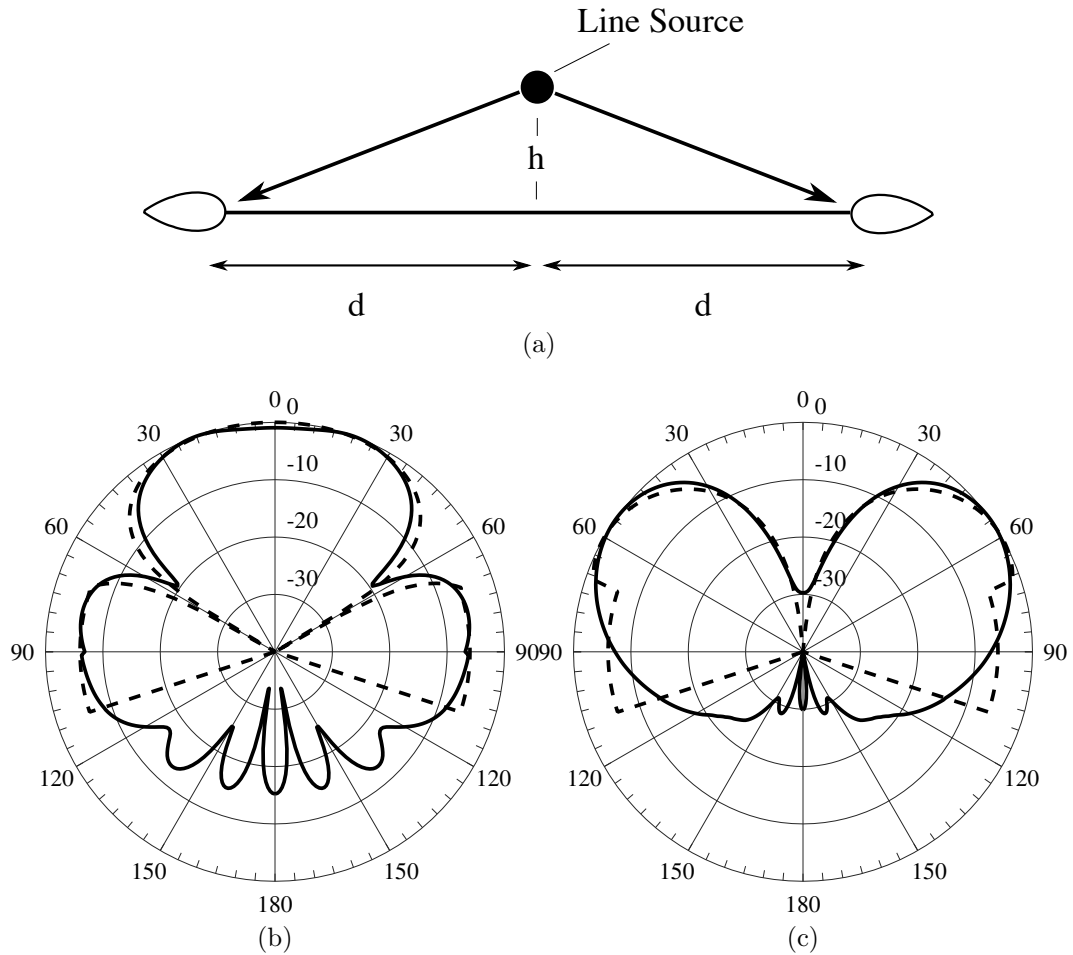
Figure 3.16: Total field of a (a) centered line source placed between two points of diffraction with (a) hard and (b) soft polarizations.

method that helps understand the implementation of the proposed method of this work is the impact that the distance to the edges has on the total radiation pattern of a given source. This variability is helpful to identify different cases of asymmetrical placement along the ground plane, hence, providing insight as to how each element's radiation pattern will look like with respect to its position about the edges of a finite ground plane.

In order to introduce a more practical scenario, the use of a two-point diffraction calculation can provide a radiation pattern where an antenna is met by two edges on either side. This is what is usually seen in practice when
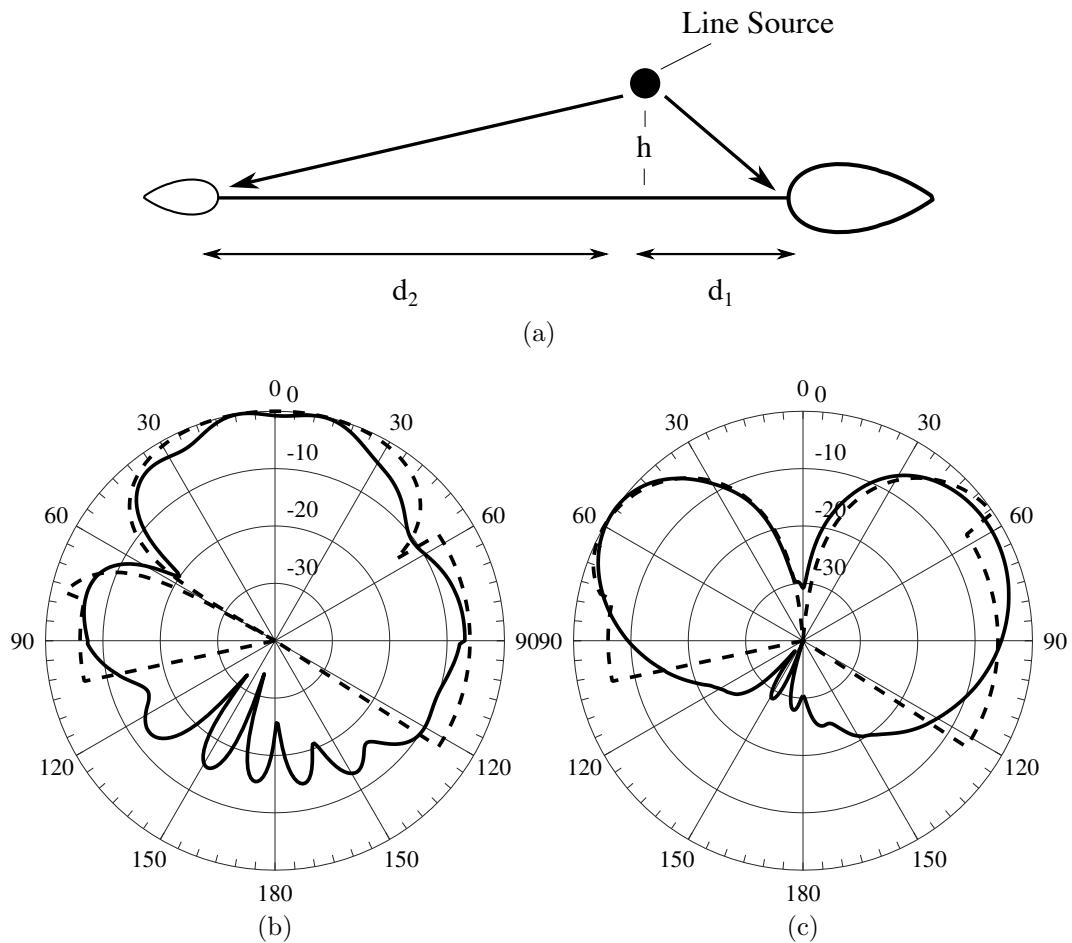
Figure 3.17: Total field of an (a) off-centered line source placed between two points of diffraction with (a) hard and (b) soft polarizations.

fabricating an antenna that is placed over a flat conductive surface as a ground plane.

Figure 3.16 shows the total field calculations for a line source with either soft or hard polarization placed over a 3λ sized ground plane. The analysis involves the superposition of the electric fields coming from the source with the two points at either side of the ground plane. In this manner, the total radiation pattern will be representative of a cut along the points of diffraction and the source. This brings the ability to place the radiation source any place between these two points, see Figure 3.17. Therefore, adds an additional

capability for studying elements at arbitrary positions along a ground plane.

It is evident that positioning the antenna at different points in between the edges produces different radiation patterns which translate to changes in phase and amplitude. This method can then be used to study the effects the edges have on individual element's gain along a phased array antenna.

3.4.2 Equivalent Current Method

The previous equations are sufficient for the co-polar components. To obtain the other component contributions coming from currents aligned in the opposite direction and the interaction along all the edge must be considered as a line of current in space, as shown in Figure 3.18. The ECM's approach is to model equivalent currents along the edges of the ground plane (x, y) plane, as shown in Figure 3.19, producing both far-field components using vector potentials.

A magnetic current I^m is used to produce the diffracted fields from such incident E_θ fields [25].

$$I_{x,y}^m = -\eta H_{x,y}^i(Q_D)\sqrt{\frac{8\pi}{k}}D_h e^{-j\frac{\pi}{4}} \tag{3.21}$$

$H_{x,y}^i$ being the incident magnetic field at any point along the edges along the x-axis and y-axis. Once the magnetic current is determined for each point along the edge, the radiation integrals using vector potential F for a magnetic current lines are calculated [25].

$$\mathbf{L} = \int \mathbf{I}_{x,y}^m e^{jks\cos\psi}\,dl \tag{3.22}$$

80
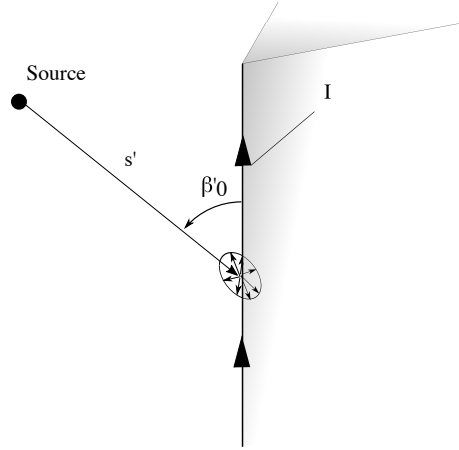
Figure 3.18: Equivalent current modeled by the diffraction along the wedge.

$$\mathbf{F} = \frac{\epsilon e^{-jkR}}{4\pi R}\mathbf{L} \tag{3.23}$$

$$\begin{bmatrix} E_\phi^D = j\omega\eta F_\theta \\ E_\theta^D = -j\omega\eta F_\phi \end{bmatrix} \tag{3.24}$$

Now that both components are determined, they can be added to the total radiated field:

$$\mathbf{E}^{Total}(\theta, \phi) = \mathbf{E}^{GO}(\theta, \phi) + \mathbf{E}^D(\theta, \phi) \tag{3.25}$$

where E^{GO} is the monopole's geometric optics (GO) electric field pattern, which takes into account the reflections of an infinite conductive surface, and E^D is the diffracted electric field from the calculated vector potential of the equivalent currents at the edges taking into account both E_θ and E_ϕ components.

Having all mutual coupling parameters (S_{mn}) between the element of in-

terest and its neighboring elements, one can add these diffracted fields to both compontents of the radiation pattern in order to have a more accurate and complete representation of the embedded element pattern.

$$\mathbf{E}_m^e(\theta,\phi) \quad = \quad \left(\mathbf{E}^{isol}(\theta,\phi) + \mathbf{E}_m^D(\theta,\phi)\right)\left(1 + \sum_{n=1}^{N} \mathbf{S}_{mn} e^{-jk(r_n' - r_m')\cdot\hat{r}}\right) \quad (3.26)$$

3.4.3   Four-Edge Equivalent Current Model

This proposed equation for an embedded element pattern (E_m^e) placed in any arbitrary position (m) of the conductive surface or ground, now includes the effects of diffracted fields from the edges at each location (E_m^D) as well as the mutual coupling parameters of the array to an isolated element pattern, represented by E^{isol}. It also takes into account the cross-polarized component when it is usually neglected.

Magnetic Incident Field

Using the monopole radiation pattern as an example, the incident electric field will be expressed as:

$$E_\theta^i = \frac{1}{2}E_o \frac{\cos\left(\frac{\pi}{2}\cos\theta\right)}{\sin\theta} \frac{e^{-jks_{x,y}'}}{s_{x,y}'} \quad (3.27)$$
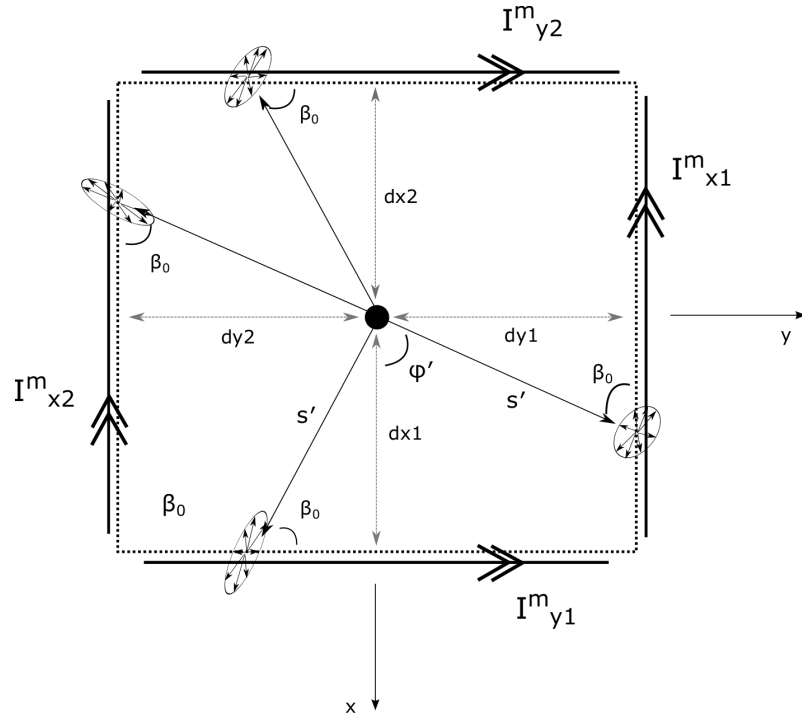
Figure 3.19: Illustration of the modeled four-edge equivalent currents.

$$\begin{bmatrix} s'_x = \sqrt{x'^2 + d_y{}^2} \\ s'_y = \sqrt{y'^2 + d_x{}^2} \end{bmatrix} \tag{3.28}$$

Given the expressions for the radiating element's electric field $E_\theta(\theta, \phi)$, the incident magnetic fields at the edges will be:

$$H_\phi^i = \frac{E_\theta^i}{\eta} \tag{3.29}$$

$$\begin{bmatrix} H_x^i = -H_\phi^i \sin\phi' \\ H_y^i = H_\phi^i \cos\phi' \end{bmatrix} \tag{3.30}$$

83

Diffraction Coefficient for Oblique Incidence

The implementation of the diffraction coefficient needs to be expressed as a function of the oblique angle β'_o and the distance from the source to the point of diffraction along the edges. Therefore, in the case of a hard diffraction, the magnetic incident fields will then be dependent on the distance to all the points along the edges, as well as the azimuth angle ϕ, which will determine the oblique incidence used in the diffraction coefficient function as well as the distance parameters.

$$D_h(L_{x,y}, \psi, \phi' = 0, \beta'_o, n = 2) \tag{3.31}$$

$$L_x = s'_x \sin^2\left(\beta'_o\right) = \frac{d_y{}^2}{s'_x} \tag{3.32}$$

Equivalent Radiating Fields

The electric fields radiated by the equivalent currents can be obtained by calculating the radiating fields from the four magnetic currents along the four edges of the ground plane. Using the magnetic currents from previous section, one can obtain the electric fields from vector potential $\mathbf{F}$:

$$\begin{bmatrix} E_\theta^F = -j\omega\eta F_\phi \\ E_\phi^F = j\omega\eta F_\theta \end{bmatrix} \tag{3.33}$$

$$\mathbf{F} = \frac{\epsilon e^{-jkR}}{4\pi R}\mathbf{L} \tag{3.34}$$

$$\mathbf{L} = \int \left[I_x + I_y + I_z \right] e^{jkr' \cos \psi} \, dl' \tag{3.35}$$

where $r' \cos \psi = x' \sin \theta \cos \phi + y' \sin \theta \sin \phi$ and $dl' = dx'$ or $dl' = dy'$

Radiating Field From Currents Along Y

$$F_y = \frac{\epsilon e^{-jkR}}{4\pi R} \left[\int \left(I_{y1}^m e^{jk\left(d_{x1} \sin \theta \cos \phi + y' \sin \theta \sin \phi\right)} \right. \right.$$
$$\left. \left. + I_{y2}^m e^{-jk\left(d_{x2} \sin \theta \cos \phi + y' \sin \theta \sin \phi\right)} \right) dy' \right] \tag{3.36}$$

$$F_\theta = F_y \cos \theta \sin \phi \tag{3.37}$$

$$F_\phi = F_y \cos \phi \tag{3.38}$$

Radiating Field From Currents Along X

$$F_x = \frac{\epsilon e^{-jkR}}{4\pi R} \left[\int \left(I_{x1}^m e^{jk\left(x' \sin \theta \cos \phi + d_{y1} \sin \theta \sin \phi\right)} \right. \right.$$
$$\left. \left. + I_{x2}^m e^{-jk\left(x' \sin \theta \cos \phi + d_{y2} \sin \theta \sin \phi\right)} \right) dx' \right] \tag{3.39}$$

$$F_\theta = F_x \cos \theta \cos \phi \tag{3.40}$$

$$F_\phi = -F_x \sin \phi \tag{3.41}$$

3.5 Summary

This chapter introduces the critical tools in diffraction theory used in this work. The use of two-point diffraction aids in the understanding of quickly placed elements along an arbitrary sized conductive surface. This provides the ability to characterize the ripples and variations in the radiation pattern caused by the diffracted fields introduced by the antenna's environment that can affect gain performance. As an expansion to this, the ECM takes in consideration every individual point of diffraction that can be calculated by the two-point procedure but throughout the complete edge, modeling the diffracted fields as an equivalent current. This brings the ability to calculate radiation fields with the use of vector potential theory in order to model the edges as though they where current sources. In the case of this study, the sources are modeled as magnetic currents, since the only used diffraction coefficient needed is for hard polarization due to the assumptions that the elements are close enough to the surface of the PEC and therefore, cancellation of the direct and reflected diffracted fields occur as shown in Section 3.3.2. In the next chapter, the use of this tools is integrated into quantifying the effect diffracted fields have on phased array antennas.

Chapter 4

Impact of Edge Diffraction in Finite Phased Array Antennas

4.1 Introduction

The tools that are provided in this manuscript aids in characterizing and quantifying in a more accurate way the effects that diffraction has on the radiation pattern performance of the antenna element in a phased array environment. This brings many questions to the discussion as to what aspects of a phased array performance can diffraction be a hindrance. The main aspects of the use of phased array technology is the capabilities of electronic scanning, high-gain with a low-profile, improved life-span of a radar with better failure rate and flexibility of beamforming techniques. However, diffraction can be a determining factor as to how well the phased array will perform under these metrics.

Specifically in weather radars, co-polarization mismatch is required to be minimized in order to have accurate estimates of the volumetric scans. It will be shown in this section under what situations can diffraction be a source of inaccuracy. Also, the cross-polarization performance, as discussed previously in Section 2.2, has to perform under certain levels in order to provide accurate
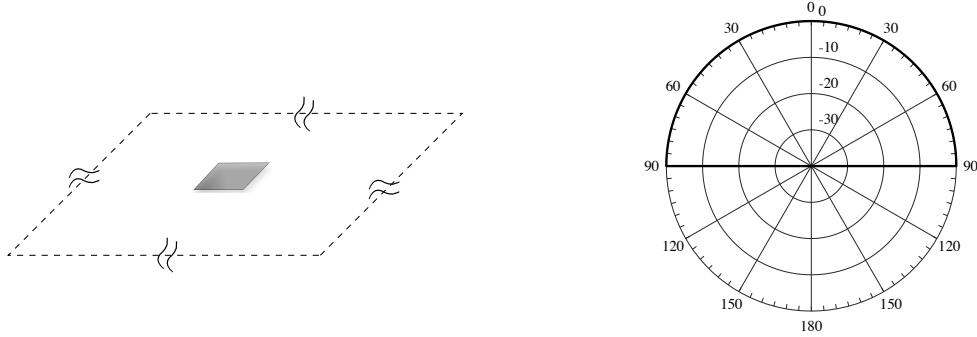
Figure 4.1: Geometric optics pattern with unit amplitude used to characterize diffracted field impact in phased array parameters.

measurements, diffraction however has a significant effect at the element level that can in situations be translated into array level detrimental pattern performance. Hence, for a large structured phased array, the introduction of gaps between panels, or internal gaps, can be additional sources of diffracted fields, that can be concerning. This chapter explores the extent at which diffracted fields play a role in these important metrics in PARs for polarimetric applications.

4.2   Co-polar Mismatch Study

Co-polar mismatch in a dual-polarized phased array antenna can be widely attributed to several factors.

1. Asymmetrical feeding between polarization ports of the radiating element.

2. Radiator structure.

3. Mutual coupling differences between polarizations.

4. Diffraction from the edges and other discontinuities.
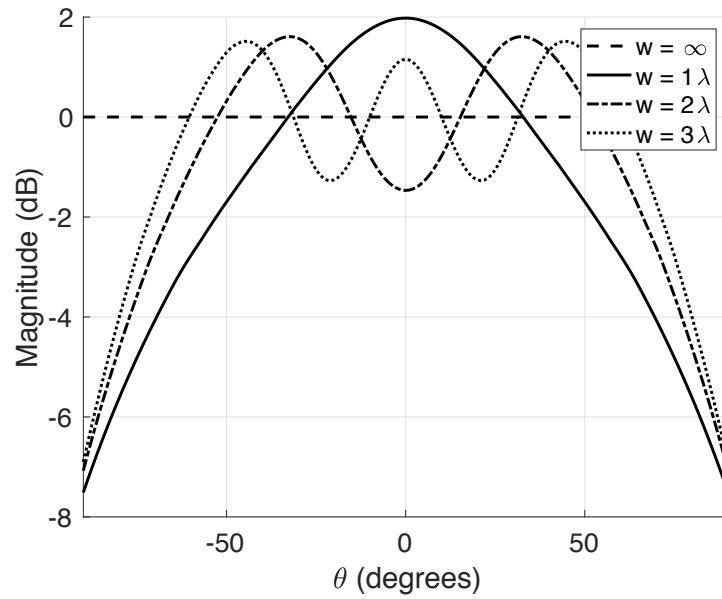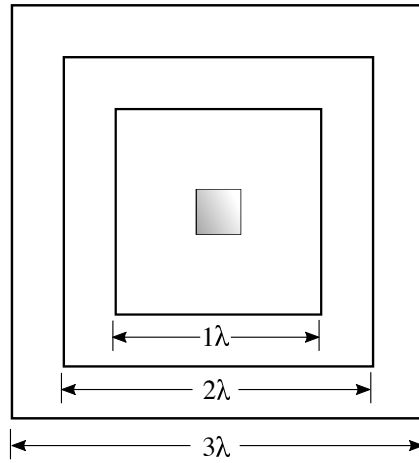
Figure 4.2: Calculated total fields of an ideal source over a ground plane of varying size (w).

In this study it will be shown what is the quantitative contribution and the behavior diffracted fields have on the overall pattern of a radiating element. As a test, a virtual ideal source of unit amplitude is used to evaluate the edge effects have in terms of diffraction to the radiation pattern. In this case, the pattern is placed in the center of a squared ground plane of PEC, see Figure 4.1.

As the size of the ground plane changes, so does the amplitude and phase of the diffracted fields that when added to the GO pattern causes rippling, as shown before in Section 3.3.2. Figure 4.2 shows how the varying size of the ground plane can have an effect on the resulting field from super-positioning the diffracted fields from point a and b. It is clear that as the distance to the element is increased, the number of ripples are increased in terms of lambda, therefore, varying the amplitude at any point close to broadside ($\theta = 0°$). Assuming that the element radiates in the orthogonal direction, representing the second polarization, the diffracted fields will have the same effect. This is because the distances from the element to both of the edges on either side, is exactly the same.

The following results show co-polar mismatch of a perfect radiation source with unit amplitude in all directions placed along the ground plane of a panel. As the element is placed in different positions of the ground plane, the amplitude of spreading of the wave in the edge is increased on one side in comparison to the other, making an asymmetrical pattern. One thing to note is that at the orthogonal dimension the distances to the edges remain equally, and an asymmetrical pattern as shown in element (1) is expected. Hence, this unequal distribution of electric fields in space will provoke a co-polar mismatch, especially when looking at broadside ($\theta = 0°$), as shown in Figure 4.3. The values of the mismatch level with respect to the element's position in a 5x5 configuration is presented in Table **??** and is illustated in Figure 4.4

Taking the diffracted values at each position of an arbitrary array of 25 elements. The points of asymmetrical illumination will give co-polarization mismatches in the embedded element pattern and therefore, diffraction is to be considered whenever it is of interest to illuminate individual elements with

90
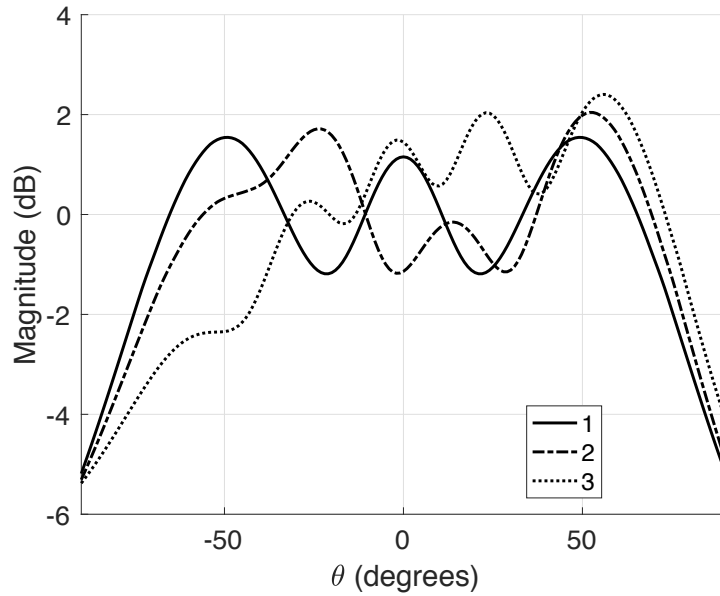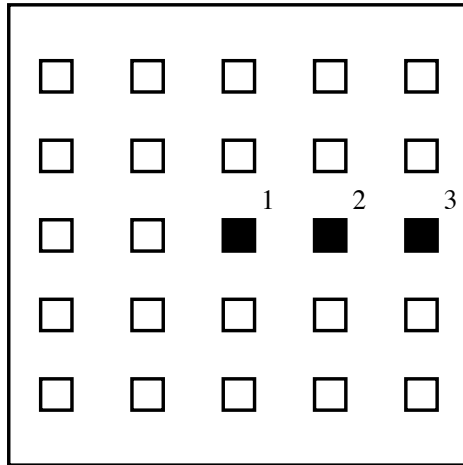
Figure 4.3: Calculation of the element patterns represented by the positioning over the ground plane.

different propagation techniques or selective illumination.

The results presented in Table **??** show the co-pol mismatch at boresight for different positions, as seen in Figure 4.4 assuming that the element radiates equally in both horizontal and vertical directions. However, it is well known that the antenna patterns for practical dual-polarized elements would
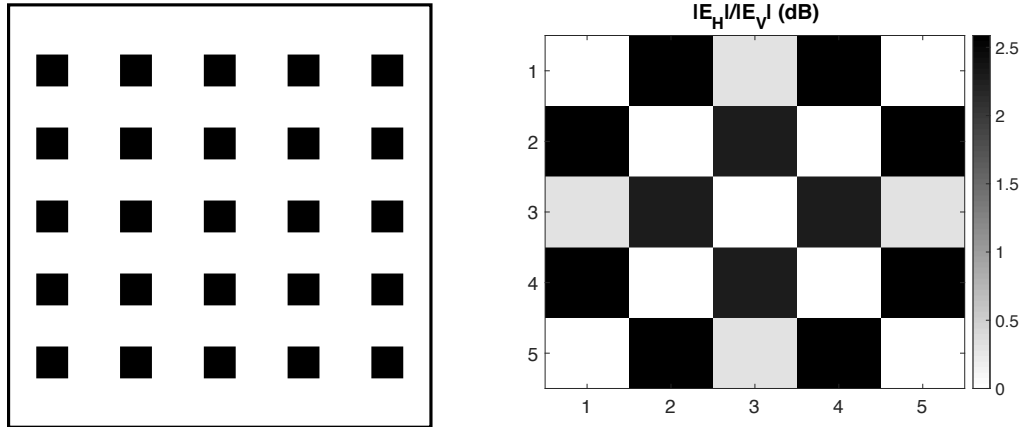
Figure 4.4: Illustration of the copolar mismatch at boresight ($\theta = 0°$) for each element of a 5x5 configuration. (a) Arrangement of elements (b) mismatch values with respect to element's position.

Table 4.1: Co-polar mismatch at boresight of the individual elements on a 5x5 array.

m/n	1	2	3	4	5
1	0.00	-2.59	0.29	-2.59	0.00
2	2.59	0.00	2.29	0.00	2.59
3	0.29	-2.29	0.00	-2.29	0.29
4	2.59	0.00	2.29	0.00	2.59
5	0.00	-2.59	0.29	-2.59	0.00

not radiate equally. This is due to the nature of the antenna structure and its radiation mechanism and how the antenna is being excited or what type of feeding structure it has. In the case of the MPA, it contains different radiation patterns for both E- and H-planes. Therefore when used as a dual-polarized element, both need to be taken into account.

4.3 The Average Embedded Element Pattern

Since the array pattern is the summation of all the embedded element patterns, the average embedded element pattern shows how the array will perform.

$$\mathbf{E}_{avg}(\theta, \phi) = \frac{\sum_{n=1}^{N} \sum_{m=1}^{M} \mathbf{E}_e^{nm}(\theta, \phi)}{N * M} \qquad (4.1)$$

The example shown in Figure 4.5, shows the average of all element patterns positioned along a single row of 5 different positions spaced 0.5λ apart. The diffracted fields are calculated for each position without the other elements presence or mutual coupling, therefore the elements do not interact with each other. The variation in diffracted fields will cause a rippling effect on the average element pattern. This effect is then dependent on the number of elements and the spacing between them. As the spacing is increased so does the ground plane structure over which the elements would be placed.

The array pattern will follow the amplitude of the average embedded element pattern and is evident that with the consideration of diffraction solely, there is a variation in gain when the array is scanned off of broadside ($\theta = 0°$) to 60°.

With different spacing between the elements, so does the distance between the elements to the edges and therefore, it will introduce changes in the average pattern. Another important distinction is that as the number of elements increases so does the average pattern. Its ripple will relatively flatten out for a more constant pattern but still will have some rippling present, especially at wider angles.

The rippling is therefore not solely related to mutual coupling in an array. to verify this several simulations are made in order to see what the effect that mutual coupling has on the embedded element pattern.

For an element like a MPA where the radiation pattern contains both E_θ and E_ϕ components, the average pattern would have different radiation pat-
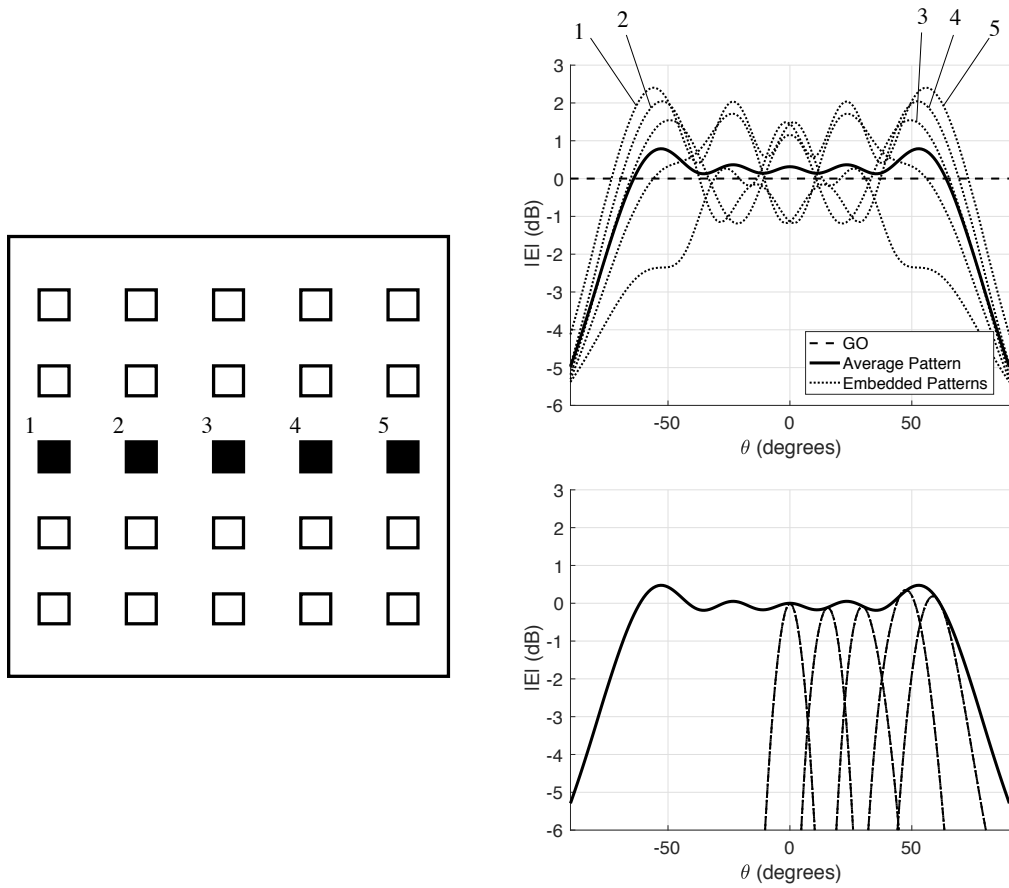
Figure 4.5: Element patterns for a 5x1 linear array are calculated with two-point diffraction and are overlapped. Below the overlapped isolated element patterns is the calculated scanned array patterns following the gain of the average element pattern.

terns in both directions. Due to boundary conditions, the roll-off and diffraction will have an effect on the pattern's gain as well as cross-pol performance.

To further analyze what is the contribution of diffraction to the general average embedded element pattern in a phased array antenna, simulations are made and analyze where the effect of mutual coupling is introduced. By simulating each element individually placed along the ground plane, mutual coupling will not be present but the element at each position will represent each isolated element.
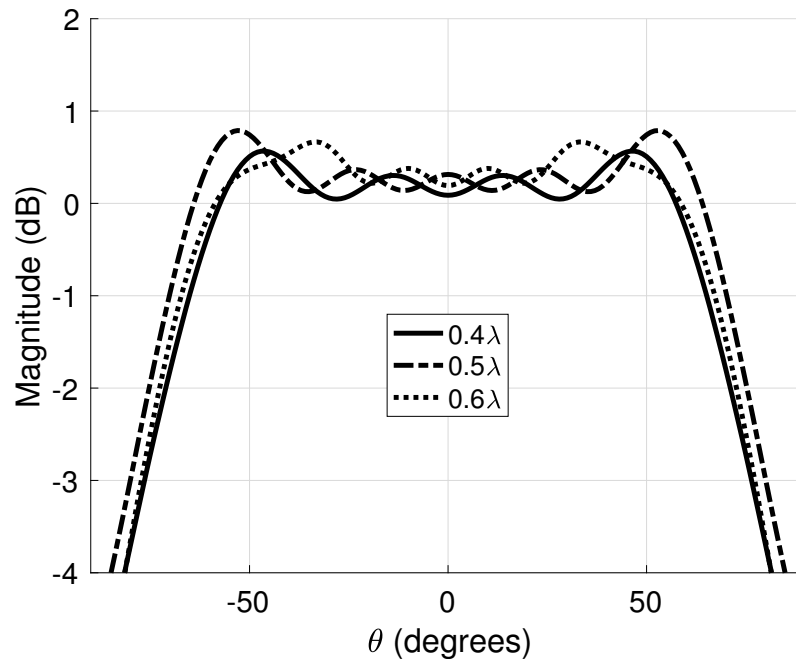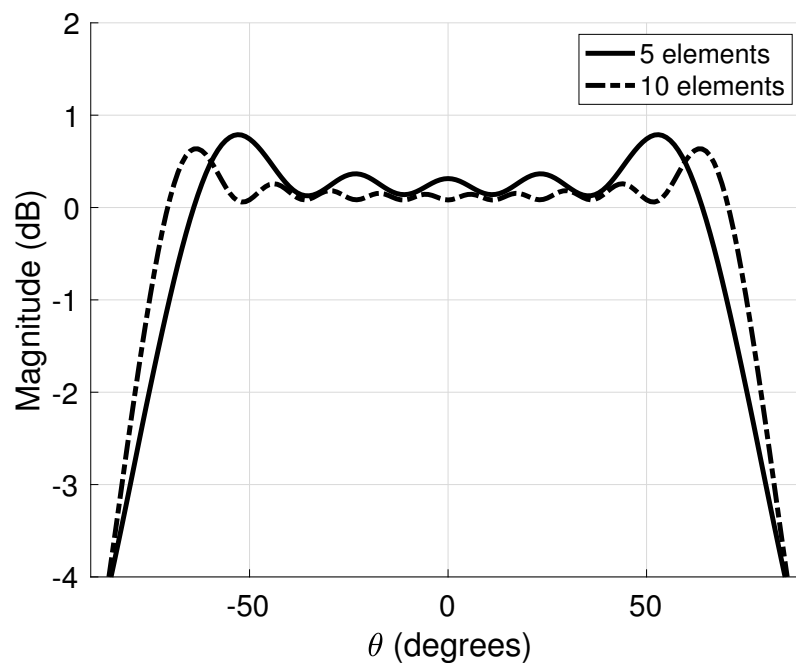
Figure 4.6: Total field calculations for (a) different element spacings for (b) an array with different number of elements.

In efforts to verify what the relationship is between the diffracted field and the average embedded element pattern, a comparison is made with and without the interaction between elements. It is well known that the phased array pattern is the summation of all the active elements in an array. The active element patterns are dependent on the mutual coupling between neighboring elements, and the diffracted fields associated with their location with respect to the edges. For this study, all elements are excited uniformly $(1\angle 0°)$ and the simulation is done for a populated array and the isolated element at each position. Hence, the results can be compared for the presence of diffraction at the element level with and without mutual coupling.

A conventional MPA fed with one probe, as shown is Figure 4.7, polarized linearly along $\phi = 90°$, is simulated for different scenarios. One where mutual coupling is along the E-plane and therefore a linear array along a row and along a column for an H-plane mutual coupling case. It is configured as a linear array along a row where the mutual coupling is then applied along the E-plane and a linear array along a column to apply mutual coupling along the H-plane.

By overlapping the embedded element patterns in this direction it is shown that there is no significant effect in the cross-pol on the E-plane. However, it is shown that in the E-plane, the rippling is present in the embedded element patterns and not in the H-plane patterns. This is because for the case of an element placed on the ground plane, only E_θ components will generate significant diffraction. Hence the co-pol pattern of the E-plane and the cross-pol pattern of the H-plane have present E_θ components where diffraction is affecting.

By simulating each individual element isolated but in a finite ground plane,
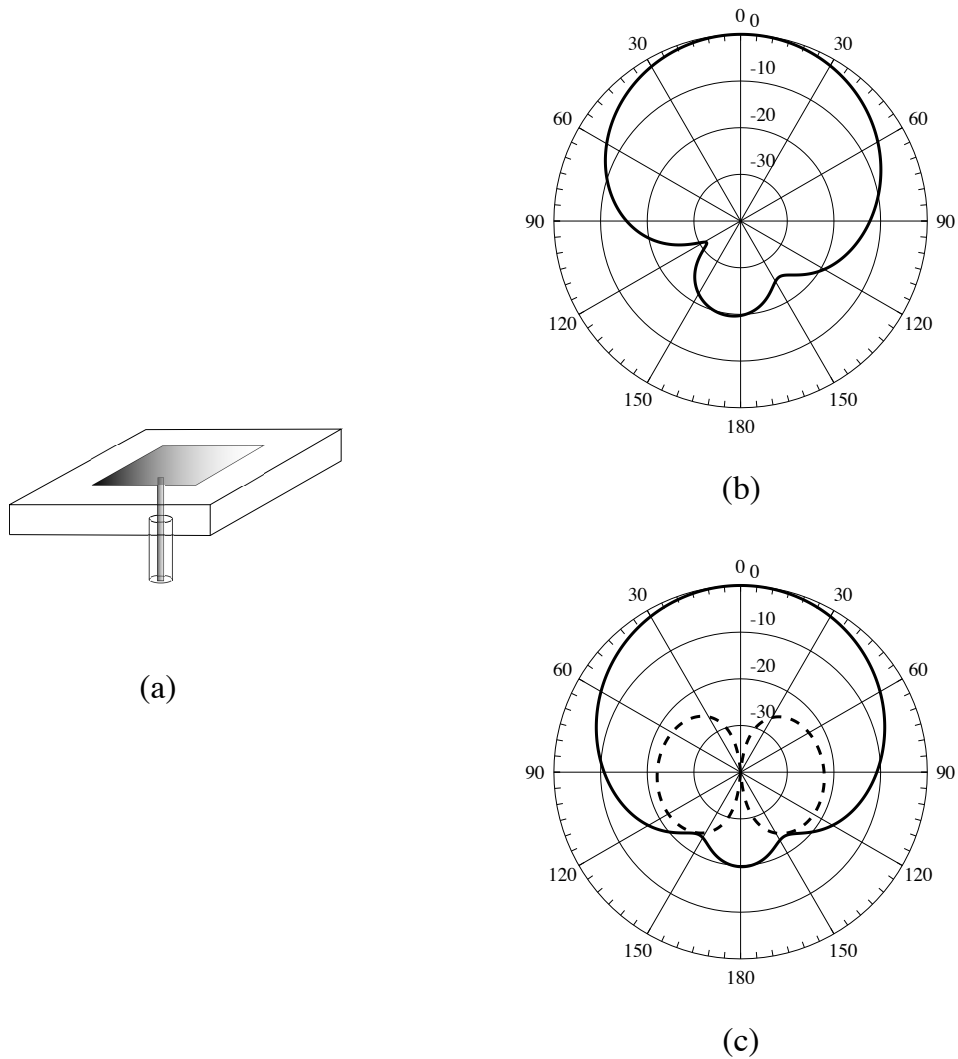
Figure 4.7: (a) One-probe single-polarized MPA unit cell used for the average pattern simulations. (b) E-plane and (c) H-plane patterns.

it is confirmed that the rippling of the pattern is solely due to the diffraction from the edges. It is interesting to note, that the cross-pol is not changing as the element is moved along the row, even though diffraction is present. In any case the cross-pol is actually higher compared to the populated case. This may be due to the fact that the energy is absorbed by the other terminated elements due to mutual coupling and consequently reducing any spurious radiation that
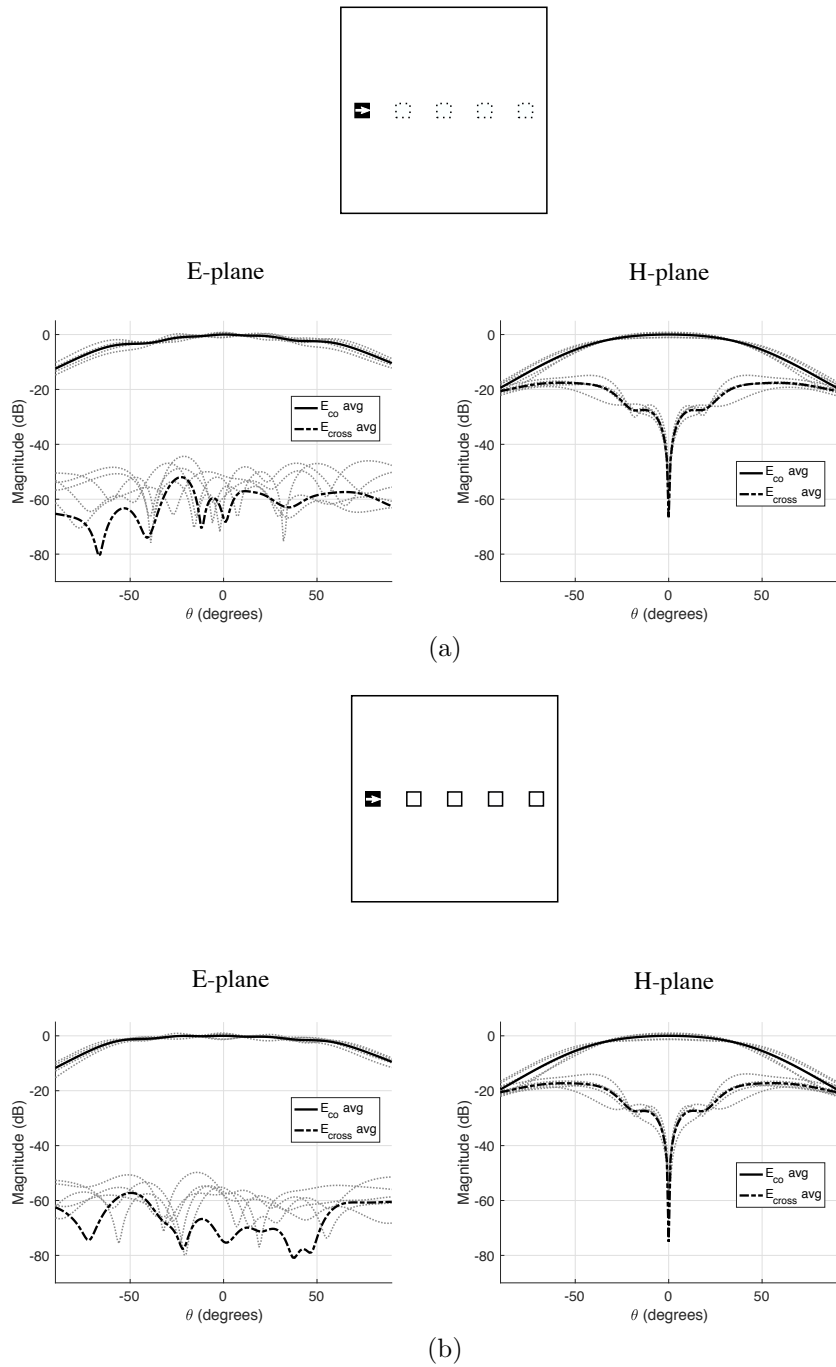
Figure 4.8: Overlapped embedded patterns for each E- and H-plane cuts at each location of a 1x5 array configuration for (a) an isolated element at each position and (b) for each element in the array environment with neighboring elements including mutual coupling.

may cause cross-polarization.

A case where a change in cross-pol can be appreciated is the elements aligned vertically in a column (along $\phi = 0°$). Something to point out is the E_θ (co-polarized field) component's ripples are barely changing element to element. In this case the elements distance to the edges in the E-plane are all equal. Therefore the diffracted fields produced are the same and hence, the pattern is not changing. Since the H-plane co-polarized field is an E_ϕ component and is tangential to the edge, the diffraction is almost negligible and therefore, does not change. Nonetheless the cross-pol in the H-plane, which is the E_θ component along $\phi = 90°$, does diffract when incident upon the edges and a small rippling can be appreciated. The cross-pol along the E-plane is where a significant change is seen from element to element, even in the isolated cases (see Figure 4.9), where the position where the lowest levels are is right at the center of the ground plane. As the element is moved closer to the edges the cross-polarized fields increase in magnitude. However, it is important to note that the average value maintains low. This phenomena suggests that the diffraction causing cross-polarized fields, if illuminated uniformly and symmetrically can cancel out. This however, may not necessarily be the case in real practical scenarios.

In almost all real scenarios for a weather radar application a full planar array is implemented. A fully populated case is simulated to show the embedded element patterns overlapped in Figure 4.10. The average patterns shown can be seen to have a lot more variation. This is due to the added element locations across the ground plane panel. For this reason, it is possible that the average cross-polarization is lower than all the other cases due to a more effective cancelation of diffracted fields. To maintain this adequate cancelation

Figure 4.9: Overlapped embedded patterns for each E- and H-plane cuts at each location of a 5x1 array configuration for (a) an isolated element at each position and (b) for each element in the array environment with neighboring elements including mutual coupling.

Figure 4.10: Overlapped embedded patterns at each location of a 5x5 array configuration for (a) an isolated element at each position and (b) for each element in the array environment with neighboring elements including mutual coupling.

all elements are assumed to be excited.

In conclusion, regardless of the presence of mutual coupling, the antenna gain variation is ultimately due to diffracted fields. The cross-polarized fields do increase dramatically per element if it is to be moved closer to edges that are tangential to the direction of polarization. To further study the effects of cross-polarized fields and diffraction in phased arrays, simulations are made with an element design that has high polarization purity and can be used for weather applications.

4.4 Cross-polarization Performance Study

As previously shown, cross-pol variations caused by diffracted fields can be sensitive in the E-plane. Simulating a differential-fed MPA the cross-polarized fields are reduced substantially the principal planes (E- and H-planes). Since the H-plane cross-polarized fields are significantly lower than a one-probe design, the changes in cross-pol, if any, in this cut can be appreciated. There is an effect from diffraction in this cut but only in the elements that are at the extremes, or right at the edges of the ground plane.

Since in the weather radar community the interest is to use radiating elements with low cross-pol in all of the scanning planes the element used for this study is a differential-fed MPA. In this particular design both ports are directly opposing each other with a 180° phase shift between port excitations. An illustration of this element is shown in Figure 4.11. With this phase shift, a uniform distribution of fields in the cavity allow for adequate cancellation of cross-polarized fields providing low cross-pol even in the H-plane compared to the conventional one probe design.

To demonstrate, the average embedded element pattern is shown in Fig-
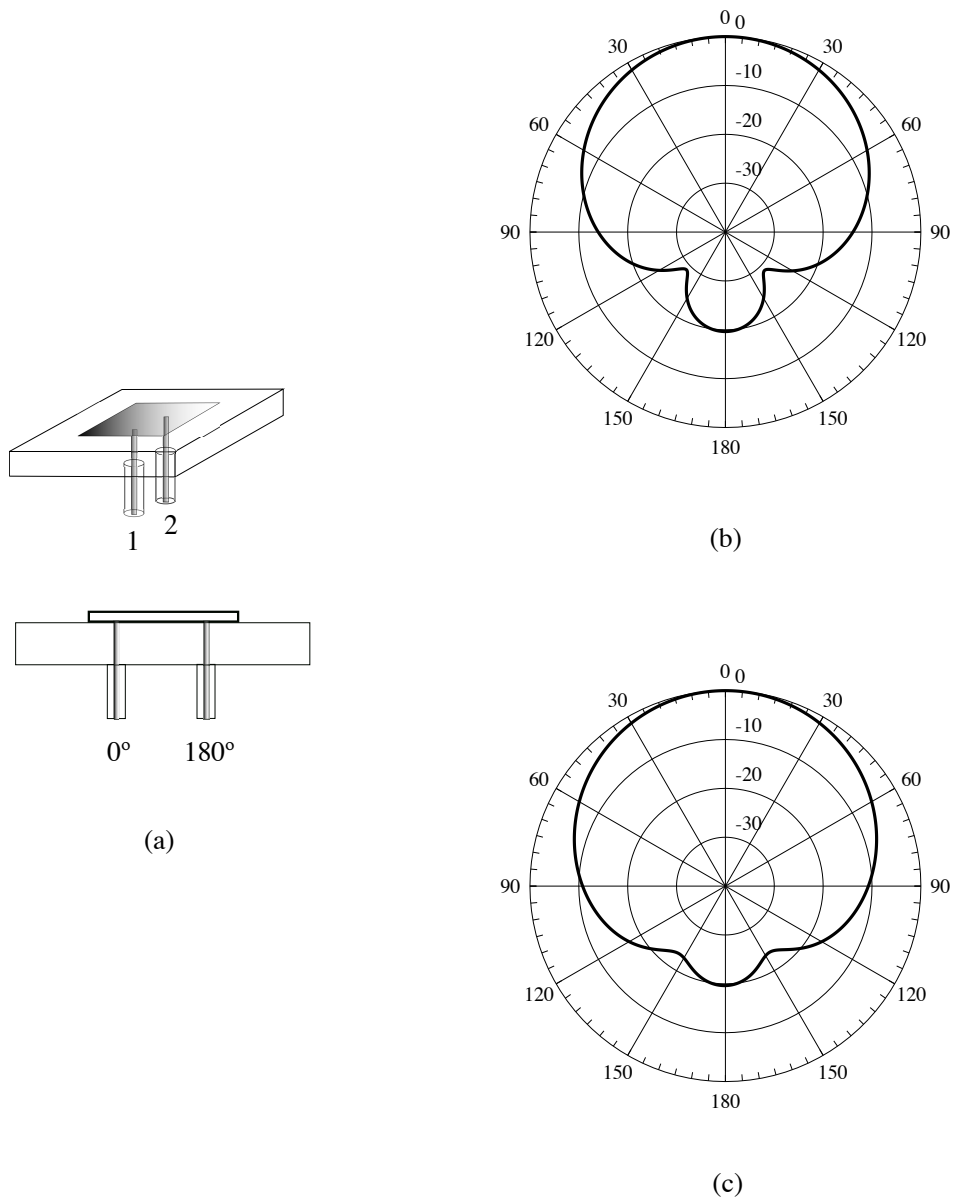
Figure 4.11: (a) Differential-fed single-polarized MPA unit cell horizontally polarized used for the average pattern simulations and cross-polarization characterization. (b) E-plane and (c) H-plane patterns.

ure 4.12 for both planes in both row and column configurations. Here, we can appreciate now any contributions in cross-pol degradation that could occur in the H-plane. It is observed that even though it is much lower, some locations
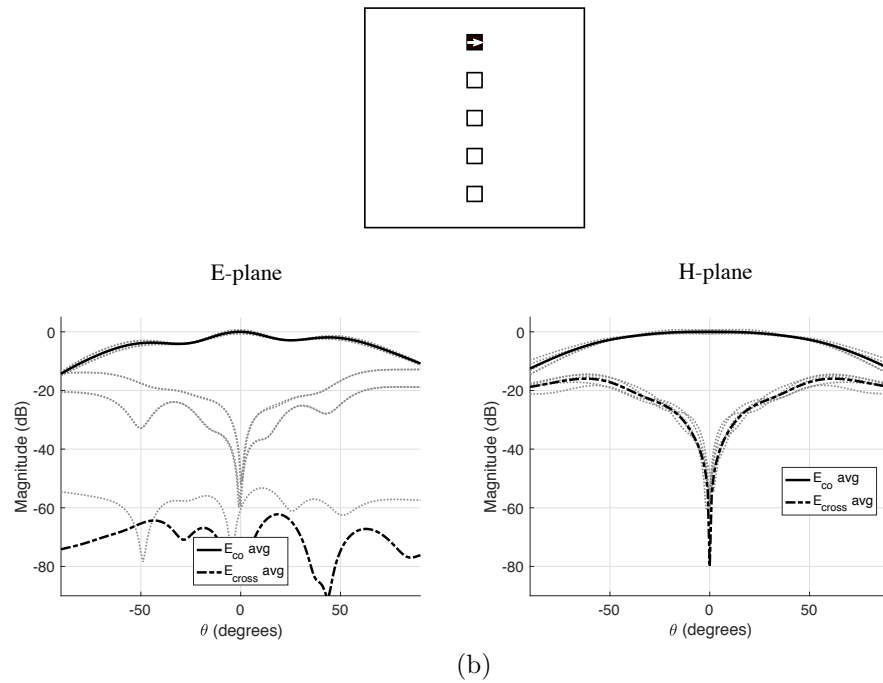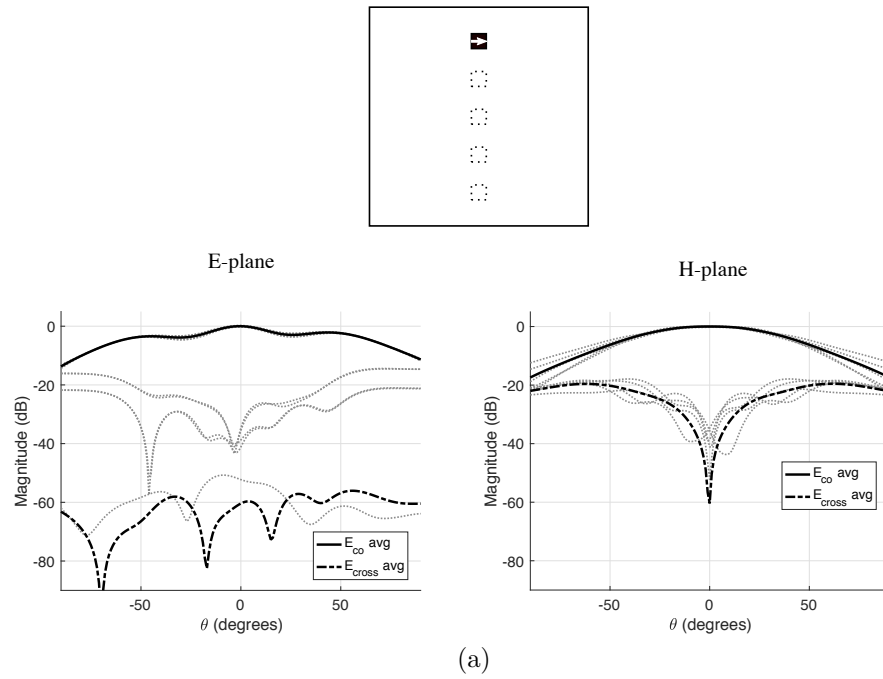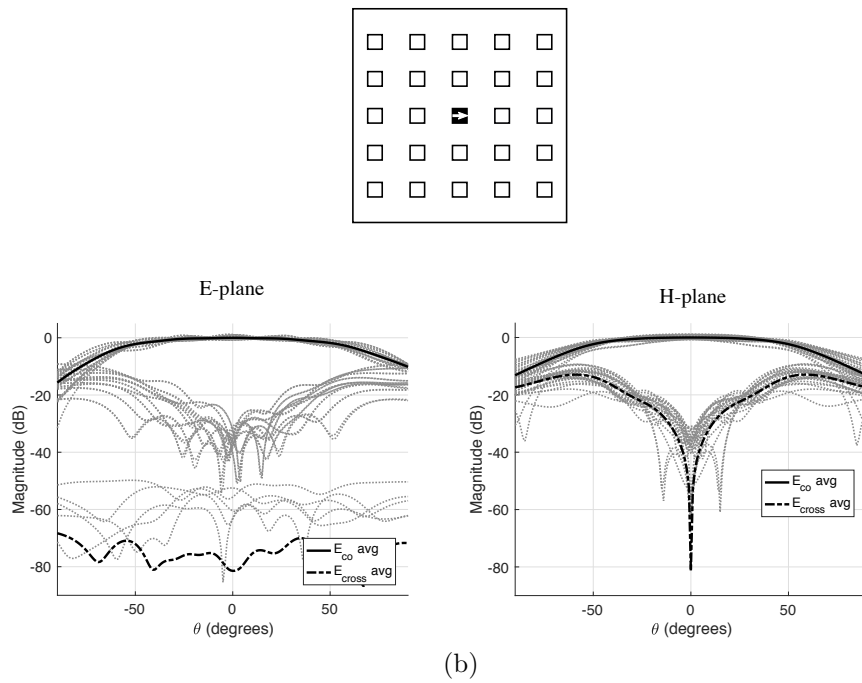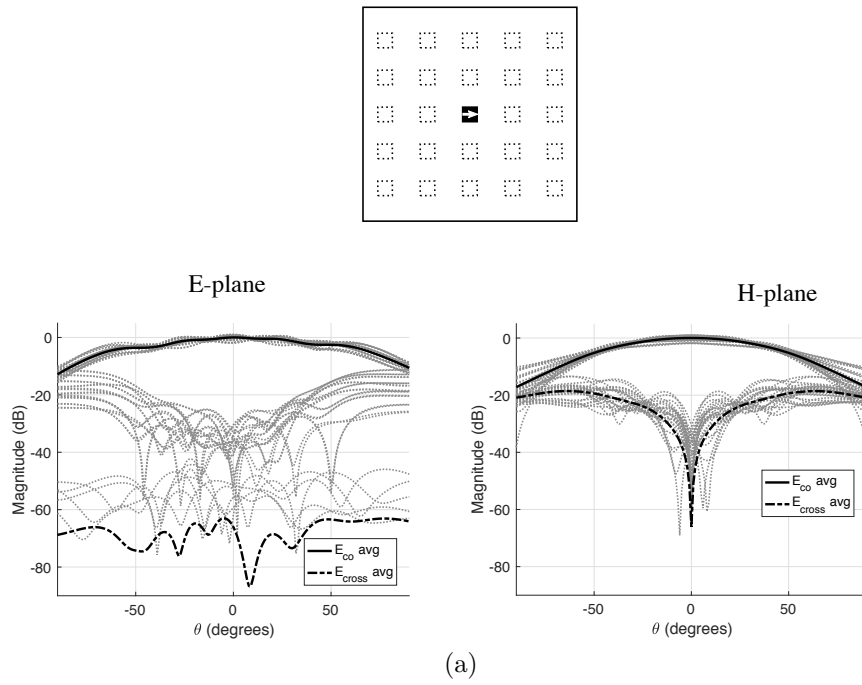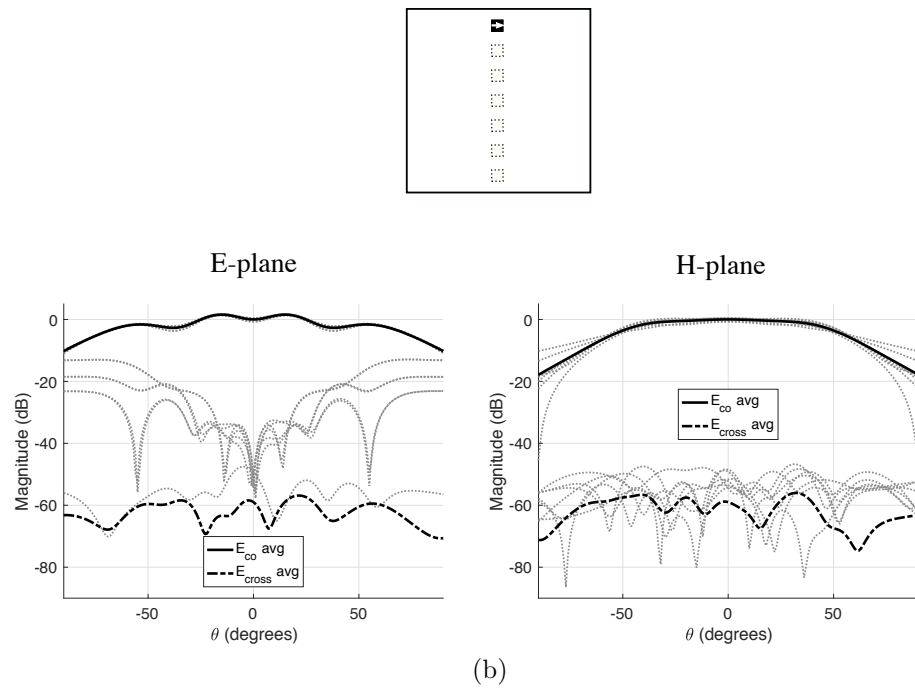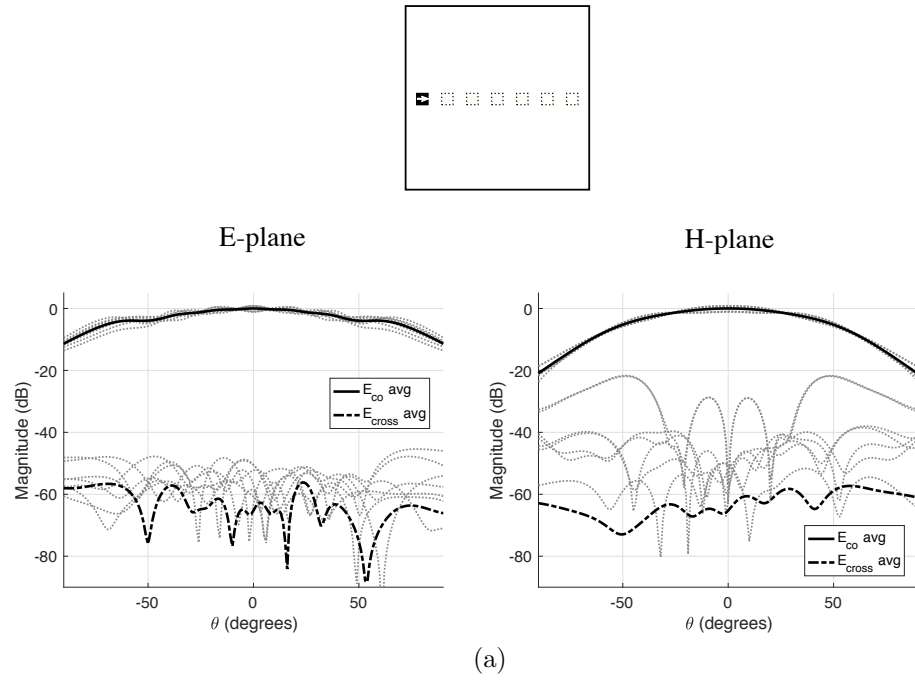
Figure 4.12: Overlapped embedded patterns at each location of an array configuration for (a) an isolated element at each position of a center row of 1x7 and (b) for each element in each position of a center column of 7x1 and their corresponding E and H-plane patterns respectively.

closer to the edge to give high cross-polarization values. However, it is less common than in the E-plane when the element is placed with its polarization parallel to the edge, as discussed before in Section 4.3.

To verify how the cross-polarization of an array is affected by diffraction, two different sized arrays are simulated for odd and even-numbered array. In Figure 4.13 both E-planes are shown for both array sizes. Even for this highly-pure element the observed behavior in cross-pol increase throughout the array is seen. Even-though the average pattern shows a low cross-pol on both configurations, the odd numbered array shows more cases where the cross-pol is maintained low. This is because these elements are in the middle row therefore the symmetry doesn't generate diffracted fields that would show up as E_ϕ components. However, in the even array since there isn't a middle row, but all elements are off center or off-axis, therefore if every single element is considered, they all will have high cross-pol values unless they are all added and therefore, cancelled, when they are illuminated.

The even array has elements all around the origin but not exactly in the center of a coordinate. The odd numbered array has elements along ($x = 0, y = 0$), ($x = x', y = 0$), and ($x = 0, y = y'$). Therefore, these considerations are important because the elements at which lie in the center of the panel have different cross-pol components (potentially co-pol as well) between H- and V-polarizations. Therefore a failed element test is to be done in order to verify the feasibility of using either.

From the current results taken from the even array it is confirmed that all of the elements have a higher cross-polarization on their own. However when added and averaged it is way below. However this adds elements with higher cross-pol that are more dependent on the symmetry of illumination.

(6x6)

(7x7)
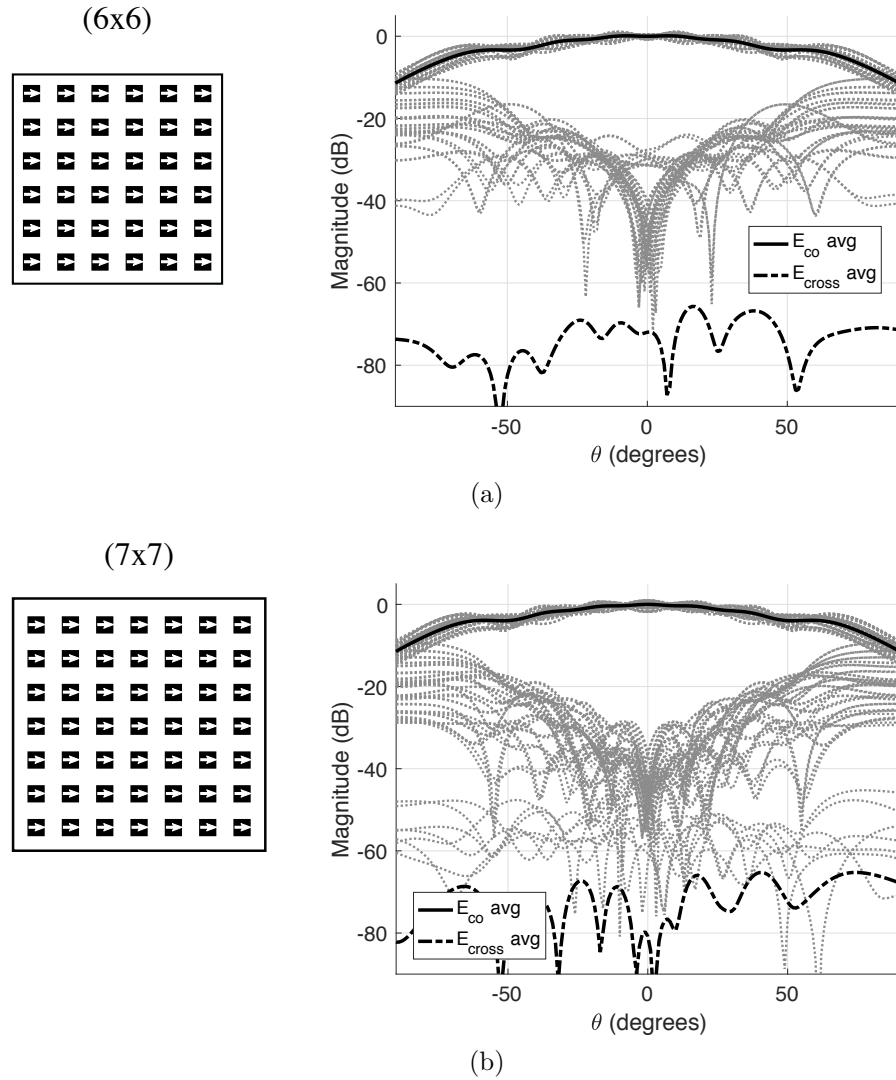
Figure 4.13: Overlapped element patterns at each location of a (a) 6x6 even-numbered array configuration and a (b) 7x7 odd-numbered array configuration.

In order to verify the feasibility of the phased array performance whenever it is operating long term, a failed element analysis is done. In order to ensure it will work properly for polarimetric weather measurements, the phased array must perform under the required sidelobe level, co-polar mismatch, and cross-polarization performances throughout the phased array's scanning range. In

0.37	0.47	0.61	0.61	0.47	0.37
0.47	0.60	0.77	0.77	0.60	0.47
0.61	0.77	1.00	1.00	0.77	0.61
0.61	0.77	1.00	1.00	0.77	0.61
0.47	0.60	0.77	0.77	0.60	0.47
0.37	0.47	0.61	0.61	0.47	0.37

E-plane | H-plane

(a)
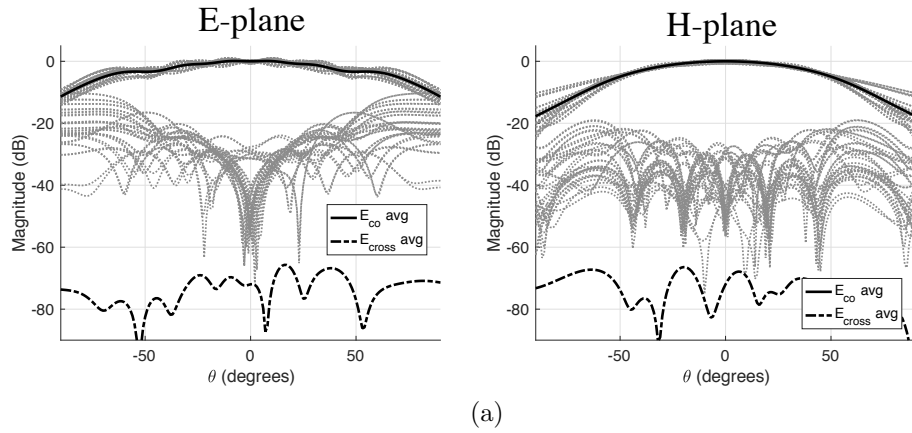
0.37	0.47	0.61	0	0.47	0.37
0.47	0.60	0.77	0.77	0.60	0.47
0.61	0.77	1.00	1.00	0	0.61
0.61	0.77	1.00	1.00	0.77	0.61
0.47	0.60	0.77	0.77	0.60	0.47
0.37	0.47	0.61	0.61	0.47	0.37

E-plane | H-plane

(b)
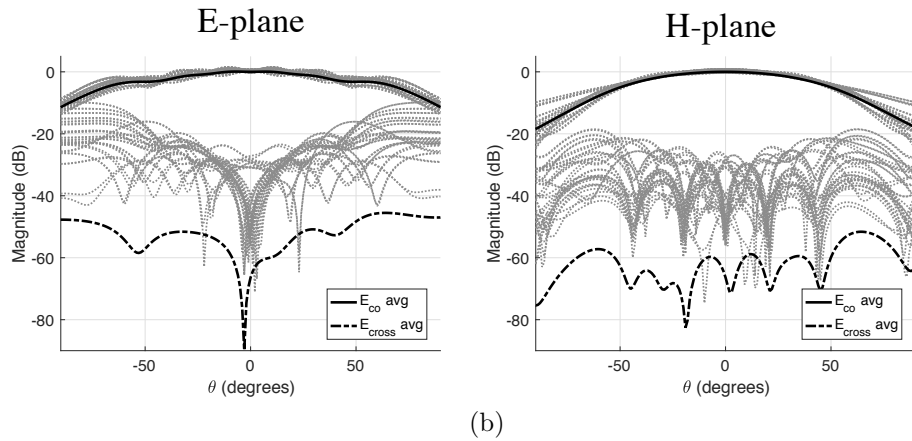
Figure 4.14: Overlapped embedded patterns at each location for a 6x6 array configuration with (a) tapering and no failed elements and (b) for tapering with a 5% element failure without the presence of mutual coupling.
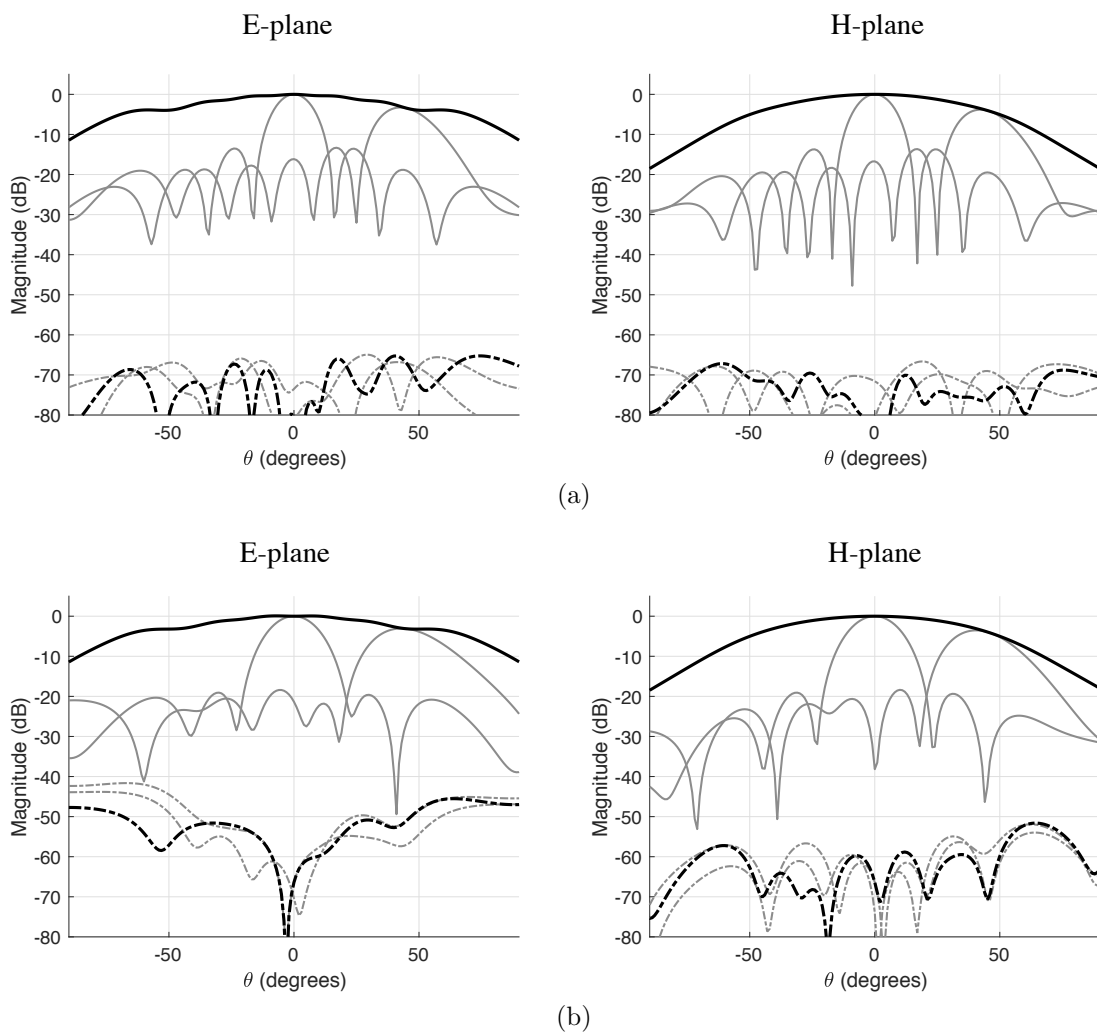
Figure 4.15: Overlapped array scanned patterns with the average embedded element pattern for the previously discussed 6x6 configuration of differential-fed MPA showing (a) all elements active and (b) a 5% element failure.

this study both the odd-numbered and even-numbered arrays are introduced a failure rate percentage in order to verify the performance of the configurations for long-term assessment.

A simulation is done for both panels and with a 5.56% failure rate, for a 36 element array once can easily see a significant increase in cross-pol levels of about 20 dB, which can be detrimental if the individual radiating elements have a limited cross-polarization at about the requirement. This is why it is

important to use well isolated elements from the start.

Using the metrics specified in this work, the overall cross-polarization level thought the scanning range can show the impact a percentage of failed elements can have on both situations, which can be potentially modeled using the 4-edge ECM method discussed in this work.

4.4.1 Internal Gaps

It is common practice that PARs be designed for scalable capabilities. Large structures are extremely hard to fabricate let alone do maintenance on. When the failure of elements arises or any other type of complications in the system, subarray panels can be swapped easily and effortlessly. The use of subarray panels however, introduce multiple points of discontinuity around the antenna elements. This can potential affect multiple elements, especially the elements at the edges [13].

In Figure 4.16 a simulation shows the added cross-polarization due to these "internal gaps". An interesting observation is that the co-polarized pattern is practically unchanged. The real problem comes with electric fields of low magnitude start to affect low-magnitude fields such as the cross-polarized fields in a pure polarized element.

What this shows is a confirmation that the level of polarization is highly dependent on the polarization of the excited element and its positional relation to the edge. Furthermore, the mere presence of a discontinuity has an effect in the cross-polarization. For instance, in this example, just small increases of only 0.01λ are enough to cause perturbations in the cross-polarized fields.
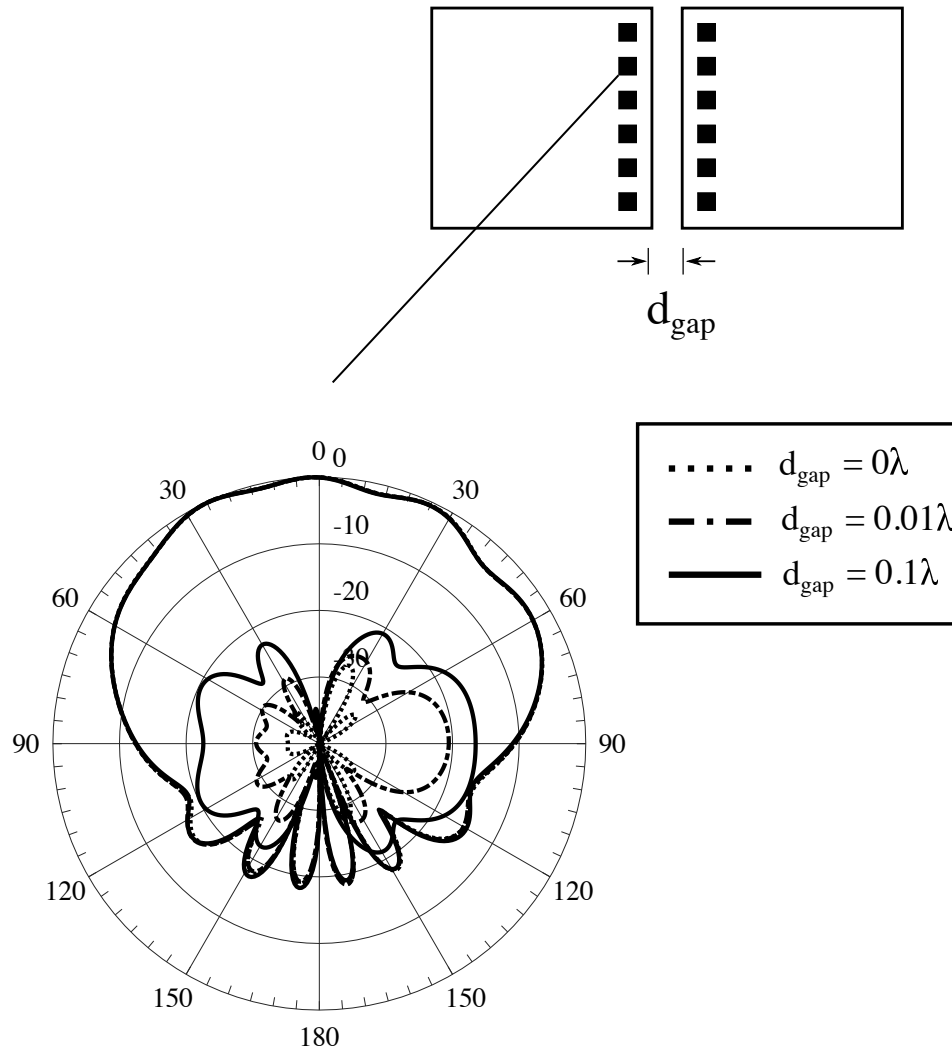
Figure 4.16: Simulated results of radiation pattern of element tangentially polarized to the internal gaps between two panels.

4.5 Mutual Coupling

Mutual coupling in the monopole antenna case is strong, since the maximum radiation intensity is at end-fire and therefore, towards the other neighboring antennas. However, reflections are so large that it causes stronger scattering at the edges. Therefore, this is why it is of interest to study the effects of mutual coupling with the monopole array. First we will look into when does
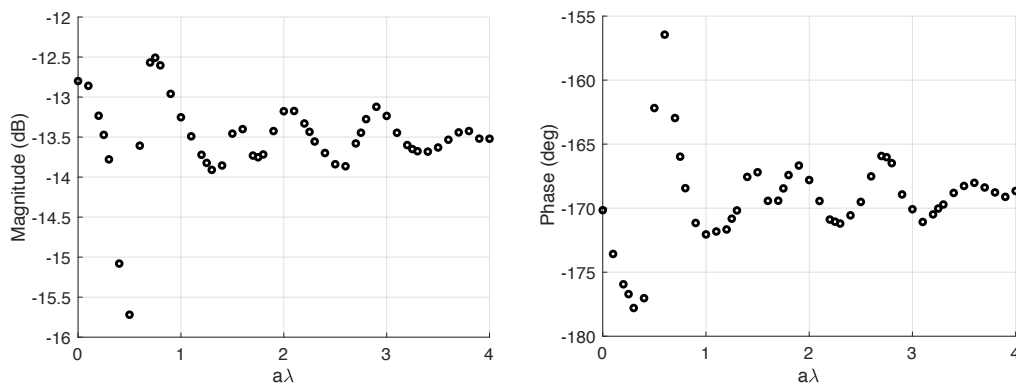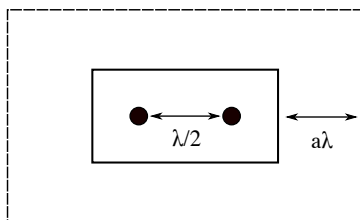
Figure 4.17: Two $\lambda/2$ sized unit cells containing monopoles are placed with a fixed separation of $\lambda/2$ and the ground plane is increased by a factor of a in terms of λ. The magnitude and phase of the mutual coupling between the two elements is illustrated.

the edges have an effect on the mutual coupling between two fixed antennas with $\lambda/2$ separation (see Figure 4.17).

These results can show the variability that edges can impose on the mutual coupling between elements. Until reaching a uniform contribution at an extended ground plane of 1λ or more. Therefore elements at right at the edges or discontinuities in a ground plane are prone to mutual coupling variances. Figure 4.18 shows how the presence of a finite ground plane can affect the mutual coupling for a column of elements. The added scattering from the diffracted edges add to the mutual coupling parameter's intensity along the edge. This is of importance to notice when an array now is populated by gaps in between subarray panels.
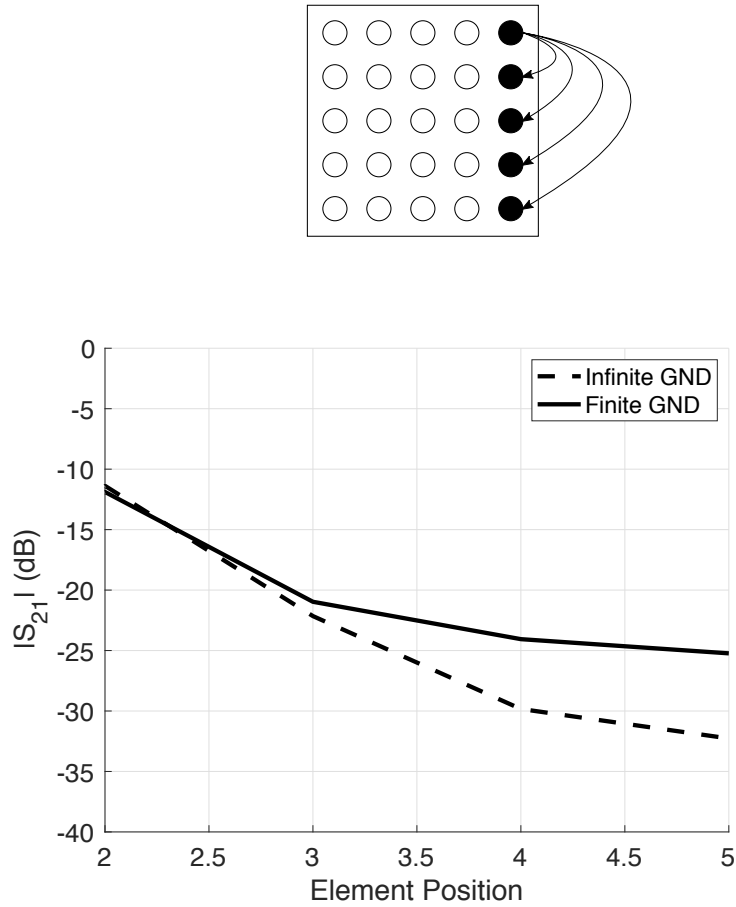
Figure 4.18: Simulated 5x5 configuration of monopoles with an infinite and a finite conductive surface (2.5λ) to show the effects of added scattering from the edges to the final column of the array.

4.6 Summary

This chapter illustrates the general impact edge diffracted fields have on the performance of phased array antennas. An analysis based on the positioning and polarization excitation is done in order to show the effects edge diffraction has on the individual element patterns of an array. This then translate to differences when steering the beam of the phased array. The results show that for elements with low levels of cross-polarization isolation, once they are moved from a central position of the ground plane, cross-polarization contamination

solely due to its positioning with respect to the edges is introduced.

Hence, depending on the number of elements in a phased array, the individual active element patterns will have different levels of distortion. However, once all of them are taken into account as a whole, these diffracted field contributions can cancel out and null itself. This is only if, the element is exactly the same throughout and has the same radiation characteristics for every element in position. If there is a slight shift in position or performance this cancellation might not be as effective.

Another important observation done in this chapter is the effect that the element excitation errors may potentially have on the array performance. The array performance will be dictated by the average embedded element pattern. Hence when a number of excitation errors are in the form of failed elements, the average embedded element pattern shows an ineffective cancelation of the edge effects. Therefore, the embedded element pattern shows higher cross-polarization levels, which results in higher cross-pol when scanning the array. Finally, this is even truer for the case where there are multiple sources of diffraction, as is the internal gaps between subarray panels in a larger-scaled PAR.

Considering the effect the reflections caused by the edges have on the mutual coupling parameters of the array is another important consideration. The last few figures show the importance of knowing the effects the edges can have on the mutual coupling between elements, especially along the edges. This then is translated to the active impedance of the elements and in turn could affect calibration techniques based on mutual coupling as well as the scanning performance of the PAR.

Chapter 5

Analytical Model Validation and Results

5.1 Introduction

In recent years, antenna performance requirements in cross-polarization levels have pushed boundaries in design. One good example is the design of radiating elements for the use of weather radar phased array technology. In this application, simultaneous transmit and simultaneous receive (STSR) polarization mode is used, where the cross-pol level requirements are down to -40 dB for scanning the array in principal planes and -35 dB for scanning in nonprincipal planes [50], [68]. The design of arrays for weather radar applications requires large panels that are produced in tiles or subarrays to comply with fabrication and mechanical limitations. This introduces gap discontinuities between subarrays when mounted in the front panel of the system.

Discontinuities in the conductive plane of antenna arrays produce diffracted field levels that can reach about -30 dB and affect the performance of elements the closer they are to the discontinuities or edges of finite arrays [13]. These fields can greatly disrupt the cross-polarization level of individual elements and can result in higher levels when scanning an array pattern off of broadside and at nonprincipal planes. This should be of great importance especially

for cases like large fully-digital phased arrays, where individual elements are excited independently to form multiple beams from different sections of the array [69]. The effects of the discontinuities could greatly contaminate the cross-polarized fields for individual scanned patterns. A mathematical model is ideal to predict such scanned patterns where an extensive array might require too much resources for numerical simulations.

There has been previous attempts to model the embedded elements of an array and their cross-polar components including the mutual coupling in the presence of edge effects [42]. However, this does not take into account the diffraction effects directly in the pattern. The element patterns can be affected by the presence of mutual coupling as well as edge effects [70]. This work only considers the effect in the mutual coupling parameters and no emphasis done to cross-polar components of the radiation pattern. For a monopole antenna array, the effect of mutual coupling is considered theoretically and experimentally [71]. Yet, there has not been a study where the individual embedded elements and the contribution of edge effects to the shape and amplitude of the individual cross-polar patterns based on their location in a finite ground plane.

The calculation of fields present in the radiating element's illuminated and shadow regions, usually referring to the front and backside of the ground plane respectfully, are made possible with the use of the Uniform Theory of Diffraction (UTD) [72]. This theory provides a dyadic diffraction coefficient capable of producing an approximation based on an asymptotic solution of the diffracted fields due to discontinuities in conductive surfaces and wedges. Further implementation of this model is seen for calculating diffraction due to a geometry's finite edge where radiation integrals are necessary to produce the fields at

the caustic region by means of equivalent currents [73]. The use of the UTD method and its extension, to what is known as the equivalent current method, is used to evaluate diffraction from ground plane edges in common antenna elements, such as aperture antennas, in both its principal E- and H-planes [29]. This provides a combination of diffraction techniques and radiation integrals in order to produce a solution for the fields produced by wedges of finite lengths.

As will be shown in this chapter, the effects diffracted fields have on the antenna radiation pattern can be in the form of amplitude and phase errors for each individual element, which are translated into calibration issues, as well as degradation of cross-polarization isolation. Diffracted fields are produced by an incident field upon a discontinuity in a conductive surface. These discontinuities are usually in form of vertex, edges, or curved surfaces. Depending on what geometry the incident field comes upon and the distance from the radiating source, the diffracted field can cause certain effects, which will be shown in this study.

The following sections will present the implementation of the analytical model to various cases. The first case involves the monopole antenna, which as mentioned before in this dissertation, it is a great tool to theoretically prove the generation of cross-polarized fields from a wire antenna which contains purely co-polarized fields. Experimental results are shown as well as an analysis based on simulation and calculation of the displacement of the antenna and the cross-polarized levels generated. Last, a MPA element is introduced to validate the 4-edge ECM analytical model. A combination of numerical analysis, which includes FEM from a simulated antenna element with an infinite ground plane, is used to calculate the effects from the edges analytically and compare with

likewise simulated FEM results from a finite ground plane of the same size.

5.2 Monopole

The monopole antenna, as seen in Figure 5.1, is a fundamentally basic element that theoretically produces E_θ components along all azimuth (ϕ) angles. This element is chosen for this study because its theoretical value for the cross-polarized component (E_ϕ) is zero. Besides being an element of theoretically pure polarization along elevation (θ) angles, it is also an element that radiates uniformly in all directions along every azimuthal cut. Because of these reasons, the monopole proves to be a good case for identifying and illustrating the effects that an antenna element would be subject to when introduced to finite edges, particularly a dual-polarized antenna. Figure 5.2a and b show a comparison of simulated monopole antenna patterns in its array environment in two different positions with and without neighboring elements that introduce mutual coupling. This clearly demonstrates that the monopole antenna in the center is purely polarized in θ, even with mutual coupling introduced, while the ϕ components are present solely due to diffracted fields from the edges.

The most straightforward way to predict the radiation pattern of an element with the effects of the diffracted fields from the edges of a conducting surface is by calculating the two-point diffraction with the use of the dyadic coefficients in diffraction theory. The diffraction coefficients are determined by the distance from the source to the point of diffraction, the angle of incidence, and the geometry of the wedge. This method only needs a point of diffraction on each side of the ground plane in a single cut in azimuth (ϕ). For the case of this study, the ground plane has four straight edges and assumed to be a strip where the wedge has no angle.
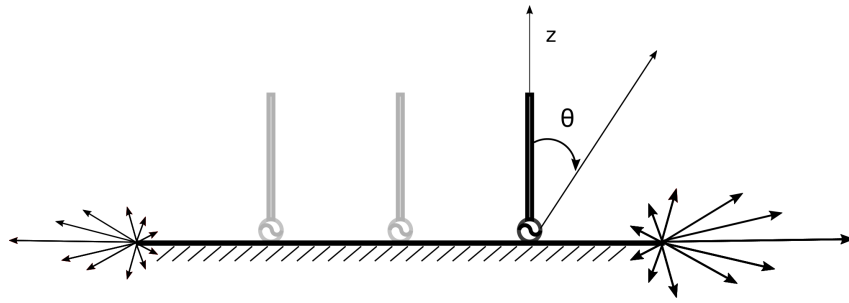
(a)
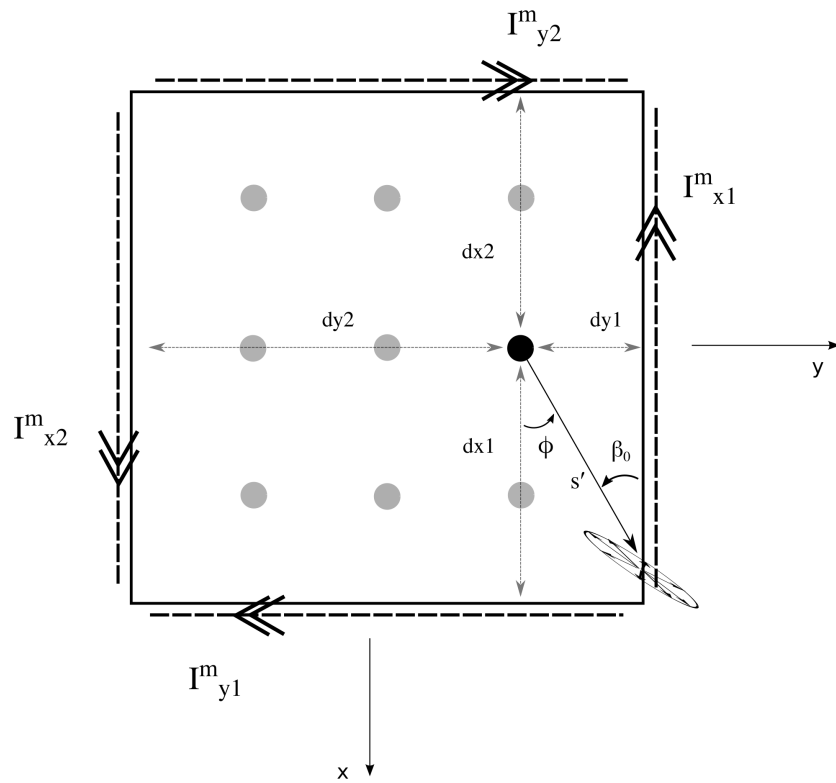
(b)

Figure 5.1: (a) Side view illustration of diffracted fields generated by the placement of a monopole along a ground plane and (b) a top view including the equivalent currents generated by a monopole antenna of about $\lambda/4$ in length on a finite ground plane [62].
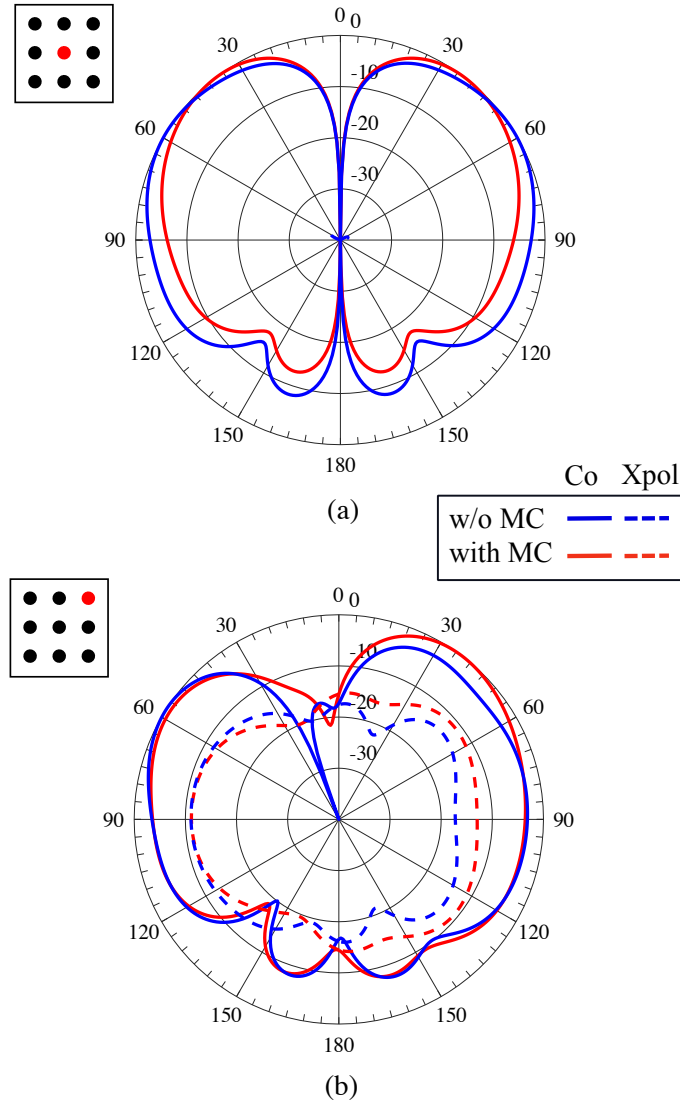
Figure 5.2: A comparison of a simulated $\lambda/4$ monopole element at 5.45 GHz placed in the (a) center [0,0] position and (b) corner [1,1] position of a $\lambda/2$ spacing 3x3 array configuration with and without neighboring elements for mutual coupling [62].

Since, for the case of the monopole antenna, E_ϕ is theoretically zero, the diffracted fields using the two-point diffraction can only be determined for E_θ components at any point Q_D along the edge, shown as $E_\theta^i(Q_D)$. The diffraction coefficient used is determined by the orientation of the incident field upon the
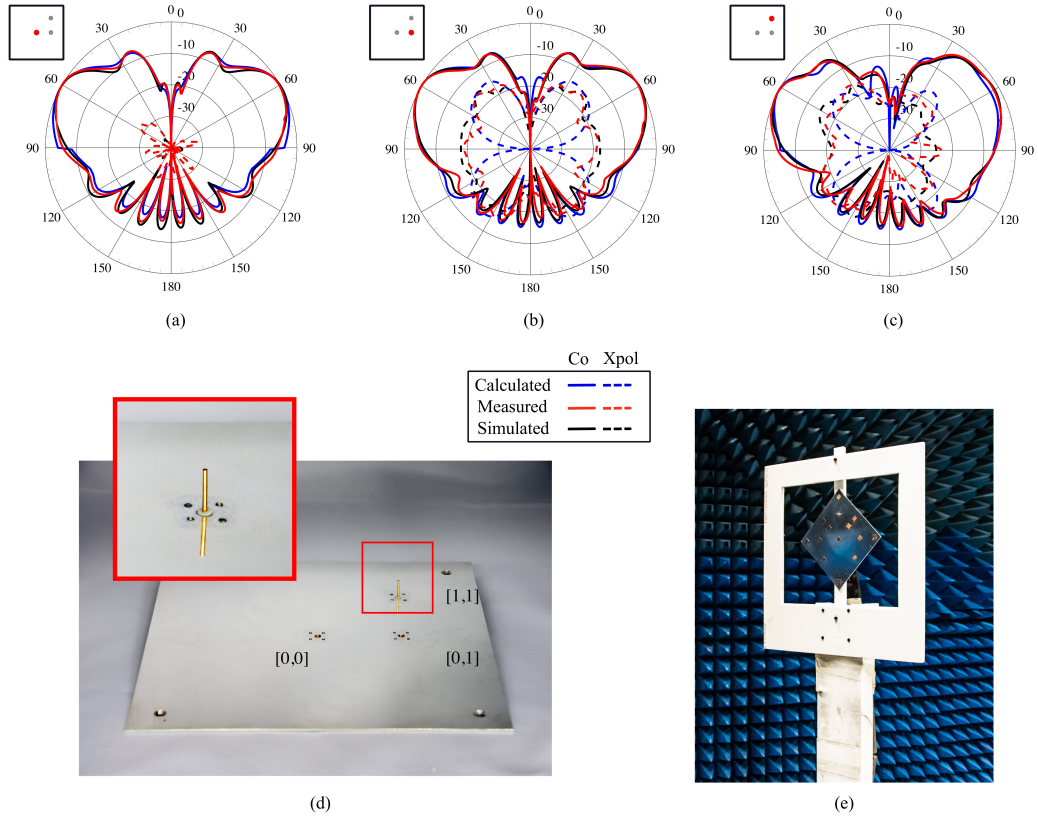
Figure 5.3: Comparison of theoretical (proposed method), simulations, and measured results of an isolated monopole antenna patterns with the effect of diffracted fields on co- and cross-pol when placed at (a) center [0,0] position, (b) edge [0,1] position, and (c) corner [1,1] position on a 4λ sized ground plane at 5.45 GHz. The (d) relatively thin (1.57 mm) aluminum sheet is (e) mounted on an electromagnetically invisible pedestal for far-field measurements [62].

wedge. All incident field components from the monopole are perpendicular to the edge, therefore, only hard diffraction coefficient is considered. Considering that E_ϕ components are zero and the grazing angle of the incident field with respect to the surface is considered to be $0°$, the soft diffraction coefficient is omitted and only E_θ^D diffracted fields can be determined. However, due to the diffraction phenomena itself there are diffracted fields that have E_ϕ components in practice, as seen in Figure 5.2b.

In theory, one of the sources of cross-polarization contamination is known

to be mutual coupling of antenna elements in an array [74]. There is cross-polarization increase whenever an element is in the presence of mutual coupling as does its radiation characteristics in general due to changes in its input impedance. However, Figure 5.2 shows that diffraction will be a predominant factor introduced into specific antenna elements, especially when the fields that are being diffracted originate from asymmetrical positioning of the elements.

The monopole cases presented in Figure 5.3 show proof that a highly-pure element such as a line of current along z, presented here as a monopole, cross-polarized fields of high levels are introduced entirely out of diffraction from the edges. This can be confirmed by the theoretical model presented in this manuscript where the element at the center, shown in Figure 5.3a, has no cross-polarized fields due to cancellation of symmetrical equivalent currents. When the antenna element is moved asymmetrically (off-center), as illustrated in Figure 5.3b and c, cross-polarization levels increases significantly due to added E_ϕ components. This is because contributions of diffracted fields from edges that are illuminated asymmetrically do are being amplified by the edges and not cancelling.

When moved to an asymmetrical position such as Figure 5.3b, the points of diffraction in currents along y are of the same distance, therefore when looking at the cut in $\phi = 0°$ the co-polarized pattern (E_θ) looks symmetrical, but the cross-polarized fields (E_ϕ) come from asymmetrical sources since the equivalent current from diffraction is stronger along $+x$ removing the ability for these fields from both x currents to counteract each other. The result is a cross-polarized pattern increase from well under -40 dB to greater than -20 dB.

Figure 5.4 shows the integrated cross-polarization values for each position

displaced from the center of the ground plane to the edge. The limits of the integration are taken to be between $\pm 60°$, which usually is the desired scanning range that could be attainable at the most with a broadside array. It can be observed that for the monopole case, where diffraction is strong along all of the edges, the diffracted fields produce significant cross-pol contamination with the slightest displacement of the antenna element. The theoretical model satisfactorily predicts this rise in cross-polarized fields, especially around boresight ($\theta = \pm 60°$) where phased array patterns are usually scanned.

For most array antenna elements, mutual coupling is a critical component in the performance of the array. In some cases like microstrip patches, it can greatly affect the cross-polarization performance. Results in this manuscript point to the fact that if it is critical to have low cross-polarization patterns for scanning arrays and there is a presence of periodic conductive surface discontinuities, diffraction can be an even greater limitation towards desired performance. In the case of the monopole shown, mutual coupling is barely a contributor to increases in cross-polarization patterns. The steps shown here provide a more accurate representation of what diffraction will contribute to an antenna element's performance in such environment.

It is proven with this concept by means of calculations, simulations, and measurements that cross-polarized fields are generated significantly by antenna elements positions asymmetrically and close to the edges of a finite phased array. With the use of diffraction theory and an extension of equivalent current method, the E_ϕ cross-polarized fields can be determined with good agreement and therefore can be used to predict in a range between $\theta = \pm 60°$. Therefore, phased array antennas with low cross-polarization requirements that have ground discontinuities can have diffraction fields presence in multiple sections
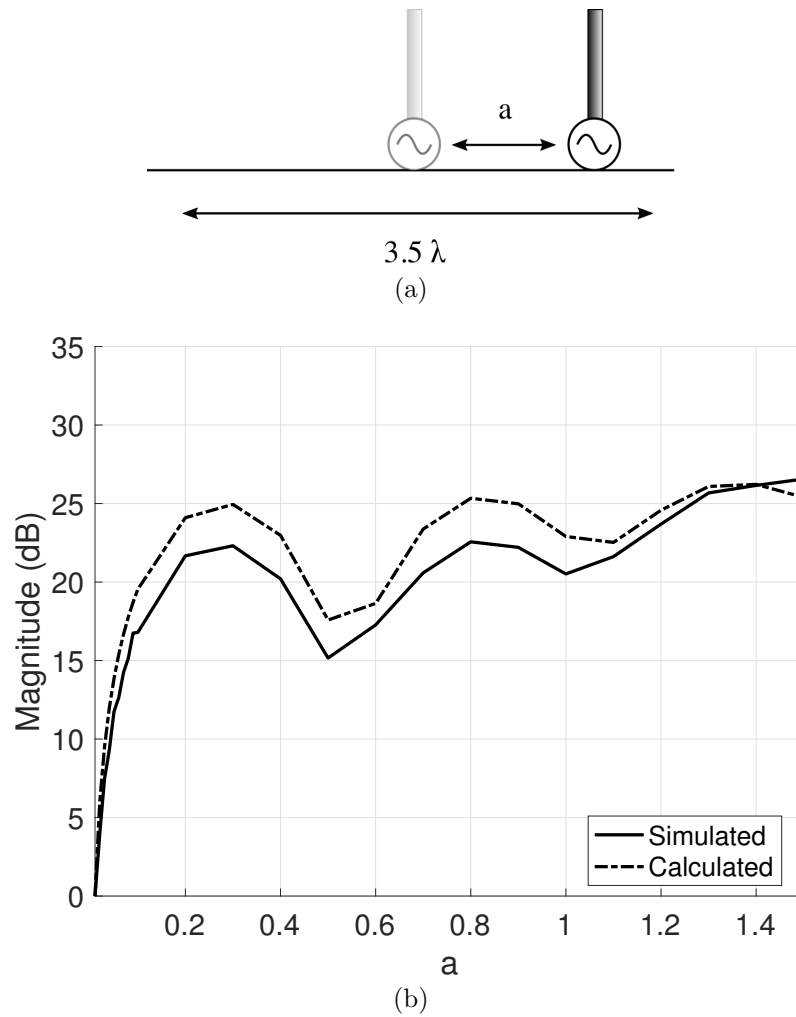
Figure 5.4: Integrated cross-polarization levels of a displaced quarter-wavelength monopole with respect to the distance from the center of the 3.5λ ground plane.

of the array. Diffraction should be evaluated for individual elements and it is made possible with the proposed model.

5.3   Microstrip Patch Antenna

As a way of validating the approximation model, an infinite ground plane solution using finite element method (FEM) is implemented into the proposed
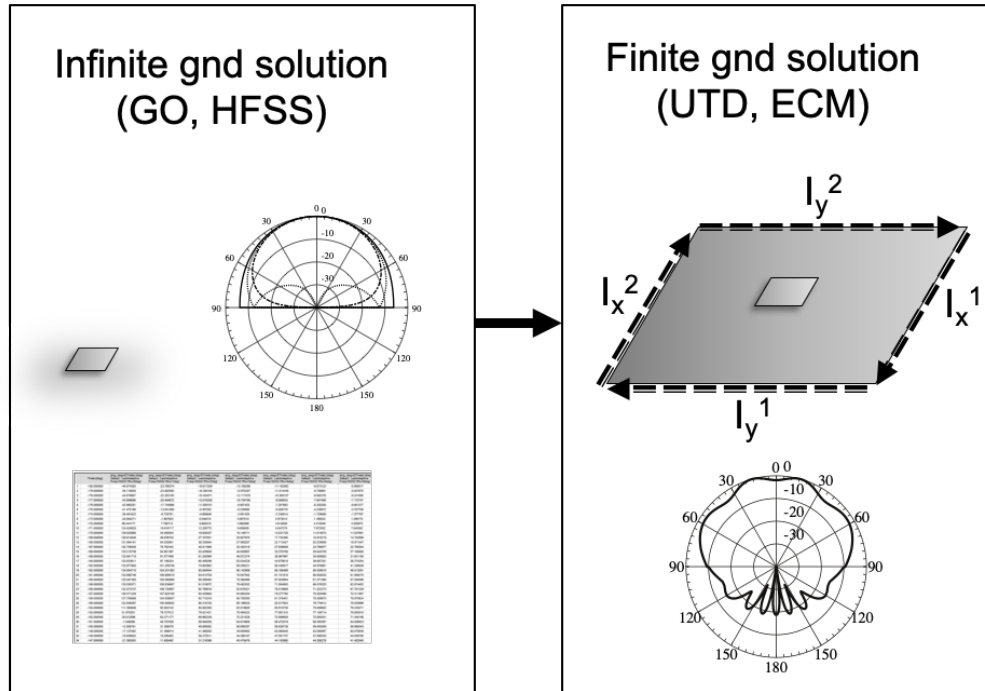
Figure 5.5: Procedure to develop the finite gnd plane solutions for an arbitrary element FEM solution data with infinite ground plane.

model. With the capability of calculating the diffracted fields using equivalent currents around the edges, it is possible to approximate the total fields even at nonprincipal planes. The procedure, as shown in Figure 5.5, involves the calculation of the radiation patterns of a single antenna element placed over an infinite ground plane. These fields are then imported into the analytical model, which with the calculation of the previously discussed 4-edge ECM the finite ground plane solution is produced. The result shown in Figure 5.6, is the E-plane of the antenna element placed over a 3.5λ sized ground plane for calculations of a 7x7 array positions. Figure 5.7 shows the results of infinite ground plane solutions once it is introduced into a ground plane in the D-plane ($\phi = 45°$) using Ludwig 3 definitions [47]. It is interesting to note that the element, regardless of being in the center of the ground plane, it experiences increases in cross-polarization levels in the nonprincipal planes.

Infinite ground plane

Finite ground plane

3.5λ
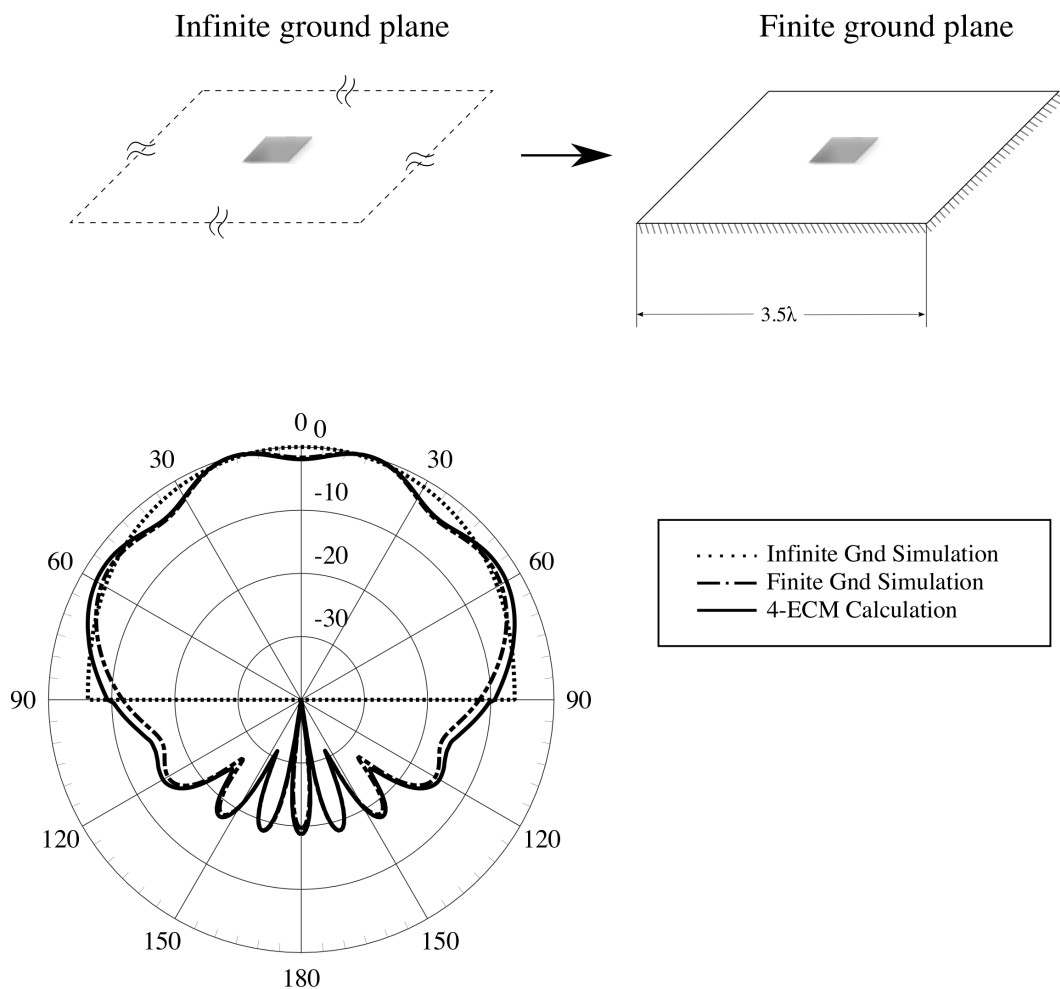
Figure 5.6: Comparison of the FEM results for both infinite and finite ground planes with the calculated results using the proposed analytical model. The patterns of the infinite ground plane FEM solution is introduced to the 4-edge ECM analytical model in order to be compared with the predicted finite ground FEM solution.

In order to validate the prediction of cross-polarized field contamination to the element pattern, the calculations are done with varying positions along the ground plane. The same solutions from the infinite ground plane are then imported with the right parameters for the element at a 0.5λ movement to the right. It is then expected that the cross-polarized fields will remain at the original levels since the element is polarized perpendicularly to the edge at
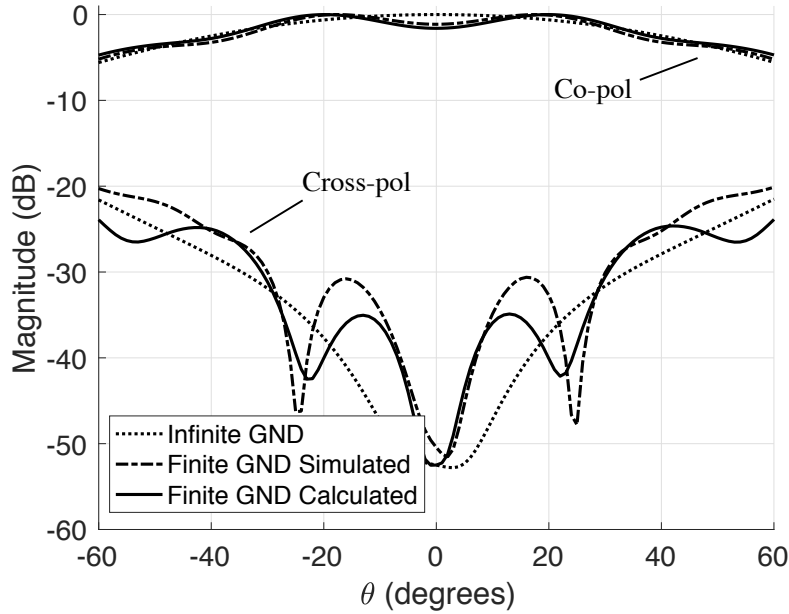
Figure 5.7: Results for an nonprincipal plane (D-plane) of the infinite and finite ground plane FEM solutions compared to the approximations using the 4-edge ECM analytical model. The calculations are done for an element at the exact center of the ground plane.

which it is being moved towards to. Figure 5.8 shows these expected results where only a shift in the co-pol ripples cause by the location with respect to the edges changes. However, cross-polarization levels are mantained below -50 dB, this is due to the cancelations from all quasi-symmetrically illuminated edges. However, at these low levels of cross-polarization component is extremely sensitive to higher-order diffraction and therefore, it is quite complicated to model with the current analytical tool. In order to see the effects on the cross-polarization levels more clearly the element is moved towards the parallel horizontal edges, as seen in Figure 5.9. This shows significant increases in cross-polarization. The levels are captured fairly well with the analytical 4-edge ECM analysis, showing that just a slight movement of the element distorts the cross-polarization greatly by about more than 25 dB in this case.

126
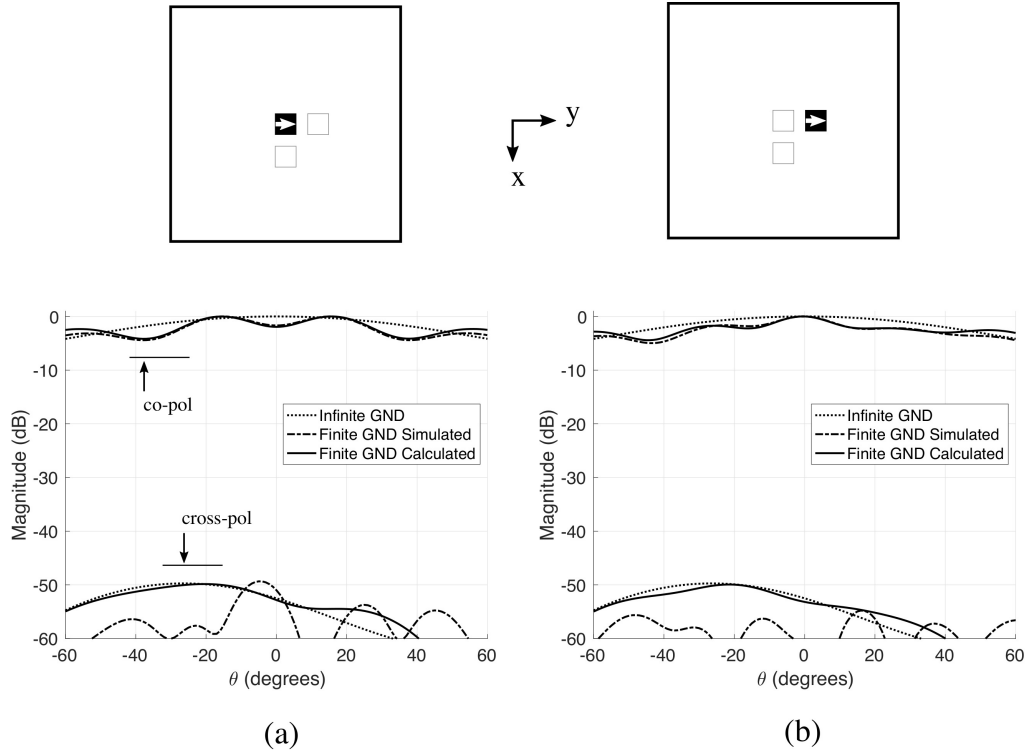
Figure 5.8: Antenna element displaced from the (a) center (0,0) to a position closer to (b) the edges (0,1) along x-axis or perpendicular to the polarization.

The diagonal movement is shown in Figure 5.10, where both co- and cross-polarized fields are distorted by the edge effects and are predicted by the calculations of the analytical model as well. Like wise, moving closer towards the corner, as shown in Figure 5.12, the analytical model is still capturing the cross-polarization levels well. These results prove that, even with the complications that lead to this effects, having so much higher-order responses, especially from corners where there are multiple points of diffraction from edge to edge, the analytical model can predict the overall levels for failure and error analysis to predict adequate performance of the array.
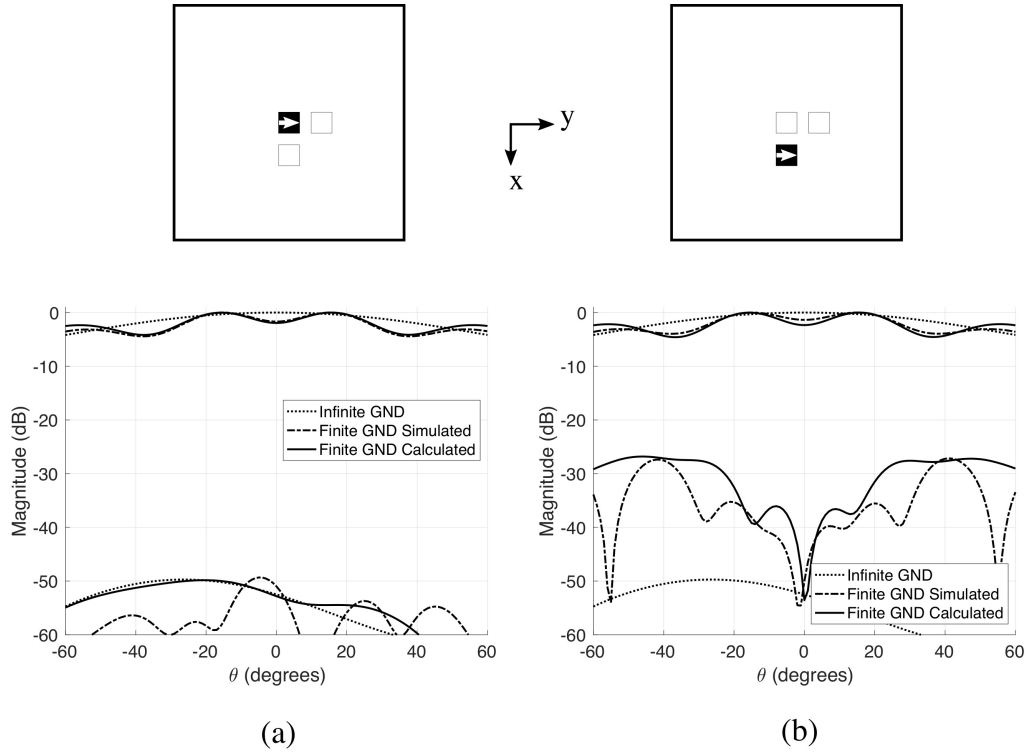
Figure 5.9: Antenna element displaced from the (a) center (0,0) to a position closer to (b) the edges (1,0) along y-axis or parallel to the polarization.

5.4 Summary

The 4-edge ECM can approximate well the results, hence proving to be an effective and quick solution to approximate the fields even for a larger array. The experimental results are shown for the monopole case, where the radiation is strong along all the edges, producing strong cross-polarized fields even moving the element slightly off the center. The same can be mentioned for the microstrip patch antenna element moved along the ground plane. The 4-ECM also proves to be an accurate approximation for any antenna that is simulated in a FEM such as HFSS. The fields taken from the FEM solution are then used to calculate the edge effects accurately matching those of the finite ground plane FEM solutions. This proves to be a useful too where it is
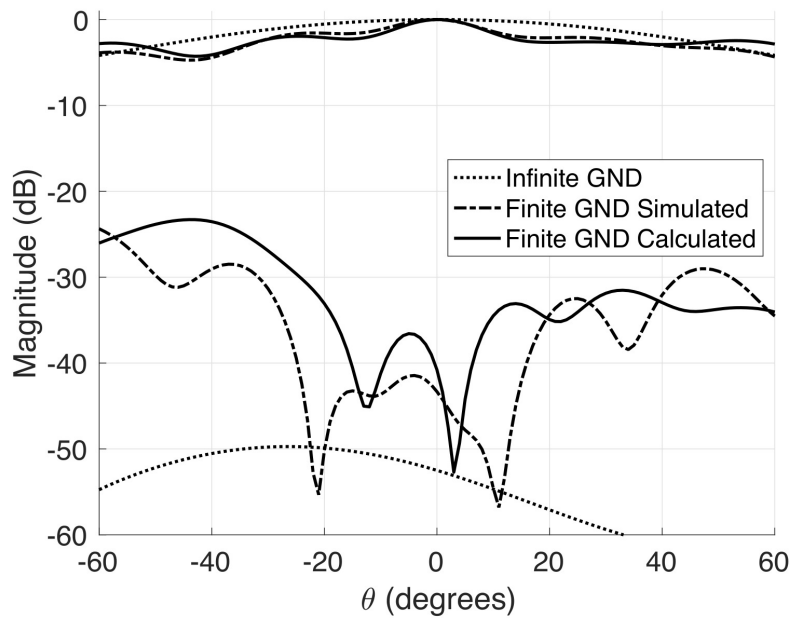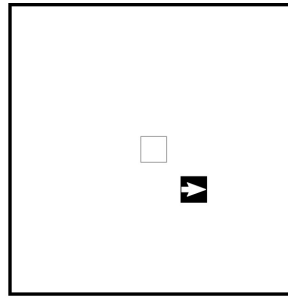
Figure 5.10: Antenna element displaced from the center to a position closer to the edges along x-axis and y-axis (1,1) with a diagonal movement.

desired to predict the fields of larger-scaled structures which would otherwise require a large demand in resources to predict the array performance.
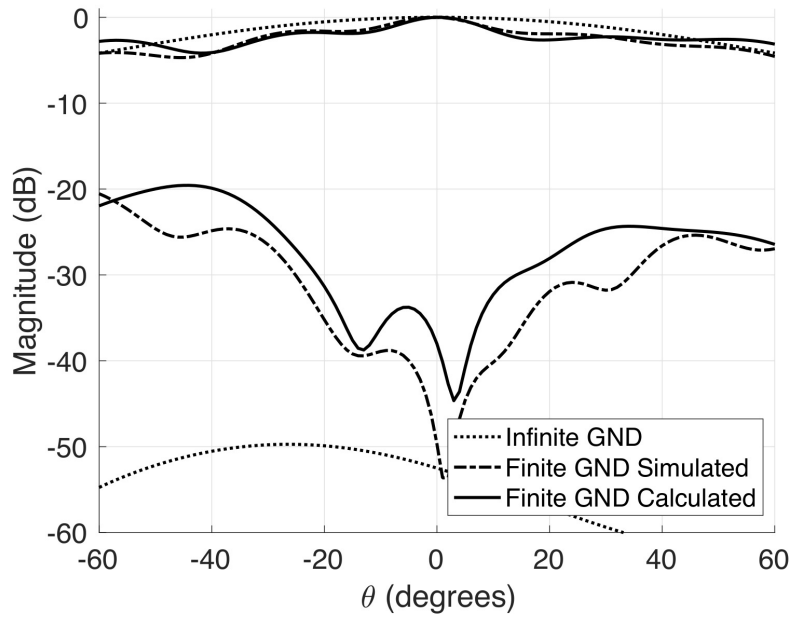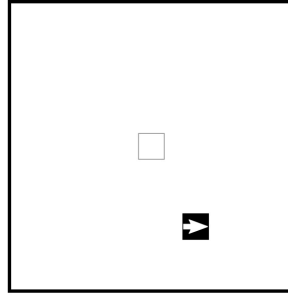
Figure 5.11: Antenna element displaced from the center to a position closer to the edges along x-axis and y-axis (2,1) with a diagonal movement.
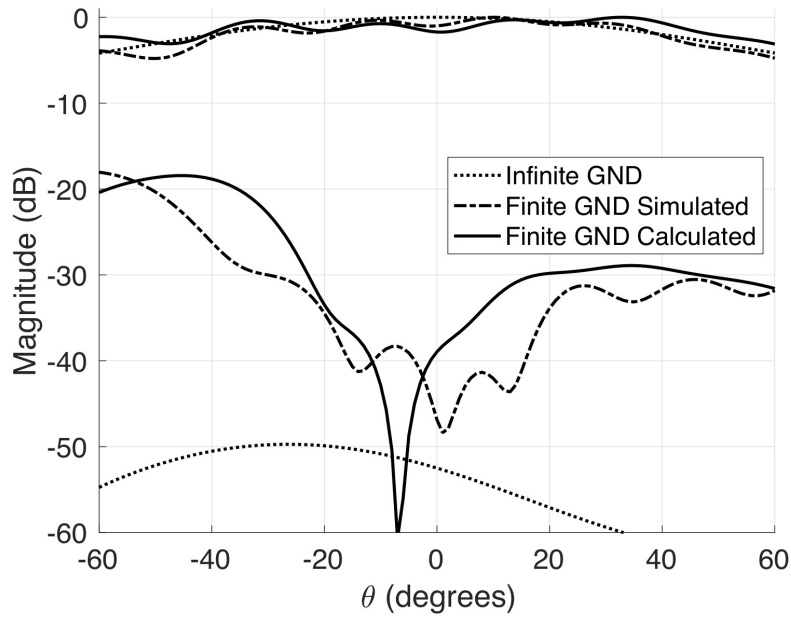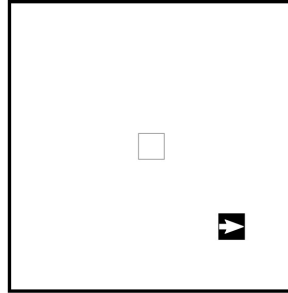
Figure 5.12: Antenna element displaced from the center with twice the diagonal movement along the x-axis and y-axis (2,2).

Chapter 6

Epilogue

6.1 Summary

This work has presented a thorough analysis into the effects that edge diffraction has in a PAR. A special focus is done in the fields radiated from these edges and how they affect the performance of individual elements of the array. Besides the reflections and scattering caused by the edges that can disturb the impedance responses of the embedded elements, especially along the edges, the contribution of the edge effects can be seen at the element level throughout all of the embedded element patterns along the subarray. Knowing this, the effects usually are not looked into because diffracted fields usually would cancel or destructively add itself. However this mainly happens when the array is illuminated uniformly and has all of the elements perfectly placed and are all exactly the same. PARs usually have fabrication limitations where the elements might be shifted, antenna elements with slight shifts in frequency also have different radiation characteristics, or where the elements have failed ports where the array can introduce errors, which can disrupt the adequate cancellation of fields. The study shown provides an insight as to how and when the radiation fields from the elements disrupt the radiation performance.

The polarization definitions for PAR where presented in order to give context to the requirements polarimetric PAR have for weather measurements. The importance to address many challenges for low cross-polarization requirements that arise with the use of electronic beam steering and shaping are discussed. One such challenge is in the form of polarization projections of the fields radiating form the PAR and being backscattered from the medium being detected. Added to this PAR require high-performance radiating elements and design of these elements have crucial factors involved such as, feeding techniques and the radiating nature of the antenna structures. These antenna elements are also placed over complicated structures, such as scalable subarray panels which introduce multiple points of discontinuity, which generate diffracted fields. These diffracted fields have been detected, but the contribution to cross-polarized fields have not been analytically quantified until this work. Other important factors in the adequate performance of the PAR like mutual coupling is discussed. These parameters are of importance to techniques such as calibration of PAR at the element level, where the edges are also a well known issue in literature.

Chapter 3 introduced the critical tools in diffraction theory used in this work. The use of two-point diffraction aids in the understanding of the arbitrary placement elements along a specifically sized conductive surface. This provides the ability to characterize the ripples and variations caused by the diffracted fields introduced by the antenna's environment that can cause changes in gain performance. As an expansion to this, the ECM takes in consideration every individual point of diffraction that can be calculated by the two-point procedure but throughout the complete edge, modeling the diffracted fields as an equivalent current. This brings the ability to calcu-

late radiation fields with the use of vector potential theory in order to model the edges as though they where current sources. In the case of this study, the sources are modeled as magnetic currents, since the only used diffraction coefficient needed is for hard polarization due to the assumptions that the elements are close enough to the surface of the PEC and therefore, cancellation of the direct and reflected diffracted fields occur as shown in Section 3.3.2. In the next chapter, the use of this tools is integrated into quantifying the effect diffracted fields have on phased array antennas.

Illustrated in Chapter 4 is the general impact edge diffracted fields have on the performance of phased array antennas. An analysis based on the positioning and polarization excitation is done in order to show the effects edge diffraction has on the individual element patterns of an array. This then translate to differences when steering the beam of the phased array. The results show that for elements with low levels of cross-polarization isolation, once they are moved from a central position of the ground plane, cross-polarization contamination solely due to its positioning with respect to the edges is introduced.

Hence, depending on the number of elements in a phased array, the individual active element patterns will have different levels of distortion. However, once all of them are taken into account as a whole, these diffracted field contributions can cancel out and null itself. This is only if, the element is exactly the same throughout and has the same radiation characteristics for every element in position. If there is a slight shift in position or performance this cancellation might not be as effective.

Another important observation was discussed in Chapter 5 as the effect that the element excitation errors may potentially have on the array performance. The array performance will be dictated by the average embedded

element pattern. Hence, when a number of excitation errors are in the form of failed elements, the average embedded element pattern shows an ineffective cancelation of the edge effects. Therefore, the embedded element pattern shows higher cross-polarization levels, which results in higher cross-pol when scanning the array. This is truer for the case where there are multiple sources of diffraction, as is the internal gaps between subarray panels in a larger-scaled PAR.

In efforts to predict the contribution of the edges in the cross-polarization levels of each array element the 4-edge ECM is introduced. It can approximate well the results, hence proving to be an effective and quick solution to approximate the fields even for a larger array. The experimental results are shown for the monopole case, where the radiation is strong along all the edges, producing strong cross-polarized fields even moving the element slightly off the center. The same can be said for the microstrip patch antenna element moved along the ground plane. The 4-ECM also proves to be an accurate approximation for any antenna that is simulated in a FEM such as HFSS. The fields taken from the FEM solution are then used to calculate the edge effects accurately matching those of the finite ground plane FEM solutions. This proves to be a useful too where it is desired to predict the fields of larger-scaled structures which would otherwise require a large demand in resources to predict the array performance.

6.2 Conclusions

The findings in this work point towards edge diffractions as a main contributor to cross-polarization level increases by the mere presence of finite ground plane edges. Extensive studies are done in order to gain insight as to how

a polarized element's radiation pattern performance, specifically in terms of co- and cross-polarization mismatches, is affected by diffracted fields from the edges. Theoretical studies show that polarization, distance to the edge, and the angle of incidence is important factors for diffracted fields and how they will interact with the antenna element.

A clear representation of a polarized element shows that as the element is moved from the center of the ground plane, cross-polarization levels are increased substantially, as well as ripples and errors in the co-polarization fields can be introduced. Cross-polarized fields are noticeable especially when the element is polarized in a certain direction and the asymmetric illumination of the parallel edges to the polarized fields produce substantial mismatches at the element level. If the array is illuminated uniformly these fields can be potentially canceled out, however, the research shows that with element excitation errors or any percentage of failed elements can contribute to a not so effective cancelation of diffracted fields. This brings forth the conclusion that any slight errors in antenna placement, fabrication errors, or elements that are not exactly replicated throughout the array should be taken into consideration in order to reassure proper performance of the PAR. In order to do so, proper tools should be implemented to successfully predict what the embedded element patterns throughout the array will be to ensure adequate performance of the array.

In this dissertation an analytical model is proposed in order to predict the effects the diffracted fields introduce to the overall patterns of the elements in an array. A combination of diffraction theory and an expansion of the modeling of diffracted fields as equivalent currents is introduced for a flat 4-edged ground plane in order to capture the undesired cross-polarization contributions that

are solely from the edges. These contributions even though they might not be the only ones, are proven to be the main source of cross-polarization at the element level of the array. The study is applied to the monopole radiation pattern, because of its uniformly strong radiation along all azimuth angles, which illuminate the edges uniformly to understand how this diffraction phenomena interacts with the positioning of the element. Furthermore, the MPA is used by mean of FEM simulation results to show that it is possible to include any design of interest in some FEM calculation to predict the cross-polarization performance of the overall elements and array.

6.3 Contribution

The main contribution of this work is an analytical model that can approximate the effect that diffracted fields have on an individual antenna element placed above a ground plane. This opens the possibilities of scaling larger phased array performance predictions without the need of high resource demanding procedures such as the common FEM analysis. The proven concept involves the expansion of diffraction theory concepts such as the equivalent current method to calculate the currents along all four edges of the ground plane with arbitrary radiating element positions. Furthermore, studies using diffraction theory and simulations are done to gain further insight as to how diffraction fields interact with an array at an element level.

The studies done take into account different element types with different ground plane sizes in the element level. Analytical experiments include different locations and array sizes to further complete a study that can be expanded to larger scale structures. Included in these experiments are analytically built element patterns and the contributions that the edge effects have on cross-

polarization and mutual coupling of an array. Finally the model is extended to be applicable to expandable arrays with multiple tiles and gap separations between them and how these separations impact the performance of the array.

A better prediction of the array pattern behavior is achieved with experiments on element frequency response, element patterns based on location over ground plane, and the analytical model for predicting the effects of diffracted fields on the radiation pattern of each individual element of the array. With this model it is shown that a more accurate representation of a phased array performance is possible by including edge effects into the calculations. Making this analytical model valuable for in-detailed predictions of high-performance PAR.

1. A stronger, clearer insight as to how edge diffraction affects the radiation performance of each element in an array. Specifically what field orientations interact more significantly with which specific edges

2. Analytical studies of different sized arrays and how they might differ in performance and what is the importance of array configurations

3. Different uses for several diffraction theory techniques and how they can provide insight into how diffracted fields are generated and affect radiation performance

4. An expanded equivalent current method for the prediction of cross-polarization levels for any sized array with introduced excitation errors such as element failures

5. The capacity for scalable applications where a quick prediction and determination of up to par performance with regards to operational requirements

6. A proven successful procedure that can import any desired FEM antenna radiation pattern solution and apply a scalable algorithm to produce the total radiation pattern with the calculation of the diffracted fields from all four edges of any arbitrarily sized the ground plane and the antenna element position

7. The analytical tool is also useful when the cross-polarization fields in the nonprincipal planes such as the D-plane is of interest given that phased array antennas can electronically steer at all directions in space and not only at the principal planes

6.4 Future Work

Recommendations for future work are the implementation of impedance calculations for edge effects. This can give a better understanding of mutual coupling and impedance performance at the element level. Also, the calculations of surface waves and the diffracted fields produced by such elements increase the amplitude of diffracted fields and can further improve the accuracy of predicted patterns, especially for thicker dielectric materials and higher frequency applications.

Further work should be done in order to correct for singularities that are inherent in the calculation of the equivalent currents. Transition effects can fill up the nulls that wouldn't be there in practice and are of more interest for end-fire array applications. Expansion of this model can be done to take into account the effects of internal gaps throughout a larger-scaled array of multiple subarrays. Even though the energy dispersed is farther away from the elements, it should still be of interest to be taken into account for sensitive measurements.

Methods of mitigation have been explored before. Resistive loading is a known technique to suppress radiation from the backlobe of the antenna. Therefore, what this does in practice is reduce the diffraction caused by the edges. Besides resistive loading, other methods that involve the disruption of the ground in order to randomize diffracted fields can be further explored. Another method that can prove to be effective is the use of metamaterials in order to depolarize the wave that is being introduced into the discontinuity of the edge. Other methods includes the application of artificial boundaries hard or soft boundaries with corrugated surfaces. It is known from this work that the hard polarization is the one that affects antennas placed on a ground plane. Therefore, a technique where the edge sees a soft polarized wave instead might help with mitigating diffracted fields from the edges, and therefore the scattering that would contribute to disrupting the impedance response.

References

[1] R. J. Mailloux, *Phased array antenna handbook.* Artech house, 2017.

[2] A. J. Fenn, D. H. Temme, W. P. Delaney, and W. E. Courtney, "The development of phased-array radar technology", *Lincoln laboratory journal*, vol. 12, no. 2, pp. 321–340, 2000.

[3] D. S. Zrnic, J. F. Kimpel, D. E. Forsyth, a. Shapiro, G. Crain, R. Ferek, J. Heimmer, W. Benner, T. J. McNellis, and R. J. Vogt, "Agile-beam phased array radar for weather observations", *Bulletin of the American Meteorological Society*, vol. 88, no. 11, pp. 1753–1766, 2007, ISSN: 00030007.

[4] Y. Wang and V. Chandrasekar, "Polarization isolation requirements for linear dual-polarization weather radar in simultaneous transmission mode of operation", *IEEE Transactions on Geoscience and Remote Sensing*, vol. 44, no. 8, pp. 2019–2028, 2006, ISSN: 01962892.

[5] M. C. Leifer, V. Chandrasekar, and E. Perl, "Dual polarized array approaches for mpar air traffic and weather radar applications", in *2013 IEEE International Symposium on Phased Array Systems and Technology*, 2013, pp. 485–489.

[6] J. Herd and S. Duffy, "Overlapped digital subarray architecture for multiple beam phased array radar", in *Proceedings of the 5th European Conference on Antennas and Propagation (EUCAP)*, 2011, pp. 3027–3030.

[7] C Buck, D. M. Pozar, and C Hansen, "Cross polarization of microstrip patch antennas", pp. 731–732, 1987.

[8] G. Zhang, R. J. Doviak, D. S. Zrnic, J. Crain, D. Staiman, and Y. Al-Rashid, "Phased array radar polarimetry for weather sensing: a theoretical formulation for bias corrections", *IEEE Transactions on Geoscience and Remote Sensing*, vol. 47, no. 11, pp. 3679–3689, 2009, ISSN: 01962892.

[9] M. C. Leifer, V. Chandrasekar, and E. Perl, "Dual polarized array approaches for mpar air traffic and weather radar applications", *IEEE International Symposium on Phased Array Systems and Technology*, pp. 485–489, 2013.

[10] M. E. Weber, J. Y. Cho, J. S. Herd, J. M. Flavin, W. E. Benner, and G. S. Torok, "The next-generation multimission U.S. surveillance radar network", *Bulletin of the American Meteorological Society*, vol. 88, no. 11, pp. 1739–1751, 2007, ISSN: 00030007.

[11] C. Fulton, J. Herd, S. Karimkashi, G. Zhang, and D. Zrnic, "Dual-polarization challenges in weather radar requirements for multifunction phased array radar", *IEEE International Symposium on Phased Array Systems and Technology*, pp. 494–501, 2013.

[12] R. J. Doviak, V. Bringi, A. Ryzhkov, A. Zahrai, and D. Zrnić, "Considerations for polarimetric upgrades to operational wsr-88d radars", *Journal of Atmospheric and Oceanic Technology*, vol. 17, no. 3, pp. 257–278, 2000.

[13] J. L. Salazar, N. Aboserwal, J. D. Díaz, J. A. Ortiz, and C. Fulton, "Edge diffractions impact on the cross polarization performance of active phased array antennas", in *2016 IEEE International Symposium on Phased Array Systems and Technology (PAST)*, 2016, pp. 1–5.

[14] J Huang, "The finite ground plane effect on the microstrip antenna radiation patterns", *New York*, vol. 31, no. 4, pp. 649–653, 1983, ISSN: 0018-926X.

[15] R. G. Kouyoumjian and P. H. Pathak, "A uniform geometrical theory of diffraction for an edge in a perfectly conducting surface", *Proceedings of the IEEE*, vol. 62, no. 11, pp. 1448–1461, 1974, ISSN: 0018-9219.

[16] J. B. Keller, "Geometrical theory of diffraction", *Journal of The Optical Society of America*, vol. 52, no. 2, 1962.

[17] H. M. Ibrahim and D. T. Stephenson, "Radiation patterns of a $\lambda/4$ monopole mounted on thick finite square and circular ground planes", *International Journal of Electronics*, vol. 64, no. 3, pp. 345–358, 1988, ISSN: 0020-7217.

[18]   C. Ryan and L. Peters, "Evaluation of edge-diffracted fields including equivalent currents for the caustic regions", *IEEE Transactions on Antennas and Propagation*, vol. 17, no. 3, pp. 292–299, 1969, ISSN: 1558-2221.

[19]   N. A. Aboserwal, "Gain and loss factor for conical horns, and impact of ground plane edge diffractions on radiation patterns of uncoated and coated circular aperture antennas", PhD thesis, Arizona State University, 2014.

[20]   C. A. Balanis, "Analysis of an array of line sources above a finite ground plane", *IEEE Transactions on Antennas and Propagation*, no. 2, pp. 1–20, 2004.

[21]   Arun K. Bhattacharyya, "Finite ground plane effects on the radiation patterns of a rectangular microstrip antenna", *12th European Microwave Conference, 1982*, pp. 384–389, 1982.

[22]   D. M. Pozar, "The active element pattern", *IEEE Transactions on Antennas and Propagation*, vol. 42, no. 8, pp. 1176–1178, 1994, ISSN: 15582221.

[23]   D. M. Pozar and B. Kaufman, "Design considerations for low sidelobe microstrip arrays", *IEEE Transactions on Antennas and Propagation*, vol. 38, no. 8, pp. 1176–1185, 1990, ISSN: 15582221.

[24]   J. B. Keller, "Diffraction by an aperture", *Journal of Applied Physics*, vol. 28, no. 4, pp. 426–444, 1957, ISSN: 00218979.

[25]   C. A. Balanis, *Advanced engineering electromagnetics*. John Wiley & Sons, 2012.

[26]   P. H. Pathak, G. Carluccio, and M. Albani, "The uniform geometrical theory of diffraction and some of its applications", *IEEE Antennas and Propagation Magazine*, vol. 55, no. 4, pp. 41–69, 2013, ISSN: 10459243.

[27]   P. H. Pathak, "High frequency techniques for antenna analysis", *Proceedings of the IEEE*, vol. 80, no. 1, pp. 44–65, 1992, ISSN: 15582256.

[28]   C Cockrell and P Pathak, "Diffraction theory techniques applied to aperture antennas on finite circular and square ground planes", *IEEE Transactions on Antennas and Propagation*, vol. 22, no. 3, pp. 443–448, 1974.

143

[29] N. A. Aboserwal, C. A. Balanis, and C. R. Birtcher, "Impact of finite gound plane edge diffractions on radiation patterns of aperture antennas", *Progress In Electromagnetics Research B*, vol. 55, no. August, pp. 1–21, 2013.

[30] F. A. Sikta, W. D. Burnside, L. Peters, and T. T. Chu, "First-order equivalent current and corner diffraction scattering from flat plate structures", *IEEE Transactions on Antennas and Propagation*, vol. 31, no. 4, pp. 584–589, 1983, ISSN: 15582221.

[31] A Michaeli, "Equivalent currents for second-order diffraction by the edges of perfectly conducting polygonal surfaces", *IEEE Trans. Antennas Propagat.*, vol. 35, no. 2, pp. 183–190, 1987, ISSN: 0018926X.

[32] A. K. Bhattacharyya, "Effects of finite ground plane on the radiation characteristics of a circular patch antenna", *Antennas and Propagation, IEEE Transactions on*, vol. 38, no. 2, 152 ST –Effects of finite ground plane on the ra, 1990, ISSN: 0018-926X.

[33] S Noghanian and L Shafai, "Control of microstrip antenna radiation characteristics by ground plane size and shape", *IEE Microwaves, Antennas & Propagation*, vol. 145, no. 3, pp. 207–212, 1998.

[34] E. Lier and K. R. Jakobsen, "Rectangular microstrip patch antennas with infinite and finite ground plane dimensions", *IEEE Transactions on Antennas and Propagation*, vol. 31, no. 6, pp. 978–984, 1983, ISSN: 15582221.

[35] K. L. Wong and T. W. Chiou, "Finite ground plane effects on broad-band dual polarized patch antenna properties", *IEEE Transactions on Antennas and Propagation*, vol. 51, no. 4, pp. 903–904, 2003, ISSN: 0018926X.

[36] Y. Wang and Z. Du, "Dual-polarized slot-coupled microstrip antenna array", *IEEE Transactions on Antennas and Propagation*, vol. 63, no. 9, pp. 4239–4244, 2015.

[37] J. Huang, "The finite ground plane effect on the microstrip antenna radiation patterns", *New York*, vol. 31, no. 4, pp. 649–653, 1983, ISSN: 0018-926X.

[38] T. Namiki, Y. Murayama, and K. Ito, "Improving radiation-pattern distortion of a patch antenna having a finite ground plane", *IEEE Trans-*

actions on Antennas and Propagation, vol. 51, no. 3, pp. 478–482, 2003, ISSN: 0018926X.

[39]   A. B. Smolders, R. M. C. Mestrom, A. C. F. Reniers, and A Zamanifekri, "Effect of a finite ground plane on the axial ratio of circularly - polarized microstrip arrays", pp. 203–206, 2013.

[40]   L. M. Bhowmik and C. J. Fulton, "Analysis and measurement of grating lobe effects in infinite planar arrays of finite sized subarrays", *IEEE International Symposium on Phased Array Systems and Technology*, 2017.

[41]   H. Yuan, K. Hirasawa, and Y. Zhang, "The mutual coupling and diffraction effects on the performance of a CMA adaptive array", vol. 47, no. 3, pp. 728–736, 1998.

[42]   M. Zamłyński and P. Slobodzian, "Mutual coupling modelling in presence of diffraction effects for different types of microstrip radiating elements", in *2012 19th International Conference on Microwaves, Radar Wireless Communications*, vol. 1, 2012, pp. 77–79.

[43]   M. Zamłyński and P. Słobodzian, "Antenna array radiation pattern modeling which includes mutual coupling and diffraction effects", *Proceedings of 6th European Conference on Antennas and Propagation, EuCAP 2012*, no. 5, pp. 1627–1631, 2012.

[44]   E. G. E. De Lera, "Mutual coupling edge effect approximation for phased-array antennas", no. 1, pp. 149–152, 2008.

[45]   L Josefsson, "Mutual coupling calculations including edge effects", vol. 30, no. 25, pp. 2087–2088, 1995.

[46]   D. Zrnić, R. Doviak, G. Zhang, and A. Ryzhkov, "Bias in differential reflectivity due to cross coupling through the radiation patterns of polarimetric weather radars", *Journal of Atmospheric and Oceanic Technology*, vol. 27, no. 10, pp. 1624–1637, 2010.

[47]   N. A. Aboserwal, J. L. Salazar, J. A. Ortiz, J. D. Díaz, C. Fulton, and R. D. Palmer, "Source current polarization impact on the cross-polarization definition of practical antenna elements: Theory and applications", *IEEE Transactions on Antennas and Propagation*, vol. 66, no. 9, pp. 4391–4406, 2018.

[48] P Sullivan and D Schaubert, "Analysis of an aperture coupled microstrip antenna", *IEEE Transactions on Antennas and Propagation*, vol. 34, no. 8, pp. 977–984, 1986, ISSN: 0096-1973.

[49] J. T. Aberle and D. M. Pozar, "Analysis of infinite arrays of one- and two-probe-fed circular patches", *IEEE Transactions on Antennas and Propagation*, vol. 38, no. 4, pp. 421–432, 1990, ISSN: 15582221.

[50] J. D. Díaz, J. L. Salazar-Cerreno, J. A. Ortiz, N. A. Aboserwal, R. M. Lebrón, C. Fulton, and R. D. Palmer, "A cross-stacked radiating antenna with enhanced scanning performance for digital beamforming multifunction phased-array radars", *IEEE Transactions on Antennas and Propagation*, vol. 66, no. 10, pp. 5258–5267, 2018, ISSN: 0018-926X.

[51] C. A. Balanis, *Antenna theory: Analysis and design.* John wiley & sons, 2016.

[52] D. M. Pozar, "Microstrip antennas", *Proceedings of the IEEE*, vol. 80, no. 1, pp. 79–91, 1992.

[53] D. R. Jackson and N. G. Alexopoulos, "Simple approximate formulas for input resistance, bandwidth, and efficiency of a resonant rectangular patch", *IEEE Transactions on Antennas and Propagation*, vol. 39, no. 3, pp. 407–410, 1991.

[54] R. Hansen, "Cross polarization of microstrip patch antennas", *IEEE Transactions on Antennas and Propagation*, vol. 35, no. 6, pp. 731–732, 1987.

[55] D. M. Pozar, "Scanning characteristics of infinite arrays of printed antenna subarrays", *IEEE Transactions on Antennas and Propagation*, vol. 40, no. 6, pp. 666–674, 1992.

[56] ——, "A relation between the active input impedance and the active element pattern of a phased array", *IEEE Transactions on Antennas and Propagation*, vol. 51, no. 9, pp. 2486–2489, 2003.

[57] H. M. Aumann, A. J. Fenn, and F. G. Willwerth, "Phased array antenna calibration and pattern prediction using mutual coupling measurements", *IEEE Transactions on Antennas and Propagation*, vol. 37, no. 7, pp. 844–850, 1989.

[58] D. Pozar and D. Schaubert, "Scan blindness in infinite phased arrays of printed dipoles", *IEEE Transactions on Antennas and Propagation*, vol. 32, no. 6, pp. 602–610, 1984.

[59] J. A. Ortiz, J. L. Salazar-Cerreno, J. D. Díaz, R. M. Lebrón, N. Aboserwal, and L. Jeon, "Low-cost CMOS active array solution for highly-dense X-band weather radar network", *IEEE Transactions on Antennas and Propagation*, pp. 1–1, 2020.

[60] R. M. Lebrón, P. Tsai, J. M. Emmett, C. Fulton, and J. L. Salazar-Cerreno, "Validation and testing of initial and in-situ mutual coupling-based calibration of a dual-polarized active phased array antenna", *IEEE Access*, vol. 8, pp. 78 315–78 329, 2020.

[61] H. Steyskal and J. S. Herd, "Mutual coupling compensation in small array antennas", *IEEE Transactions on Antennas and Propagation*, vol. 38, no. 12, pp. 1971–1975, 1990, ISSN: 15582221.

[62] J. A. Ortiz, N. Aboserwal, and J. L. Salazar, "A new analytical model based on diffraction theory for predicting cross-polar patterns of antenna elements in a finite phased array", in *2019 IEEE International Symposium on Phased Array System Technology (PAST)*, 2019, pp. 1–4.

[63] R. J. Mailloux, "Phased array theory and technology", *Proceedings of the IEEE*, vol. 70, no. 3, pp. 246–291, 1982.

[64] R. G. Kouyoumjian, "Asymptotic high-frequency methods", *Proceedings of the IEEE*, vol. 53, no. 8, pp. 864–876, 1965, ISSN: 15582256.

[65] P. Y. Ufimtsev, "Method of edge waves in the physical theory of diffraction", Foreign Technology Div. Wright-Patterson AFB OH, Tech. Rep., 1971.

[66] W. Richards, Yuen Lo, and D. Harrison, "An improved theory for microstrip antennas and applications", *IEEE Transactions on Antennas and Propagation*, vol. 29, no. 1, pp. 38–46, 1981, ISSN: 1558-2221.

[67] P. H. Pathak and R. Kouyoumjian, "The dyadic diffraction coefficient for a perfectly conducting wedge", Ohio State Univ. Colombus Electroscience Lab, Tech. Rep., 1970.

[68] Y. Wang and V. Chandrasekar, "Polarization isolation requirements for linear dual-polarization weather radar in simultaneous transmission mode of operation", *IEEE Transactions on Geoscience and Remote Sensing*, vol. 44, no. 8, pp. 2019–2028, 2006, ISSN: 0196-2892.

[69] D. S. Zrnic, J. F. Kimpel, D. E. Forsyth, A. Shapiro, G. Crain, R. Ferek, J. Heimmer, W. Benner, F. T. J. McNellis, and R. J. Vogt, "Agile-beam phased array radar for weather observations", *Bulletin of the American Meteorological Society*, vol. 88, no. 11, pp. 1753–1766, 2007.

[70] M. Zamłyński and P. Słobodzian, "Antenna array radiation pattern modeling which includes mutual coupling and diffraction effects", in *2012 6th European Conference on Antennas and Propagation (EUCAP)*, 2012, pp. 1627–1631.

[71] A. J. Fenn, "Theoretical and experimental study of monopole phased array antennas", *IEEE Transactions on Antennas and Propagation*, vol. 33, no. 10, pp. 1118–1126, 1985, ISSN: 15582221.

[72] R. G. Kouyoumjian and P. H. Pathak, "A uniform geometrical theory of diffraction for an edge in a perfectly conducting surface", *Proceedings of the IEEE*, vol. 62, no. 11, pp. 1448–1461, 1974, ISSN: 0018-9219.

[73] C. Ryan and L. Peters, "Evaluation of edge-diffracted fields including equivalent currents for the caustic regions", *IEEE Transactions on Antennas and Propagation*, vol. 17, no. 3, pp. 292–299, 1969, ISSN: 0018-926X.

[74] H. Yuan, K. Hirasawa, and Y. Zhang, "The mutual coupling and diffraction effects on the performance of a cma adaptive array", *IEEE Transactions on Vehicular Technology*, vol. 47, no. 3, pp. 728–736, 1998, ISSN: 0018-9545.